NASA CONTRACTOR REPORT

NASA CR-2662

NASA CR-2662

A NUMERICALLY EFFICIENT FINITE ELEMENT HYDROELASTIC ANALYSIS

Volume 1: Theory and Results

Robert N. Coppolino

Prepared by
GRUMMAN AEROSPACE CORPORATION
Bethpage, N.Y. 11714
for Langley Research Center

NATIONAL AERONAUTICS AND SPACE ADMINISTRATION • WASHINGTON, D. C. • APRIL 1976

1. Report No.	2. Government Accession No.	3. Recipient's Catalog No.
NASA CR-2662		

4. Title and Subtitle "A Numerically Efficient Finite Element Hydroelastic Analysis" Volume 1: Theory and Results	5. Report Date April 1976 6. Performing Organization Code
7. Author(s) Robert N. Coppolino	8. Performing Organization Report No.
9. Performing Organization Name and Address Grumman Aerospace Corporation Bethpage, New York 11714	10. Work Unit No. 11. Contract or Grant No. NAS1-10635-21
12. Sponsoring Agency Name and Address National Aeronautics and Space Administration Washington, DC 20546	13. Type of Report and Period Covered Contractor Report 14. Sponsoring Agency Code

15. Supplementary Notes

Langley Technical Monitor - Larry D. Pinson FINAL REPORT

16. Abstract

Symmetric finite element matrix formulations for compressible and incompressible hydroelasticity are developed on the basis of Toupin's complementary formulation of classical mechanics. Results of implementation of the new technique in the NASTRAN structural analysis program are presented which demonstrate accuracy and efficiency.

17. Key Words (Suggested by Author(s))	18. Distribution Statement
Hydroelasticity, NASTRAN, Complementary energy, fluid-structure interaction	Unclassified - Unlimited Subject Category 39 Structural Mechanics

19. Security Classif. (of this report)	20. Security Classif. (of this page)	21. No. of Pages	22. Price*
Unclassified	Unclassified	104	$5.25

*For sale by the National Technical Information Service, Springfield, Virginia 22161

FOREWORD

The work described in this report was performed at the Grumman Aerospace Corporation, Bethpage, New York, and administered by the Vibration Section of the Structures and Dynamics Division, NASA Langley Research Center, Hampton, Virginia.

The work performed under NASA Contract NAS1-10635-21 with supplementary funding provided by the Space Division, Rockwell International (POM3WXMZ-483002) included development of a fundamental finite element hydroelastic formulation applicable to NASTRAN, implementation of the theoretical developments into NASTRAN, and verification and demonstration of the new technique on various problems including the 1/8-scale space shuttle external tank model.

ABSTRACT

A finite element hydroelastic analysis formulation is developed on the basis of Toupin's complementary variational principle of classical mechanics. Emphasis is placed on the special case of an incompressible fluid model which is applicable to propellant tank hydroelastic analysis. A concise fluid inertia representation results from the assumption of incompressibility and the hydroelastic equations reduce to a simplified form associated with non-fluid filled structures. The efficiency of the incompressible hydroelastic formulation is enhanced for both fluid and structure by introduction of harmonic reduction as an alternative to Guyan reduction. The theoretical developments are implemented in NASTRAN and the modified NASTRAN hydroelastic analysis technique is verified and demonstrated as an efficient and accurate approach with a series of illustrative problems including the 1/8-scale space shuttle external tank.

List of Symbols

(A), Aik	generalized area matrix, generalized area matrix component (Eq. 2.1-11)
B	fluid bulk modulus (Eq. 2.1-2)
(C), Cij	compliance (flexibility) matrix, compliance matrix component (Eq. 2.1-10d)
E	structural elastic modulus
F	force
(G)	matrix defined in (Eq. 2.3-21c)
(Gm)	multipoint constraint matrix (Eq. 3.1-4)
($\ulcorner I \lrcorner$)	identity matrix
$I_n\left(\frac{m\pi r}{2Z}\right)$	modified Bessel function (Eq. 5.1-7b)
(K), Kij	stiffness matrix, stiffness matrix component
K_T	material thermal conductivity (Eq. C-4)
(L), Lij	inertance matrix, inertance matrix component (Eq. 2.1-10c)
L_C	complementary Lagrangian function (Eq. 2.1-6b)
(M)	mass matrix
M_θ, M_z	cylindrical shell bending moment resultants (Eq. 4.1-6)
N_θ, N_z	cylindrical shell membrane stress resultants (Eq. 4.1-6)
P	pressure
P′	pressure deviation (Eq. 2.3-15)
$P_m^n(\cos\theta)$	associated Legendre function (Eq. 4.1-2)

List of Symbols (Cont)

P_O	static pressurization level (Eq. 4.1-10)
$P_O(r_i, z_i)$, $P_K(r_i, z_i)$, $P_K^*(r_i, z_i)$	harmonic distribution pressure components (Eq. 3.1-1)
$\hat{Q}$	generalized impulsive force (Eq. A-14)
R	hemisphere radial dimension (Fig. 4-1), cylindrical shell radial dimension (Fig. 4-4)
S	surface area (Eq. 2.1-5)
T	kinetic energy function (Eq. 2.1-4a)
T_C	complementary kinetic energy function (Eq. 2.1-4b)
U	potential energy function (Eq. 2.1-4b)
U_c	complementary potential energy function (Eq. 2.1-4b)
V	volume
W_c	complementary work function (Eq. 2.1-5)
Z	cylindrical shell axial dimension (Fig. 4-4)
f	surface heat flux per unit area (Eq. C-4)
h	shell thickness (Fig. 4-4)
ℓ_o	particle inertance (Eq. A-2)
m	meridional wave index (Eq. 4.1-2)
m_f	effective fluid mass (Eq. 4.1-9b)
m_o	particle mass (Eq. A-1)
m_s	effective structure mass (Eq. 4.1-9c)
n	circumferential wave index (Eq. 4.1-2)
$\hat{n}$	surface outward normal unit vector

List of Symbols (Cont)

q	generalized displacement variable (Eq. A-18b)
r	radial coordinate in cylindrical reference frame (Fig. 3-1a)
$\vec{r}$	position vector in a Newtonian reference frame (Eq. A-1)
t	time
u, $\vec{u}$	displacement, displacement vector
z	axial coordinate in cylindrical reference frame (Fig. 3.1)
T	temperature
(Γ)	matrix defined in Eq. 2.3-21b
Δ_1	fractional frequency error (Table 3.1)
Δ_2	fractional frequency squared error (Table 3.1)
Ω	nondimensional frequency; for hemisphere see Table 4-1; for cylinder see Fig. 4-7
α	stiffness constant for hemisphere (Eq. 4.1-1)
θ	circumferential coordinate in cylindrical reference frame (Fig. 3.1a); meridional angle in spherical reference frame (Fig. 3.1b)
γ	Poisson's ratio (Eq. 4.1-10)
ρ	radial coordinate in spherical reference frame (Fig. 3.1b)
ρ_f	fluid density
ρ_s	structural density
Φ	circumferential coordinate in spherical reference frame (Fig. 3.1b)
ω	circular frequency
$\omega_{E_{mn}}$	empty circular cylinder natural frequency (Eq. 4.1.9a)

List of Symbols (Cont)

$\omega^{P}_{E_{mn}}$	pressurized empty circular cylinder natural frequency (Eq. 4.1.10)
operators:	
$d(\ )$	total differential
$\nabla\cdot(\ )$	divergence
$\nabla(\ )$	gradient
$\partial(\ )$	partial derivative
$\delta(\ )$	variation
$(\hat{\ })$	total impulse, $\int_{-\infty}^{t} (\ )\, dt$
$(\ )$	time derivative, $\frac{d(\ )}{dt}$
Subscripts	
$(\ )_e$	externally applied
$(\ )_f$	"fluid" or "free surface" as specified in text
$(\ )_i$	"internal" unless used as an index
$(\ )_s$	"structure" or structural surface as specified in text

VOLUME I CONTENTS

VOLUME I ILLUSTRATIONS

VOLUME I TABLES

1 - INTRODUCTION

The increasing complexity of launch vehicle configurations, particularly in the case of the space shuttle, recently has stimulated considerable interest in the dynamic behavior of liquid filled tanks. The task of Pogo prediction and suppression, for example, requires very complete and accurate mathematical models for the calculation of propellant tank hydroelastic modes in the Pogo-susceptible frequency range (2 - 50 Hz for the space shuttle).

A variety of automatic fluid modeling techniques has been under development ranging from finite element and finite difference techniques to approximate analytical approaches taking advantage of the properties of the fluid velocity potential and the consequences of Green's theorem (Refs. 1-5). The available hydroelastic analysis methods although in most cases theoretically rigorous, contain serious deficiencies in computational economy and/or numerical accuracy. For example, the NASTRAN hydroelastic analysis technique as formulated in the level 15 series is deficient in computational economy primarily because of an unsymmetrical eigenvalue problem resulting from the use of mixed pressure and displacement generalized coordinates.

In the NASTRAN hydroelastic formulation, the fluid coefficient matrices are interpreted according to a structural analogy. The fluid pseudo-mass and pseudo-stiffness matrices of that formulation are recognized herein as flexibility and inverse mass matrices, respectively, on the basis of the complementary principle in mechanics known as Toupin's principle (Ref. 6). This revised interpretation is central to the formulation of the hydroelastic problem presented here.

This report consists of a theoretical development, a description of NASTRAN program modifications, a program with which some familiarity is assumed, and a series of illustrative hydroelastic problems demonstrating the accuracy and efficiency of the present formulation. The theoretical sections include a derivation of the NASTRAN fluid matrix equations on the basis of Toupin's principle, a symmetric formulation for compressible hydroelasticity and a symmetric kinematic formulation for incompressible hydroelasticity. The incompressible formulation, particularly applicable in the study of propellant tank dynamics, provides a description of fluid inertia in terms of bounding surface displacements alone. This description represents a drastic reduction in system variables. In addition, harmonic reduction is introduced as an efficient alternative to Guyan reduction for geometrically axisymmetric structures to further reduce the number of system variables. Detailed theoretical discussions in the appendices include a derivation of Toupin's principle and the proposed utilization of polyhedral heat conduction elements in NASTRAN as fluid elements (according to a heat conduction-incompressible flow analogy) to accommodate the analysis of asymmetric fluid geometries such as a tilted free surface.

Volume II (Ref. 7) consists of detailed information pertinent to the NASTRAN program. Included is a description of NASTRAN program modifications, based on the above theoretical developments, consisting of DMAP modifications required in the calculation of fluid matrix data and in the calculation normal modes for fluid-filled structures with and without the effects of static pressurization. Special input bulk data considerations are discussed as an aid to the NASTRAN user. Bulk data listings for the illustrative problems are presented in the appendices and serve as supplementary user information.

A series of illustrative hydroelastic problems are presented in the final sections of this report. They have been chosen to verify the reformulated NASTRAN hydroelastic analysis and to demonstrate its economy. Exact analytical and available test results were used as verification data for the NASTRAN analysis. The relatively complex 1/8-scale space shuttle external tank model is included with the illustrative examples in spite of a lack of totally satisfactory correlation with experimental data. Correlations with exact analytical results and experimental results for all other illustrative examples, however, are excellent and it is concluded that the formulation of this report is an accurate and efficient operational approach.

2 - THEORETICAL DEVELOPMENT

The class of problems considered in the NASTRAN hydroelastic analysis technique consists of the interaction of irrotational, inviscid, compressible fluids with flexible structures for which both fluid and structural motions are assumed small compared to overall dimensions. The approach used to describe the dynamics of the fluid is a finite element technique. "Mass" and "stiffness" matrices are formed on the basis of a constructed energy principle with pressure taking the role of generalized displacement and bounding surface displacement taking the role of the forcing function. The dynamics of the structure is described in the usual way with displacement taken as the dynamic variable and applied pressure taken as the forcing function. The assembled set of hydroelastic dynamic equations consists of coupled fluid pressure and structural displacement matrix relationships containing unsymmetric coupling terms as a result of the mixed set of variables. The unsymmetric form of the NASTRAN hydroelastic equations leads to considerable analytical and numerical difficulty.

2.1 DERIVATION OF THE NASTRAN FINITE ELEMENT FLUID REPRESENTATION

The NASTRAN fluid equations are derivable on the basis of a complementary variational principle introduced by Toupin in 1952, Ref. 6. The physical interpretation of the fluid matrix relationships on the basis of this principle provides the insight required to resolve the difficulties present in the NASTRAN formulation. (A detailed derivation and discussion of Toupin's principle and its consequences is presented in Appendix A).

The equation of motion of a fluid particle is

$$\ddot{\vec{U}} = -\frac{1}{\rho_f}\nabla P \tag{2.1-1}$$

The constitutive relationship for an inviscid, compressible fluid is

$$P = -B\,\nabla\cdot\vec{U} \tag{2.1-2}$$

where $\nabla.\vec{U}$ represents the dilitational strain. In order to obtain a fluid velocity expression, with ρ_f taken as a mean fluid density, the equation of motion Eq. 2.1-1 is integrated resulting in

$$\dot{\vec{U}} = -\frac{1}{\rho_f}\nabla\hat{P} \tag{2.1-3a}$$

where P is the pressure impulse

$$\hat{P} = \int_{-\infty}^{t} P \, dt \qquad (2.1\text{-}3b)$$

or

$$P = \dot{\hat{P}} \qquad (2.1\text{-}3c)$$

The usual expressions for kinetic and strain energy may now be expressed in terms of impulsive pressure as

$$T = T_c = \frac{1}{2}\int_V \rho_f(\dot{\vec{U}} \cdot \dot{\vec{U}})dV = \frac{1}{2}\int_V \frac{1}{\rho_f}(\nabla\hat{P} \cdot \nabla\hat{P})\,dV \qquad (2.1\text{-}4a)$$

$$U = U_c = \frac{1}{2}\int_V B(\nabla \cdot \vec{U})^2 dV = \frac{1}{2}\int_V \frac{1}{B}(\dot{\hat{P}})^2 dV \qquad (2.1\text{-}4b)$$

The motion dependent and impulse dependent energy expressions are generally not equivalent; they are equivalent, however, for linear systems. The complementary virtual work performed by boundary surface displacements, $\vec{U}^*$, is

$$\delta W_c = \int_S \delta\hat{P}(\dot{\vec{U}}^* \cdot \hat{\eta})\, dS \qquad (2.1\text{-}5)$$

The complementary form of Hamilton's principle due to Toupin is

$$\delta\int_{t_0}^{t_1} L_c \, dt + \int_{t_0}^{t_1} \delta W_c \, dt = 0 \qquad (2.1\text{-}6a)$$

with

$$L_c = T_c - U_c \qquad (2.1\text{-}6b)$$

The expression of the principle in the present application is

$$\delta\int_{t_0}^{t_1}\left\{\frac{1}{2}\int_V\left[\frac{1}{\rho_f}(\hat{\nabla}P \cdot \hat{\nabla}P) - \frac{1}{B}(\dot{\hat{P}})^2\right]dV\right\}dt + \delta\int_{t_0}^{t_1}\int_S(\dot{\vec{U}}^* \cdot \hat{n})\,\delta\hat{P}\,dS\,dt = 0 \qquad (2.1\text{-}7)$$

Upon utilization of Green's theorem, integration by parts, and rearrangement of terms the final expression (taking $\delta\hat{P} = 0$ @ $t = t_0$, t_1) is

$$\int_{t_0}^{t_1}\left[\int_V\left(\frac{1}{B}\ddot{\hat{P}} - \frac{1}{\rho_f}\nabla^2\hat{P}\right)\delta\hat{P}\,dV + \int_S\left(\frac{1}{\rho_f}\nabla\hat{P} \cdot \hat{\eta} + \dot{U}_n^*\right)\delta\hat{P}\,ds\right]dt = 0 \qquad (2.1\text{-}8)$$

and by setting the integrands to zero the well known field equation and natural boundary conditions for an inviscid, incompressible fluid result which are

$$\frac{1}{B}\ddot{\hat{P}} - \frac{1}{\rho_f}\nabla^2\hat{P} = 0 \text{ in V} \tag{2.1-9a}$$

$$\dot{U}^*_n = -\frac{1}{\rho_f}\nabla\hat{P}\cdot\hat{n} \text{ or } \hat{P} \text{ prescribed on S} \tag{2.1-9b}$$

The usefullness of the complementary principle lies in approximate analysis rather than in the derivation of field equations. Consider an approximation of a fluid pressure (impulse) state in terms of a finite set of variables. The fluid complementary kinetic and strain energies are the quadratic functions

$$T_c = \frac{1}{2}\sum_i \sum_j L_{ij}\hat{P}_i\hat{P}_j \tag{2.1-10a}$$

$$U_c = \frac{1}{2}\sum_i \sum_j C_{ij}\dot{\hat{P}}_i\dot{\hat{P}}_j \tag{2.1-10b}$$

with the symmetric inertance matrix defined as

$$L_{ij} = \frac{\partial^2 T_c}{\partial\hat{P}_i\,\partial\hat{P}_j} \tag{2.1-10c}$$

and the symmetric flexibility matrix defined as

$$C_{ij} = \frac{\partial^2 U_c}{\partial\dot{\hat{P}}_i\,\partial\dot{\hat{P}}_j} \tag{2.1-10d}$$

The elements of the inertance matrix are proportional to $\frac{1}{\rho}$, and the elements of the flexibility matrix are proportional to $\frac{1}{B}$. The complementary virtual work is expressed as

$$\delta W_c = \sum_i \left[\int_S \frac{\partial\hat{P}}{\partial\hat{P}_i}\,\dot{U}^*\cdot\hat{n}\right] dS\,\delta\hat{P}_i \tag{2.1-11a}$$

For the special case in which the surface displacements are physically discretized the complementary virtual work may be expressed as

$$\delta W_c = \sum_k \sum_i A_{ik}\,\dot{U}^*_k\,\delta\hat{P}_i \tag{2.1-11b}$$

with the generalized area matrix defined as

$$A_{ik} = \int_{S_j} \left(\frac{\partial \hat{P}}{\partial \hat{P}_i}\right)\left(\frac{\partial \vec{\dot{U}}}{\partial \dot{U}_k} \cdot \hat{n}\right) dS \qquad (2.1\text{-}11c)$$

Substitution of Eq. 2.1-10 and Eq. 2.1-11 into Eq. 2.1-6 with the appropriate integrations by parts results in the complementary Euler-Lagrange equations

$$\sum_j \left(L_{ij} \hat{P}_j + C_{ij} \ddot{\hat{P}}_j \right) = - \sum_k A_{ik} \dot{U}^*_k \qquad (2.1\text{-}12a)$$

By taking the time derivative of this expression noting Eq. 2.1-3C, the Euler-Lagrange equations become

$$\sum_j \left(L_{ij} P_j + C_{ij} \ddot{P}_j \right) = - \sum_k A_{ik} \ddot{U}^*_k \qquad (2.1\text{-}12b)$$

This is the form of the fluid dynamic finite element equations for individual elements and stacked systems of elements in NASTRAN. In the case of a stacked system of elements the matrix A_{ik} represents only bounding surface generalized areas and u^*_k represents discrete surface displacements. The pressures P_j comprise the set of boundary surface and internal pressures; therefore the matrix A_{ik} is rectangular. The physical interpretations of the matrix quantities, however differ from the interpretations in the NASTRAN theoretical manual. The C_{ij} matrix is a flexibility matrix and the L_{ij} matrix is an inverse mass matrix (see Appendix A). This point is realized without interpretation of Toupin's principle by examination of two special illustrative cases. Consider first static deformation ($T_c \rightarrow 0$) in which Eq. 2.1-12b takes the form

$$\sum_j C_{ij} \ddot{P}_j = - \sum_k A_{ik} \ddot{U}^*_k \qquad (2.1\text{-}13a)$$

which twice integrated is

$$\sum_j C_{ij} P_j = - \sum_k A_{ik} U^*_k \qquad (2.1\text{-}13b)$$

The matrix C_{ij} is recognized as a flexibility matrix in terms of pressure. Further clarification is realized by noting that

$$F_\ell = \Sigma A_{\ell j} P_j = -\sum_j \sum_i \sum_k A_{\ell j} C_{ij}^{-1} A_{ik} U_k = -\sum_k K_{\ell k} U_k^* \tag{2.1-14}$$

where $K_{\ell k}$ is a stiffness matrix relating surface F_ℓ forces and displacements U_k. The second special case consists of an incompressible fluid ($C_{ij} \rightarrow 0$) in which Eq. 2.1-12b takes the form

$$\sum_j L_{ij} P_j = -\sum_k A_{ik} \ddot{U}_k \tag{2.1-15}$$

The inertance matrix, L_{ij} must contain one singularity. This singularity, which will be discussed fully in Section 2.3, is due to the fact that an incompressible fluid under uniform pressure does not deform. It is however apparent in Eq. 2.1-15 that the inertance matrix, as in the case of the flexibility matrix C_{ij}, is an inverse "mass-type" matrix.

2.2 A SYMMETRIC FORMULATION FOR COMPRESSIBLE HYDROELASTICITY

The formulation presented in the NASTRAN theoretical manual utilizes the complementary Euler-Lagrange equations for a fluid

$$(L_f)\left\{P\right\} + (C_f)\left\{\ddot{P}\right\} = -(A^T)\left\{\ddot{U}\right\} \tag{2.2-1a}$$

and a standard set of structural dynamic equations

$$(M_S)\left\{\ddot{U}\right\} + (K_S)\left\{U\right\} = (A)\left\{P\right\} \tag{2.2-1b}$$

The above are combined to form the unsymmetric set of hydroelastic equations

$$\left(\begin{array}{c|c} C_f & A^T \\ \hline 0 & M_S \end{array}\right)\left\{\begin{array}{c} \ddot{P} \\ \hline \ddot{U} \end{array}\right\} + \left(\begin{array}{c|c} L_f & \\ \hline -A & K_S \end{array}\right)\left\{\begin{array}{c} P \\ \hline U \end{array}\right\} = \left\{\begin{array}{c} 0 \\ \hline 0 \end{array}\right\} \tag{2.2-2}$$

Considerable numerical and analytical difficulty has been encountered by NASTRAN users due to the unsymmetric form of these equations.

An alternate symmetric formulation is derivable by the complementary principle or by manipulation of the structural dynamic equations. Taking the latter approach, the internal structural generalized forces, F_s, are related to the structural displacements, U, according to

$$(K_S)\left\{U\right\} = \left\{F_s\right\} \tag{2.2-3a}$$

Suppose that K_s represents a supported stiffness matrix; the transformation to internal forces is therefore defined as

$$\left\{U\right\} = (K_s^{-1})\left\{F_s\right\} \tag{2.2-3b}$$

Substitution of the above into Eq. 2.2-1b results in

$$(M_s)(K_s^{-1})\left\{\ddot{F}_s\right\} + \left\{F_s\right\} = (A)\left\{P\right\} \tag{2.2-4}$$

and premultiplication by the inverse of the structural mass matrix yields

$$(C_s)\left\{\ddot{F}_s\right\} + (L_s)\left\{F_s\right\} - (L_s)(A)\left\{P\right\} = \left\{0\right\} \tag{2.2-5a}$$

with

$$(C_s) = (K_s^{-1}) \tag{2.2-5b}$$

representing the structural flexibility matrix and

$$(L_s) = (M_s^{-1}) \tag{2.2-5c}$$

representing the structural inertance matrix. Utilizing Eq. 2.2-3b and Eq. 2.2-5a the expression for acceleration to be substituted into the fluid Eq. 2.2-1a is

$$\left\{\ddot{U}\right\} = (C_s)\left\{\ddot{F}_s\right\} = (L_s)(A)\left\{P\right\} - (L_s)\left\{F_s\right\} \tag{2.2-6}$$

and the fluid dynamic equation is rewritten as

$$(L_f)\left\{P\right\} + (C_f)\left\{\ddot{P}\right\} = -(A^T L_s A)\left\{P\right\} + (A^T)(L_s)\left\{F_s\right\} \tag{2.2-7}$$

The set of hydroelastic equations in terms of force type variables consisting of Eq. 2.2-5a and Eq. 2.2-7 now takes the symmetric form

$$\left(\begin{array}{c|c} C_f & \\ \hline & C_s \end{array}\right)\left\{\begin{array}{c} \ddot{P} \\ \hline \ddot{F}_s \end{array}\right\} + \left(\begin{array}{c|c} L_f + A^T L_s A & -A^T L_s \\ \hline -L_s A & L_s \end{array}\right)\left\{\begin{array}{c} P \\ \hline F_s \end{array}\right\} = \left\{\begin{array}{c} 0 \\ \hline 0 \end{array}\right\} \tag{2.2-8}$$

The formulation presented here provides a basis for modification of the NASTRAN formulation for inviscid, compressible fluid hydroelastic problems. The class of problems of interest in the current work, however, is limited to inviscid, incompressible fluids interacting with flexible structures and an alternate simplified kinematic formulation is derivable for this case.

2.3 A SYMMETRIC KINEMATIC FORMULATION FOR INCOMPRESSIBLE HYDRO-ELASTICITY

The complementary Euler-Lagrange matrix equation set for the special case of an incompressible fluid ($B \rightarrow 0$, $(C_f) \rightarrow 0$) in a conveniently partitioned form is

$$\left(\begin{array}{c|c|c} L_{ff} & L_{fs} & L_{fi} \\ \hline L_{sf} & L_{ss} & L_{si} \\ \hline L_{if} & L_{is} & L_{ii} \end{array}\right)\left\{\begin{array}{c} P_f \\ \hline P_s \\ \hline P_i \end{array}\right\} = -\left(\begin{array}{c|c} A^T_{ff} & A^T_{sf} \\ \hline A^T_{fs} & A^T_{ss} \\ \hline 0 & 0 \end{array}\right)\left\{\begin{array}{c} \ddot{U}_f \\ \hline \ddot{U}_s \end{array}\right\} \tag{2.3-1}$$

The pressure partitions P_f, P_s and P_i correspond to free surface, structural interface surface and internal fluid pressure sets, respectively, and the displacement partitions U_f and U_s correspond to the free surface and structural interface surface displacement sets, respectively. The structural dynamic equation set with applied fluid pressure loading is in partitioned form

$$\left(\begin{array}{c|c} 0 & 0 \\ \hline 0 & M_s \end{array}\right)\left\{\begin{array}{c} \ddot{U}_f \\ \hline \ddot{U}_s \end{array}\right\} + \left(\begin{array}{c|c} K_{ff} & K_{fs} \\ \hline K_{sf} & K_{ss} \end{array}\right)\left\{\begin{array}{c} U_f \\ \hline U_s \end{array}\right\} = \left(\begin{array}{c|c|c} A_{ff} & A_{fs} & 0 \\ \hline A_{sf} & A_{ss} & 0 \end{array}\right)\left\{\begin{array}{c} P_f \\ \hline P_s \\ \hline P_i \end{array}\right\} \tag{2.3-2}$$

where M_s is the structural mass matrix, K_{ss} is the structural stiffness matrix and K_{ff}, K_{fs}, K_{sf}, are additional stiffness matrix contributions resulting from the gravitational potential and possibly ullage pressure fluctuation.

It is obvious from Eq. 2.3-1 that the internal pressures are related to the surface pressures as

$$\left\{P_i\right\} = -(L_{ii})^{-1}(L_{if} \mid L_{is}) \begin{Bmatrix} P_f \\ \hline P_s \end{Bmatrix} . \tag{2.3-3}$$

and the reduced fluid dynamic equation set in terms of surface quantities only is

$$\begin{pmatrix} L'_{ff} & L'_{fs} \\ L'_{sf} & L'_{ss} \end{pmatrix} \begin{Bmatrix} P_f \\ P_s \end{Bmatrix} = - \begin{pmatrix} A^T_{ff} & A^T_{sf} \\ A^T_{fs} & A^T_{ss} \end{pmatrix} \begin{Bmatrix} \ddot{U}_f \\ \ddot{U}_s \end{Bmatrix} \tag{2.3-4a}$$

with

$$\begin{pmatrix} L'_{ff} & L'_{fs} \\ L'_{sf} & L'_{ss} \end{pmatrix} = \begin{pmatrix} L_{ff} & L_{fs} \\ L_{sf} & L_{ss} \end{pmatrix} - \begin{pmatrix} L_{fi} \\ L_{si} \end{pmatrix} (L_{ii})^{-1} (L_{if} \, L_{is}) \tag{2.3-4b}$$

The reduced inertance matrix is singular since an incompressible fluid under uniform pressure does not deform. This singularity must occur ideally in the individual finite element inertance matrices as it is a necessary condition for compatibility. This is analogous to the condition imposed on structural finite elements that requires no internal stresses under rigid body motion (i.e. singular element stiffness matrices). There are two approaches to eliminating the uniform pressure singularity; the first is a general approach and the second is a special case in which part of the fluid surface is at zero pressure.

In the special case of zero free surface pressure (gravitational and ullage stiffness negligible) the fluid surface dynamic equation set Eq. 2.3-4a is under the single point constraints

$$\left\{P_f\right\} = \left\{0\right\} \tag{2.3-5}$$

and the singular pressure state, uniform pressure is removed from the total surface pressure set. The partitions of Eq. 2.3-4a now reduce to

$$(L'_{fs})\left\{P_s\right\} = -(A^T_{ff})\left\{\ddot{U}_f\right\} - (A^T_{sf})\left\{\ddot{U}_s\right\} \tag{2.3-6a}$$

$$(L'_{ss})\left\{P_s\right\} = -(A^T_{fs})\left\{\ddot{U}_f\right\} - (A^T_{ss})\left\{\ddot{U}_s\right\} \tag{2.3-6b}$$

If the free surface displacements are normal to the free surface then the generalized area coupling partitions are null $((A^T_{sf}) = (0), (A^T_{fs}) = (0))$. The matrix partition, (L'_{ss}), is not singular due the constraint Eq. 2.3-5 and may now be inverted in Eq. 2.3-6b to form the structural interface pressure recovery equation set

$$\left\{P_s\right\} = -(L'_{ss})^{-1}(A^T_{ss})\left\{\ddot{U}_s\right\} \tag{2.3-7}$$

Substitution of this relationship into Eq. 2.3-6a yields

$$(L'_{fs})(L'_{ss})^{-1}(A^T_{ss})\left\{\ddot{U}_s\right\} = (A^T_{ff})\left\{\ddot{U}_f\right\} \tag{2.3-8a}$$

and since $\left\{U_f\right\}$ consists of outward normal displacements only the free surface area matrix is non-singular; thus the free surface acceleration (or displacement) recovery relationship is

$$\left\{U_f\right\} = (A_{ff})^{-T}(L'_{fs})(L'_{ss})^{-1}(A^T_{ss})\left\{U_s\right\} \tag{2.3-8b}$$

The structural dynamic equation set Eq. 2.3-2 under the constraints Eq. 2.3-5 is

$$(M_{ss})\left\{\ddot{U}_s\right\} + (K_{ss})\left\{U_s\right\} = (A_{ss})\left\{P_s\right\} \tag{2.3-9}$$

Substitution of the pressure recovery relationship Eq. 2.3-7 into the above set results in

$$(M_s + M_f)\left\{\ddot{U}_s\right\} + (K_{ss})\left\{U_s\right\} = \left\{0\right\} \tag{2.3-10a}$$

with the symmetric fluid mass matrix formed as

$$(M_f) = (A_{ss})(L'_{ss})^{-1}(A^T_{ss}) \tag{2.3-10b}$$

Thus in the special case of an incompressible, inviscid fluid with zero pressure fluctuation on a free surface, the hydroelastic dynamics problem reduces to a standard problem in structural dynamics.

Consider now the general case of incompressible fluid/structure interaction in which the entire bounding surface of the fluid interacts with flexible structure and a gravitational potential or ullage volume. As in the above special case, all internal pressures are dependent on surface pressures Eq. 2.3-3 and the resultant reduced fluid inertance matrix is singular. In the case of a fluid represented by discrete surface pressures the normalized uniform pressure state is

$$\left\{\begin{array}{c} P_f \\ \hline P_s \end{array}\right\} = \left\{\begin{array}{c} 1 \\ 1 \\ \vdots \\ 1 \end{array}\right\} \tag{2.3-11}$$

Under such loading the surface normal accelerations must be null and the necessary property of the reduced inertance matrix is

$$\sum_j L'_{ij} = 0 \tag{2.3-12}$$

for all i. The fluid representations in NASTRAN are currently limited to axisymmetric geometries in which fluid pressures are described in terms of circumferential harmonics, e.g.,

$$P(r_i, \theta_i, z_i) = \sum_{K=0,1,..}^{N} P_K(r_i, z_i)\cos K\theta_i + \sum_{K=1,2,..}^{N} P_K^*(r_i, z_i)\sin K\theta_i \qquad (2.3\text{-}13)$$

The fluid finite elements are rectangular and triangular solids of revolution and the generalized pressure degrees of freedom are the amplitudes P_K and P_K^*. In this case the zeroth harmonic (n = O) generalized pressure subset contains the uniform pressure state and the higher harmonic (n > O) subsets by definition do not contain the uniform pressure state. Thus the discrete pressure considerations described by Eq. 2.3-11 and Eq. 2.3-12 hold for the zeroth harmonic. The singularity in the reduced inertance matrix is removable by artificially setting one pressure to zero (in the case of generalized harmonic pressures this pressure must be in the zeroth harmonic subset). For convenience let the pressure partitions $\{P_f\}$ and $\{P_s\}$ represent the single artificially nulled pressure and the remaining pressures, respectively; in addition let $\{P_f\}$ represent a pressure associated with the fluid free surface. The artificially constrained pressure set is denoted as

$$\begin{Bmatrix} P_f \\ P_s \end{Bmatrix} = \begin{Bmatrix} 0 \\ P_s' \end{Bmatrix} \qquad (2.3\text{-}14)$$

in which the primed set represents pressure deviations from a uniform pressure state of value, P_f, i.e.,

$$P_{s_i} = P_{s_i} - P_f \qquad (2.3\text{-}15)$$

Assuming that the area coupling partitions are null $((A_{sf}^T) = 0,\ (A_{fs})^T = (0))$ the pressure deviations are related to the surface displacements as

$$(L_{fs}')\{P_s'\} = -(A_{ff}^T)\{\ddot{U}_f\} \qquad (2.3\text{-}16a)$$

$$(L_{ss}')\{P_s'\} = -(A_{ss}^T)\{\ddot{U}_s\} \qquad (2.3\text{-}16b)$$

Solution for the pressure deviations in Eq. 2.3-16b and substitution of the result into Eq. 2.3-16a yields the pressure deviation recovery relationship

$$\left\{P'_s\right\} = -\,(L'_{ss})^{-1}(A^T_{ss})\left\{\ddot{U}_s\right\} \tag{2.3-17a}$$

and the displacement recovery relationship

$$\left\{\begin{array}{c} U_f \\ \hline U_s \end{array}\right\} = \left(\begin{array}{c} A^{-T}_{ff} L'_{fs} L'^{-1}_{ss} A^T_{ss} \\ \hline I \end{array}\right) \left\{ U_s \right\} \tag{2.3-17b}$$

The above result is equivalent to imposing a kinematic constraint on outward normal surface flow (incompressibility)

$$\left\{\begin{array}{c} 0 \\ \hline A^T_{ss} U_s \end{array}\right\} = \left(\begin{array}{c|c} I & -L'_{fs} L'^{-1}_{ss} \\ \hline 0 & I \end{array}\right) \left\{\begin{array}{c} A^T_{ff} U_f \\ A^T_{ss} U_s \end{array}\right\} \tag{2.3-18}$$

The companion pressure constraint expression is

$$\left\{\begin{array}{c} P_f \\ \hline P_s \end{array}\right\} = \left(\begin{array}{c|c} I & 0 \\ \hline -L'^{-1}_{ss} L'_{sf} & I \end{array}\right) \left\{\begin{array}{c} P_f \\ P'_s \end{array}\right\} \tag{2.3-19}$$

Substitution of Eq. 2.3-18 and Eq. 2.3-19 into Eq. 2.3-4a yields the result already obtained in Eq. 2.3-16b

$$\left(\begin{array}{c|c} 0 & 0 \\ \hline 0 & L'_{ss} \end{array}\right) \left\{\begin{array}{c} P_f \\ P'_s \end{array}\right\} = -\left\{\begin{array}{c} 0 \\ \hline A^T_{ss} \ddot{U}_s \end{array}\right\} \tag{2.3-20a}$$

where the singularity condition is expressed as

$$(L'_{ff}) - (L'_{fs})(L'_{ss})^{-1}(L'_{sf}) = (0) \tag{2.3-20b}$$

The constraints presented in Eq. 2.3-18 and Eq. 2.3-19 are now applied to the structural dynamic equation set Eq. 2.3-2 as

$$(\Gamma^T \mid I)\left(\begin{array}{c|c} 0 & 0 \\ \hline 0 & M_s \end{array}\right)\left(\begin{array}{c} \Gamma \\ \hline I \end{array}\right)\left\{\ddot{U}_s\right\} + (\Gamma^T \mid I)\left(\begin{array}{c|c} K_{ff} & K_{fs} \\ \hline K_{sf} & K_{ss} \end{array}\right)\left(\begin{array}{c} \Gamma \\ \hline I \end{array}\right)\left\{U_s\right\}$$

$$= (\Gamma^T \mid I)\left(\begin{array}{c|c} A_{ff} & 0 \\ \hline 0 & A_{ss} \end{array}\right)\left(\begin{array}{c|c} 1 & 0 \\ \hline G^T & I \end{array}\right)\left\{\begin{array}{c} P_f' \\ P_s \end{array}\right\} \tag{2.3-21a}$$

where

$$(\Gamma) = (A_{ff}^{-T})(L_{fs}')(L_{ss}')^{-1}(A_{ss}^{T}) \tag{2.3-21b}$$

$$(G) = -(L_{fs}')(L_{ss}')^{-1} \tag{2.3-21c}$$

The coefficient matrix on the right side of Eq. 2.3-21a reduces to

$$(\Gamma^T A_{ff} + A_{ss} G^T \mid A_{ss}) = (0 \mid A_{ss}) \tag{2.3-22}$$

Substitution of the pressure deviation recovery relationship Eq. 2.3-17a into Eq. 2.3-21a noting Eq. 2.3-22 results in the symmetric kinematic equation set

$$(M_s + M_f)\left\{\ddot{U}_s\right\} + (K_s^*)\left\{U_s\right\} = \left\{0\right\} \tag{2.3-23a}$$

where the fluid mass matrix is as in the special case, Eq. 2.3-10b

$$(M_f) = A_{ss} L_{ss}'^{-1} A_{ss}^T \tag{2.3-23b}$$

and the hydroelastic stiffness matrix is

$$(K_s^*) = \Gamma^T K_{ff} \Gamma + \Gamma^T K_{fs} + K_{sf} \Gamma + K_{ss} \tag{2.3-23c}$$

Complete displacement recovery is obtained through Eq. 2.3-17b and pressure deviation recovery is obtained through Eq. 2.3-17a. Complete pressure recovery is achieved by combining the upper partition equation set in Eq. 2.3-2 with Eq. 2.3-17 and Eq. 2.3-19; thus the pressure recovery equation set is

$$\left\{P_f\right\} = (A_{ff}^{-1} K_{ff}\, \Gamma + K_{fs}) \left\{U_s\right\} \tag{2.3-24a}$$

$$\left\{\begin{array}{c} P_f \\ \hline P_s \end{array}\right\} = \left(\begin{array}{c|c} I & 0 \\ \hline G^T & I \end{array}\right) \left\{\begin{array}{c} P_f \\ \hline P_s' \end{array}\right\} \tag{2.3-24b}$$

The general symmetric kinematic formulation developed above is useful in hydroelastic analyses for which free surface strain energy and structural strain energy are equally significant. In most practical analyses involving liquid filled tanks the free surface strain energy is much smaller than the structural strain energy. Thus low frequency slosh dynamics is usually approximated with rigid structure, and flexible structure/fluid interaction is usually approximated with zero free surface pressure (the special case first developed in this section).

3 - HARMONIC REDUCTION OF GEOMETRICALLY AXISYMMETRIC STRUCTURES

The NASTRAN hydroelastic analysis provides for a description of dynamics of axisymmetrically configured fluids in terms of circumferential harmonic pressure distributions. The distribution of pressure is

$$P(r_i, \theta_i, z_i) = P_o(r_i, z_i) + \sum_{k=1}^{N} \left\{ P_K(r_i, z_i) \cos k\theta_i + P_K^*(r_i, z_i) \sin k\theta_i \right\} \tag{3.1-1}$$

The fluid containing structure is described in terms of discrete physical displacements so that the structural representation is not limited to structurally axisymmetric containers. Coupling of harmonic pressure distributions with discrete structural displacements in the NASTRAN formulation is not strictly consistent; moreover, in many cases it is inefficient. When a structure described in terms of discrete displacements is coupled with a fluid described in terms of circumferential harmonics, inconsistencies may arise if too few pressure harmonics are utilized; structural deformation shapes associated with higher harmonics not included in the fluid representation will reflect a lack of fluid inertia loading. Alternatively, when the discrete structural grid is too coarse to accurately describe the highest harmonic pressure distributions, large errors in the mode shapes associated with higher harmonics will be present.

A consistent grid representation is realized by imposing a kinematic set of constraints on the structure restricting it to deform in circumferential harmonic patterns. For cylindrical coordinates (Fig. 3-1a) the relationships between a discrete displacement and the harmonic displacement amplitudes are:

$$U_1(r_i, \theta_i, z_i) = \sum_{k=0}^{N} \left[U_{1_k}(r_i, z_i) \cos k\theta_i + U_{1_k}^*(r_i, z_i) \sin k\theta_i \right] \tag{3.1-2a}$$

(A) CYLINDRICAL

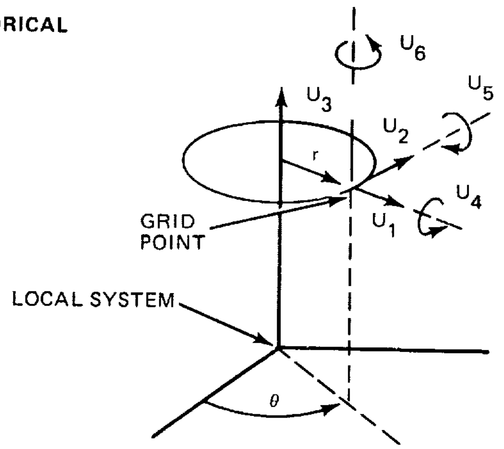

(B) SPHERICAL

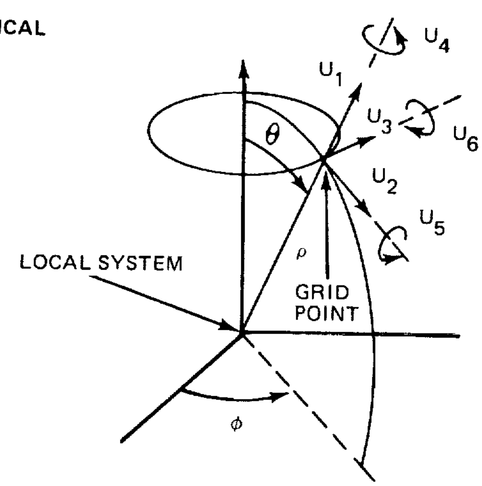

Fig. 3-1 Cylindrical and Spherical Reference Frames

$$U_2(r_i, \theta_i, z_i) = \sum_{k=0}^{N} \left[U_{2_k}(r_i, z_i) \sin k\theta_i + U^*_{2_k}(r_i, z_i) \cos k\theta_i \right] \tag{3.1-2b}$$

$$U_3(r_i, \theta_i, z_i) = \sum_{k=0}^{N} \left[U_{3_k}(r_i, z_i) \cos k\theta_i + U^*_{3_k}(r_i, z_i) \sin k\theta_i \right] \tag{3.1-2c}$$

$$U_4(r_i, \theta_i, z_i) = \sum_{k=0}^{N} \left[U_{4_k}(r_i, z_i) \sin k\theta_i + U^*_{4_k}(r_i, z_i) \cos k\theta_i \right] \tag{3.1-2d}$$

$$U_5(r_i, \theta_i, z_i) = \sum_{k=0}^{N} \left[U_{5_k}(r_i, z_i) \cos k\theta_i + U^*_{5_k}(r_i, z_i) \sin k\theta_i \right] \tag{3.1-2e}$$

$$U_6(r_i, \theta_i, z_i) = \sum_{k=0}^{N} \left[U_{6_k}(r_i, z_i) \sin k\theta_i + U^*_{6_k}(r_i, z_i) \cos k\theta_i \right] \tag{3.1-2f}$$

For spherical coordinates (Fig. 3-1b) the relationships are:

$$U_{1_k}(\rho_i, \theta_i, \phi_i) = \sum_{k=0}^{N} \left[U_{1_k}(\rho_i, \theta_i) \cos k\phi_i + U^*_{1_k}(\rho_i, \theta_i) \sin k\phi_i \right] \tag{(3.1-3a)}$$

$$U_{2_k}(\rho_i, \theta_i, \phi_i) = \sum_{k=0}^{N} \left[U_{2_k}(\rho_i, \theta_i) \cos k\phi_i + U^*_{2_k}(\rho_i, \theta_i) \sin k\phi_i \right] \tag{3.1-3b}$$

$$U_{3_k}(\rho_i, \theta_i, \phi_i) = \sum_{k=0}^{N} \left[U_{3_k}(\rho_i, \theta_i) \sin k\phi_i + U^*_{3_k}(\rho_i, \theta_i) \cos k\phi_i \right] \tag{3.1-3c}$$

$$U_{4_k}(\rho_i, \theta_i, \phi_i) = \sum_{k=0}^{N} \left[U_{4_k}(\rho_i, \theta_i) \sin k\phi_i + U^*_{4_k}(\rho_i, \theta_i) \cos k\phi_i \right] \tag{3.1-3d}$$

$$U_{5_k}(\rho_i, \theta_i, \phi_i) = \sum_{k=0}^{N} \left[U_{5_k}(\rho_i, \theta_i)\sin k\phi_i + U_{5_k}^*(\rho_i, \theta_i)\cos k\phi_i \right] \tag{3.1-3e}$$

$$U_{6_k}(\rho_i, \theta_i, \phi_i) = \sum_{k=0}^{N} \left[U_{6_k}(\rho_i, \theta_i)\cos k\phi_i + U_{6_k}^*(\rho_i, \theta_i)\sin k\phi_i \right] \tag{3.1-3f}$$

Symmetric and antisymmetric displacement distributions are represented by unstarred and starred variables, respectively. It should be noted that all rigid body motions are represented by the above displacement distributions.

Harmonic transformation of a discrete structural grid is accomplished in NASTRAN by the use of multipoint constraint (MPC) statements. The harmonic degrees of freedom must be accounted for by supplementary grid points (in addition to the physical discrete grid). The general form of the harmonic transformation is

$$\left\{U_m\right\} = (G_m)\left\{U_n\right\} \tag{3.1-4}$$

where U_m corresponds to the physical grid degrees of freedom to be transformed, and U_n corresponds to the harmonic degrees of freedom (plus any discrete degrees of freedom not transformed). The transformation or constraint matrix Gm is composed of the appropriate sinusoidal functions evaluated at the discrete variable locations in accordance with the relationships outlined in Eq. 3.1-2 and Eq. 3.1-3. For a typical structure with JxK grid points such that there are J meridional rows and K circumferential points in a row, the grid "g" set has typically 6xJxK degrees of freedom and the matrix semibandwidths are 6xK (assuming $K<J$). Application of the harmonic transformation as a reduction scheme where the number of harmonics, N, is much less than K results in a U_N set of 6xJxN generalized coordinates with matrix semibandwidths of 6xN. If $N \ll K$ harmonic reduction represents a radical reduction in the number of degrees of freedom as well as matrix bandwidth. Further reduction of the system description is possible by a small Guyan reduction by choosing the generalized rotation degrees of freedom and tangential displacements as members of the omitted set of displacements. In such a case the analysis set consists of JxN degrees of freedom. This represents a radical reduction in degrees of freedom by a factor of (N/6K) without a costly large matrix decomposition typical of Guyan reduction.

The economy and accuracy of harmonic reduction was first tested on the spherical cap with uniform thickness illustrated in Fig. 3-2. A nodal grid consisting of 20 circumferential divisions in a semicircle and 10 meridional divisions was chosen resulting in a 1266 DOF "g-set" structural model. Three circumferential harmonics (0, 1, 2) were chosen for harmonic reduction. It should be noted that the apex node is left in terms of rectangular coordinates since the polar degrees of freedom have no meaning at this node. After application of the fixed-base boundary condition and symmetric kinematic constraints at the pole the reduced representation consists of a 138 DOF "f-set". A small Guyan reduction omitting the non-zero displacements at the pole and rotational and circumferential generalized displacements yields a 72 DOF "a-set". At this point, all natural frequencies and the first 15 modes were calculated by the Givens method.

The results of the above strategy were then compared to STARS-II (Ref. 8) results which were assumed exact. In addition, NASTRAN results utilizing various Guyan reduction strategies illustrated in Figs. 3-3 and 3-4 were compared to the STARS-II and harmonic reduction results.

A comparison of natural frequency results (Table 3-1) indicates that the overall accuracy of the 72 DOF harmonic reduction representation is better than the 190 DOF Guyan reduction representation. The quantities Δ_1 are representative of fractional frequency errors and Δ_2, the frequency squared errors, are representative of mode shape errors. Comparisons of the first two axisymmetric mode shapes illustrated in Fig. 3-5 indicate that although frequencies are rather accurate, mode shapes may contain large local errors. Mode shapes resulting from harmonic reduction are clearly more accurate than those resulting from Guyan reduction.

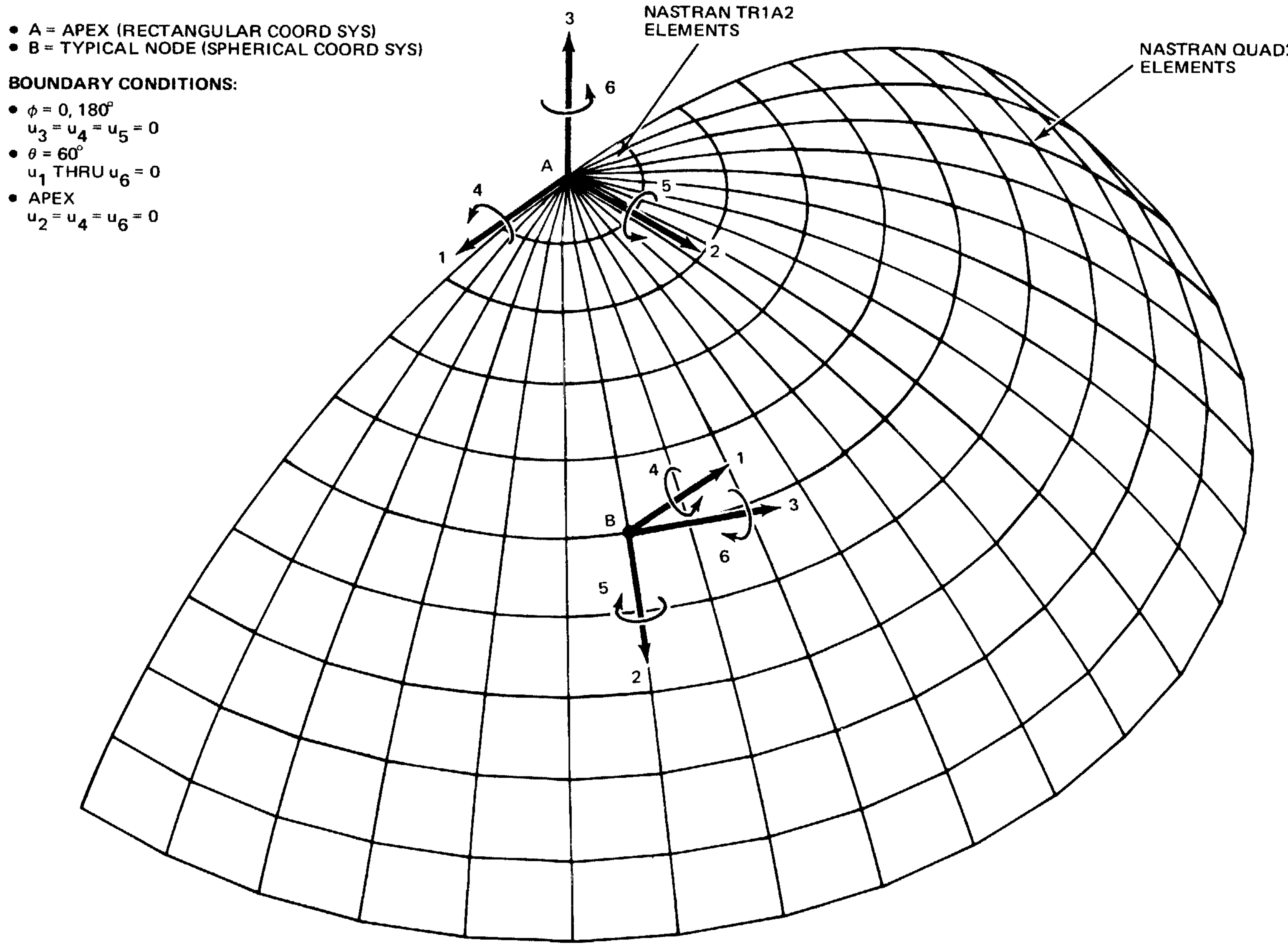

Fig. 3-2 60° Spherical Cap Model, (h/R) = 0.05

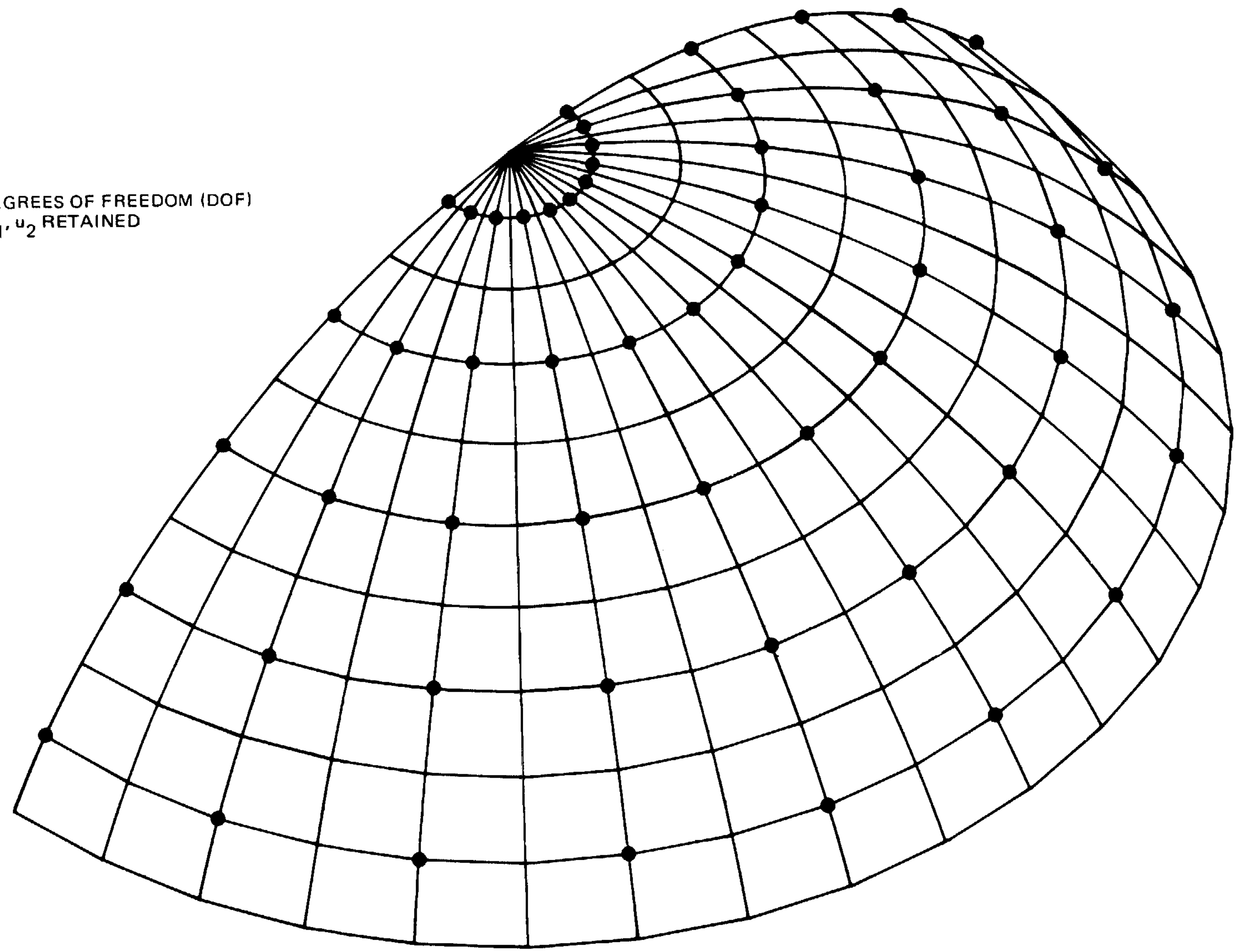

• DEGREES OF FREEDOM (DOF) u_1, u_2 RETAINED

Fig. 3-3 Analysis Set Nodes for Guyan Reduction G–110

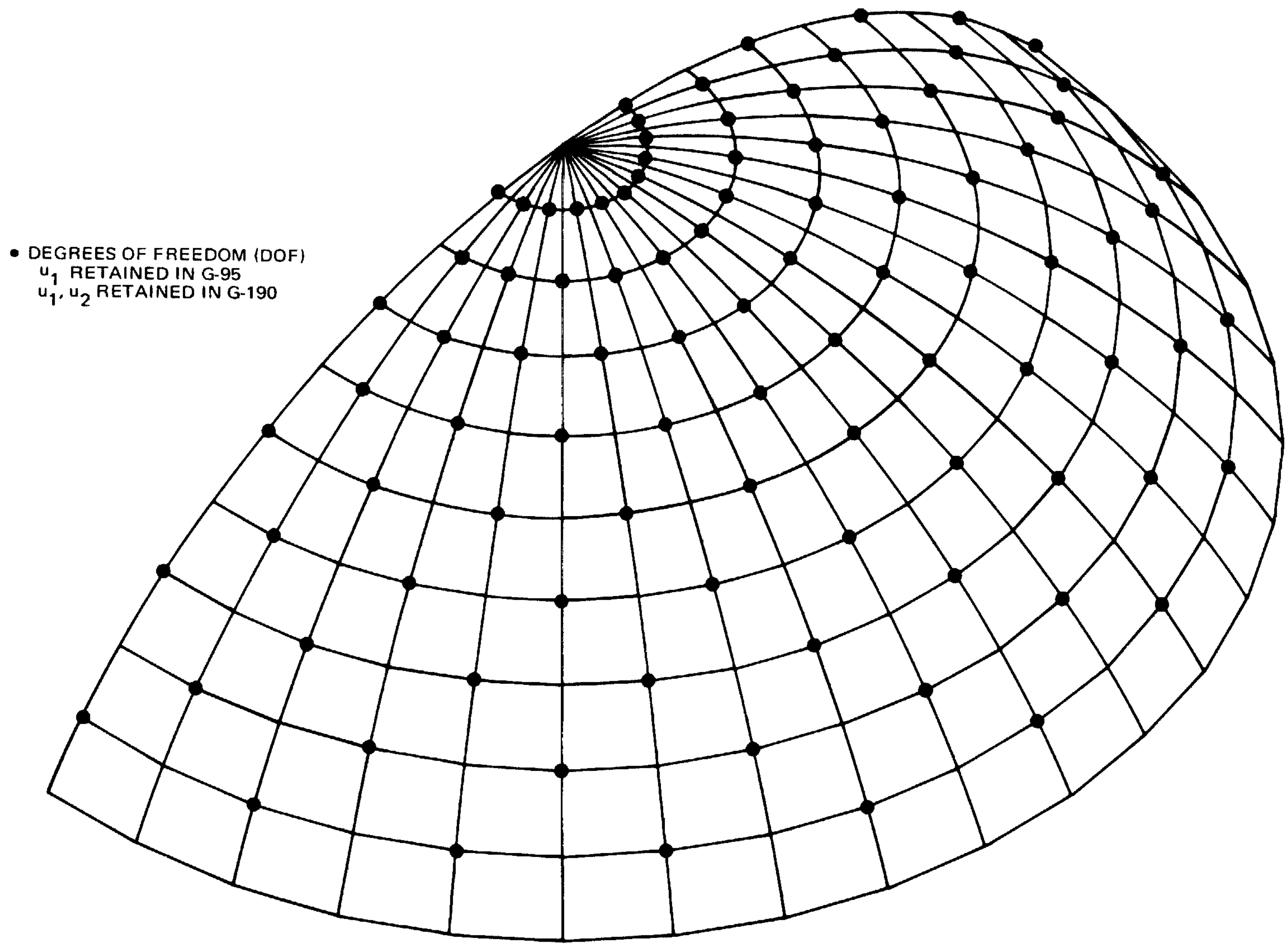

Fig. 3-4 Analysis Set Nodes for Guyan Reduction G – 95 and G – 190

Table 3-1 60° Spherical Cap – Comparison of Modal Frequencies

$\Delta_1 = \omega/\omega_s - 1, \ \Delta_2 = (\omega/\omega_s)^2 - 1$

Mode		STARS	Harm. Red. H-72			Guyan Red. G-110			GUYAN Red. G-95			GUYAN Red. G-190		
M	N	Ω_s	Ω	Δ_1	Δ_2	Ω	Δ_1	Δ_2	Ω	Δ_1	Δ_2	Ω	Δ_1	Δ_2
1	0	637	647	0.015	0.030	682	0.071	0.146	664	0.042	0.085	656	0.029	0.060
2		697	700	0.004	0.008	734	0.053	0.109	717	0.030	0.060	711	0.020	0.041
3		720	732	0.016	0.033	815	0.132	0.281	767	0.065	0.135	757	0.051	0.105
4		760	778	0.023	0.047	–	–	–	–	–	–	–	–	–
5		820	843	0.028	0.057	–	–	–	–	–	–	–	–	–
1	1	611	616	0.008	0.016	679	0.111	0.235	670	0.096	0.200	640	0.047	0.096
2		687	696	0.012	0.024	768	0.118	0.250	725	0.054	0.111	713	0.037	0.075
3		715	726	0.015	0.030	807	0.129	0.274	759	0.062	0.127	747	0.045	0.092
4		738	760	0.029	0.060	827	0.121	0.256	769	0.041	0.085	793	0.074	0.153
5		810	810	–	–	–	–	–	805	–.006	–.012	–	–	–
1	2	684	700	0.023	0.047	800	0.170	0.368	732	0.070	0.146	730	0.067	0.138
2		711	731	0.029	0.060	825	0.160	0.346	813	0.144	0.308	764	0.075	0.156
3		742	762	0.027	0.055	869	0.171	0.372	–	–	–	804	0.084	0.175
4		765	801	0.060	0.123	–	–	–	–	–	–	–	–	–
5		831	861	0.036	0.074	–	–	–	–	–	–	–	–	–
1	3	694	–	–	–	841	0.212	0.468	757	0.091	0.191	755	0.088	0.184
2		714	–	–	–	846	0.185	0.404	792	0.109	0.230	788	0.103	0.217
1	4	–	–	–	–	867	–	–	781	–	–	779	–	–
2		–	–	–	–	879	–	–	814	–	–	811	–	–
1	5	–	–	–	–	–	–	–	803	–	–	801	–	–

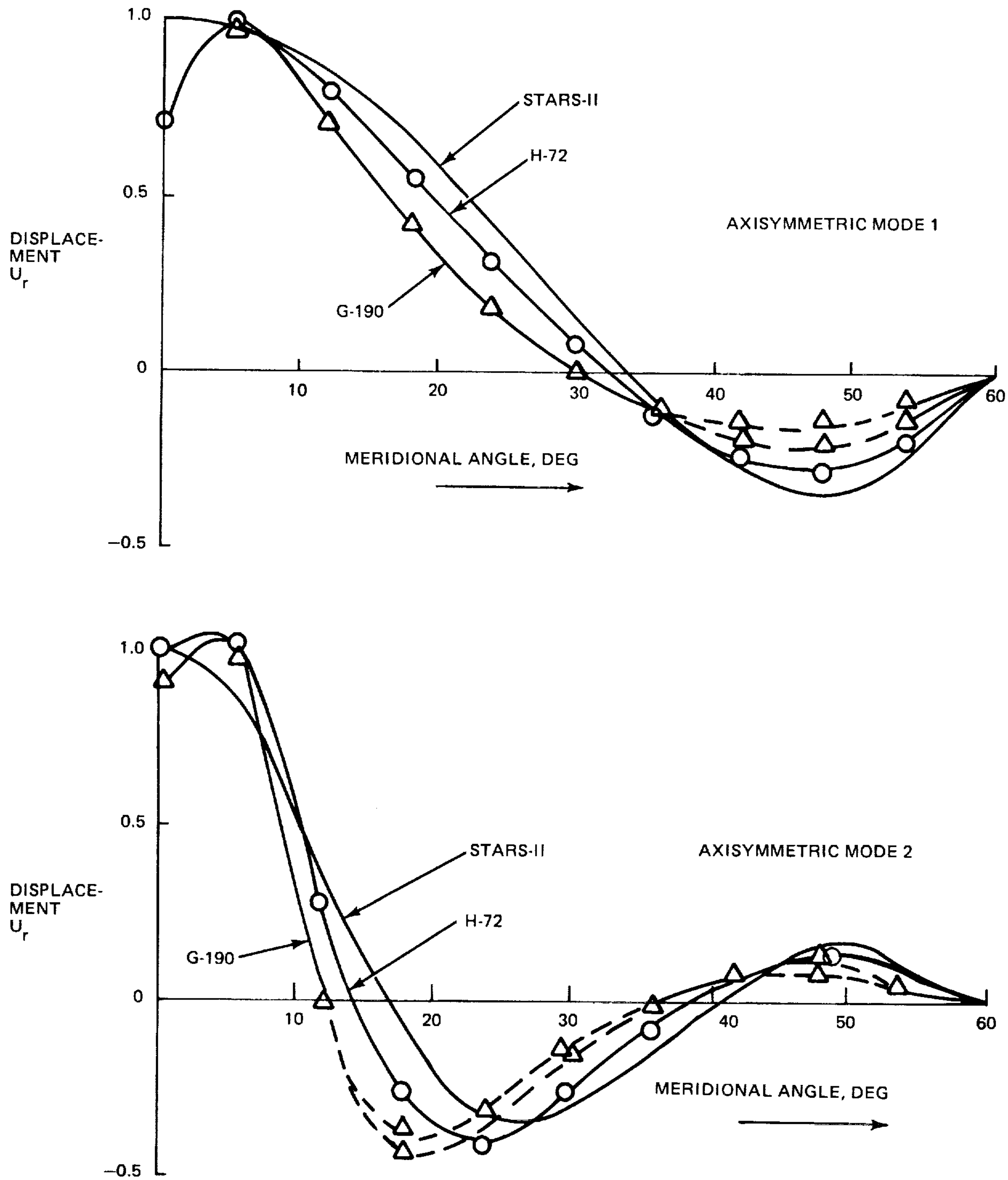

Fig. 3-5 60° Spherical Cap, Fixed Base Mode Shape Comparisons

Another aspect of the harmonic reduction technique is its relative efficiency. A comparision of harmonic and Guyan reduction Central Processor Unit (CPU) times presented in Table 3-2 indicates a significantly lower reduction CPU time for harmonic reduction. This is attributed to elimination of a large scale matrix decomposition, characteristic of the Guyan reduction, and to the fact that fewer degrees of freedom are required for comparable accuracy (e. g. , harmonic 72 DOF-5% accuracy vs. Guyan 190 DOF-12% accuracy). The CPU time associated with eigenvalue analysis of the harmonic analysis set is naturally much less than that associated with the Guyan reduction analysis set.

For the current structural model, circumferential harmonics were uncoupled due to the axisymmetry of shell thickness. In cases where thickness varies with circumferential location (θ) harmonics will be coupled. The degree of coupling is a function of the relative abruptness or smoothness of thickness distribution and the thickness asymmetry.

A general purpose FORTRAN IV computer program for generation of multipoint constraint bulk data cards, HARM, has since been written for typically large hydroelastic problems, many constraint statements must be prepared. A listing and description of this program are presented in Appendix A of Volume II.

Table 3-2 60° Spherical Cap Modal Accuracy/Cost Comparisons (1266 DOF Grid Set)

Reduction Scheme	Analysis Set Size	Modal Accuracy* (15 Modes)	Total Central Processor Unit Time (Sec)
Harmonic	72	0.053	238
Guyan	110	0.276	346
Guyan	95	0.149	328
Guyan	190	0.117	531

$$^{*}\text{Error} = \frac{1}{N}\sum_{i=1}^{N}\left[\left(\omega_i/\omega_{S_i}\right)^2 - 1\right]^2$$

4 - NUMERICAL RESULTS

The present hydroelastic analysis has been implemented in NASTRAN and verified and demonstrated on a number of problems. The problems fall into two categories, namely, analytical verification problems for which exact solutions are known and demonstration problems for which experimental data are available. The 1/8-scale shuttle external tank is included in the second category.

4.1 ANALYTICAL VERIFICATION PROBLEMS

Ex. 1. Fluid Filled Hemispherical Container

This first problem consists of the fluid filled hemispherical container illustrated in Fig. 4-1. The container is massless and follows the artificial structural law

$$P = \alpha U_r \tag{4.1-1}$$

The exact free vibration solution for this problem is expressed in terms of spherical harmonics (Ref. 9). The modal displacements on the structural surface and free surface are

$$U_r = P_m^n(\cos\theta)\cos n\varphi \tag{4.1-2a}$$

$$U_\theta = \left(\frac{r}{R}\right)^{m-1} \frac{dP_m^n(\cos\theta)}{d\theta} \cos n\varphi \tag{4.1-2b}$$

respectively. The modal pressure function is

$$P = \left(\frac{\rho_f R\omega_{mn}^2}{m}\right)\left(\frac{r}{R}\right)^m P_m^n(\cos\theta)\cos n\varphi \tag{4.1-3}$$

and the natural frequencies are

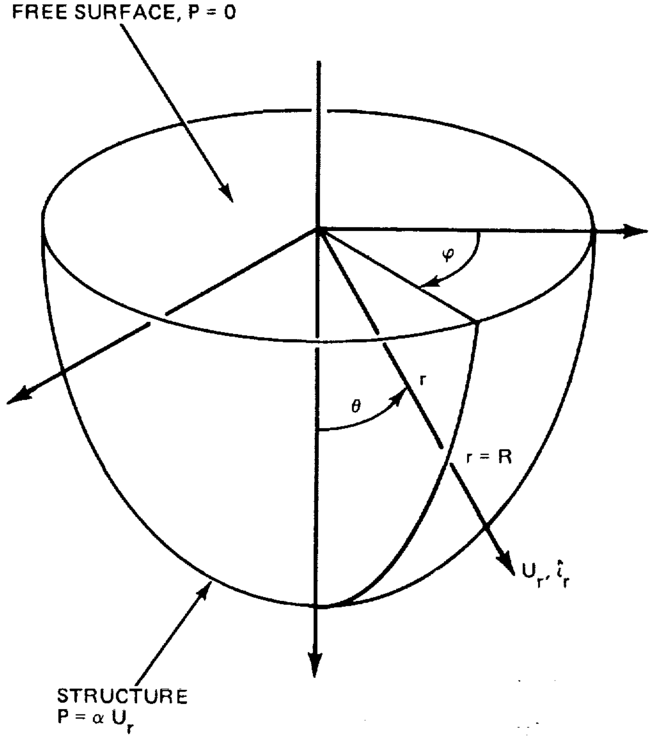

Fig. 4-1 Fluid in a Hemispherical Container

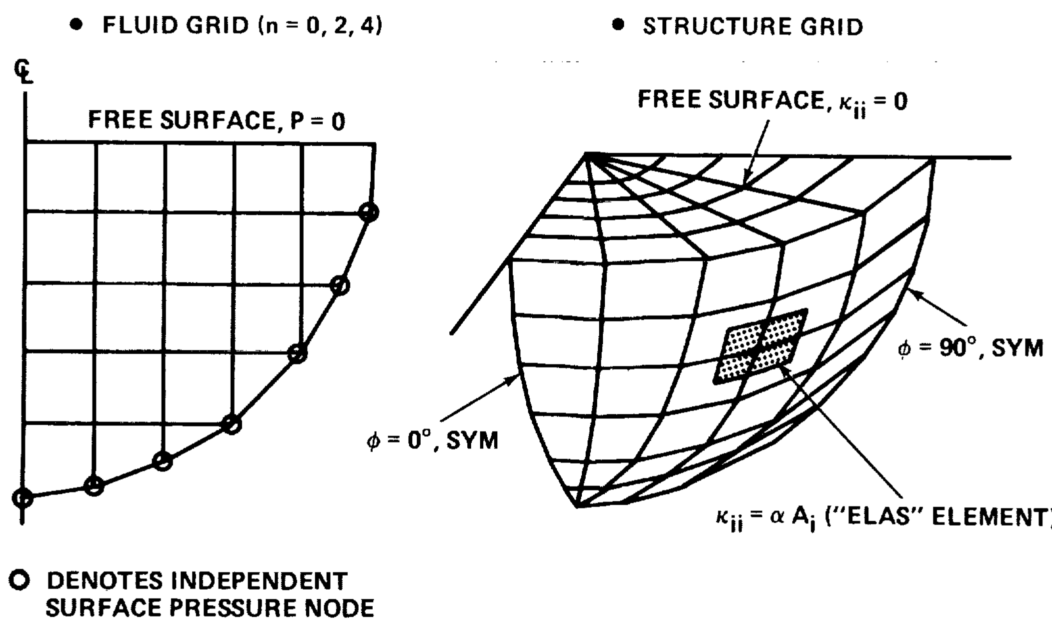

Fig. 4-2 Fluid in a Hemispherical Container – Finite Element Model

$$\omega_{mn} = \sqrt{\frac{m\,\alpha}{\rho_f R}} \qquad (4.1\text{-}4)$$

The function $P_m^n(\cos\,\theta)$ is the associated Legendre function for which m is the meridional wave index and n is the circumferential wave index. The allowable indices are such that the sum m+n must be odd with $m \geq n$.

The finite element model of the hemispherical fluid filled container is illustrated in Fig. 4-2. As a result of the structural law Eq. 4.1-1 the structural stiffness matrix is diagonal with entries

$$K_{ii} = \alpha A_i \qquad (4.1\text{-}5)$$

where A_i is the area associated with the "ith" (radial) degree of freedom. All diagonal entries not associated with radial degrees of freedom are null. The fluid model is expressed in terms of the circumferential pressure harmonics n = 0, 2, 4 and the structural surface and free surface grids are reduced by harmonic reduction accordingly. The fluid mass matrix developed in the modified Rigid Format 7 version is expressed in terms of a 21-degree of freedom analysis set of structural radial displacements (7 meridional locations, circumferential harmonics n = 0, 2, 4).

Natural frequencies and mode shapes for the finite element model were calculated in Rigid Format 3 by the Givens method. A comparison of exact and NASTRAN calculated nondimensional natural frequencies is presented in Table 4-1 and comparisons of selected modal displacement distributions are presented in Fig. 4-3. In general the finite element results are in excellent agreement with the exact solution; as expected in any finite element analysis the level of accuracy decreases with modal complexity.

Ex. 2. Fluid Filled Circular Cylindrical Shell

The second verification problem consists of the fluid filled circular cylindrical shell illustrated in Fig. 4-4. The shell structure is taken as one with bending as well as membrane stiffness. The geometric properties of the shell consist of a cylinder aspect ratio Z/R = 2 and a thickness ratio h/R = 0.01. In addition, the fluid to structure density ratio is $\rho f/\rho s = 1/3$ and the structural material Poisson ratio is $\nu = .3$ An exact hydroelastic modal solution is known for an infinitely long cylinder which holds for the present problem when the structure is subjected to the boundary conditions

$$U_r = M_\theta = N_\theta = N_z = 0 \text{ (shear diaphragm) @ } z = Z,\ r = R \tag{4.1-6a}$$

$$P = 0 \text{ (free surface) @ } z = Z,\ r \leq R \tag{4.1-6b}$$

$$\frac{\partial U_r}{\partial z} = U_z = \frac{\partial M_z}{\partial_z} = N_\theta = 0 \text{ (symmetry) @ } z=0,\ r=R \tag{4.1-6c}$$

$$U_z = 0 \text{ (fixed bottom) @ } z=0,\ r \leq R \tag{4.1-6d}$$

The exact free vibration solution is expressed in terms of cylindrical harmonics (Ref. 10). The normalized modal displacements on the structural surface ($r=R$, $0 \leq z \leq Z$) and the free surface ($r \leq R$, $z = Z$) are

$$U_r = \cos\frac{m\pi z}{2Z} \cos n\theta \tag{4.1-7a}$$

$$U_z = \frac{-\frac{m\pi}{2Z} I_n \frac{m\pi r}{2Z}}{\frac{d}{dr} \mathrm{In}\left(\frac{m\pi r}{2Z}\right)\Big|_{r=R}} \cos n\theta \tag{4.1-7b}$$

respectively, where $I_n (\frac{m\pi r}{2Z})$ is a modified Bessel function. The modal pressure function on the structural surface is

$$P = \frac{\rho_f \omega^2_{mn} I_n \left(\frac{m\pi R}{2Z}\right)}{\left(\frac{m\pi}{2Z}\right) \frac{d}{dr} I_n \left(\frac{m\pi r}{2Z}\right)_{r=R}} \cos n\theta \cos \frac{m\pi z}{2z} \tag{4.1-8}$$

Table 4-1 Fluid in a Hemispherical Container Natural Frequency Comparisons

	N = 0			N = 2			N = 4		
M	Exact*	Nastran	Error**	Exact	Nastran	Error	Exact	Nastran	Error
1	1	1	0						
3	1.732	1.697	−0.02	1.732	1.886	0.089			
5	2.236	2.193	−0.02	2.236	2.367	0.059	2.236	2.308	0.032
7	2.646	2.474	−0.065	2.646	2.714	0.026	2.646	2.698	0.020
9	3.	2.875	−0.042	3.	2.990	−0.003	3.	2.844	−0.052
11	3.317	2.976	−0.103	3.317	3.272	−0.014	3.317	3.192	−0.038
13	3.606	3.	−0.168	3.606	3.863	0.071	3.606	3.343	−0.073
15	3.872	–	–	3.872	–	–	3.872	4.940	0.276
17	4.123	–	–	4.123	–	–	4.123	–	–

*$\Omega_{EXACT} = \sqrt{M}$ M, ODD > N (See Pef 8 for details)

**$ERROR = \frac{\Omega_{NASTRAN}}{\Omega_{EXACT}} - 1$

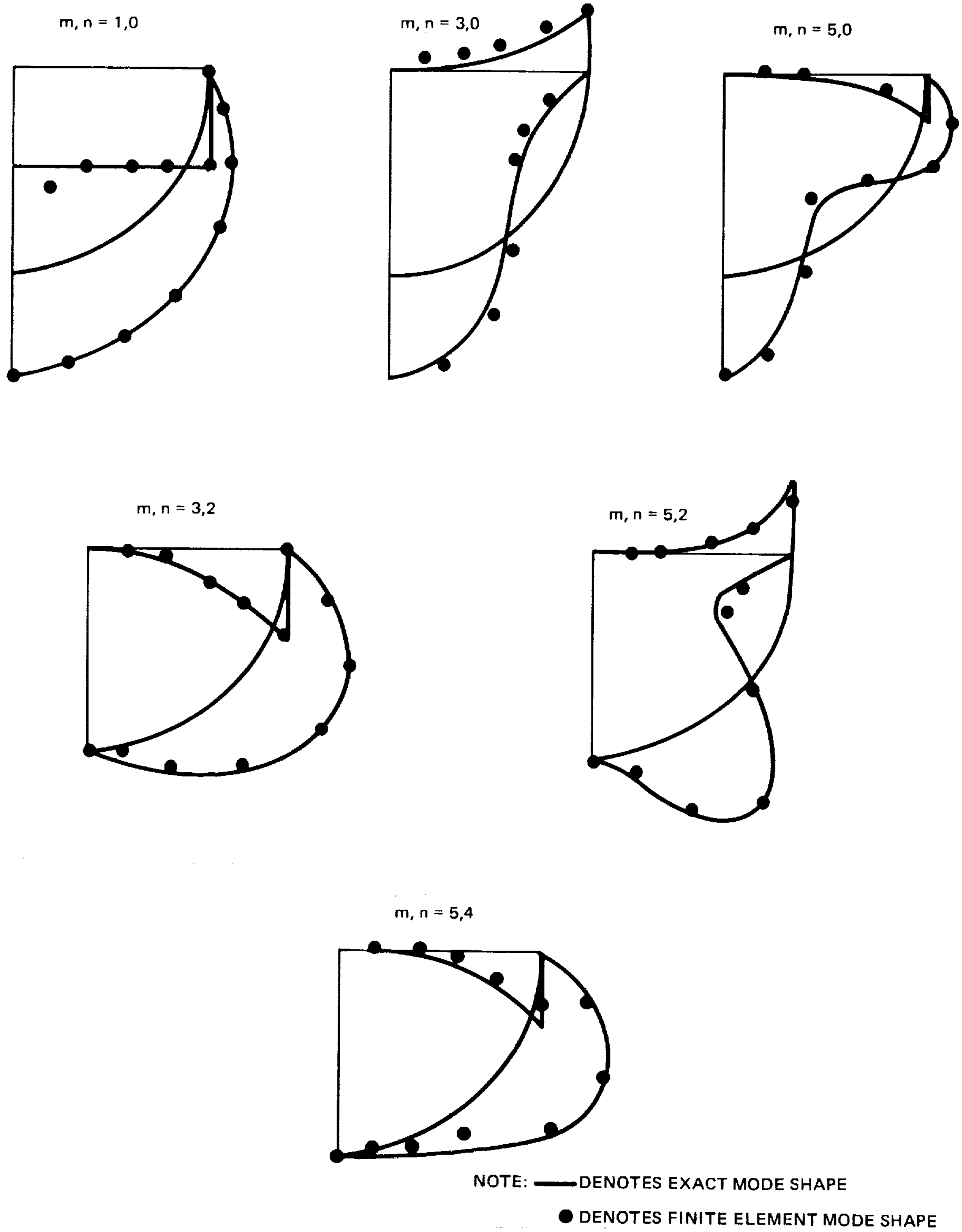

Fig. 4-3 Fluid in Hemispherical Container – Mode Shape Comparisons

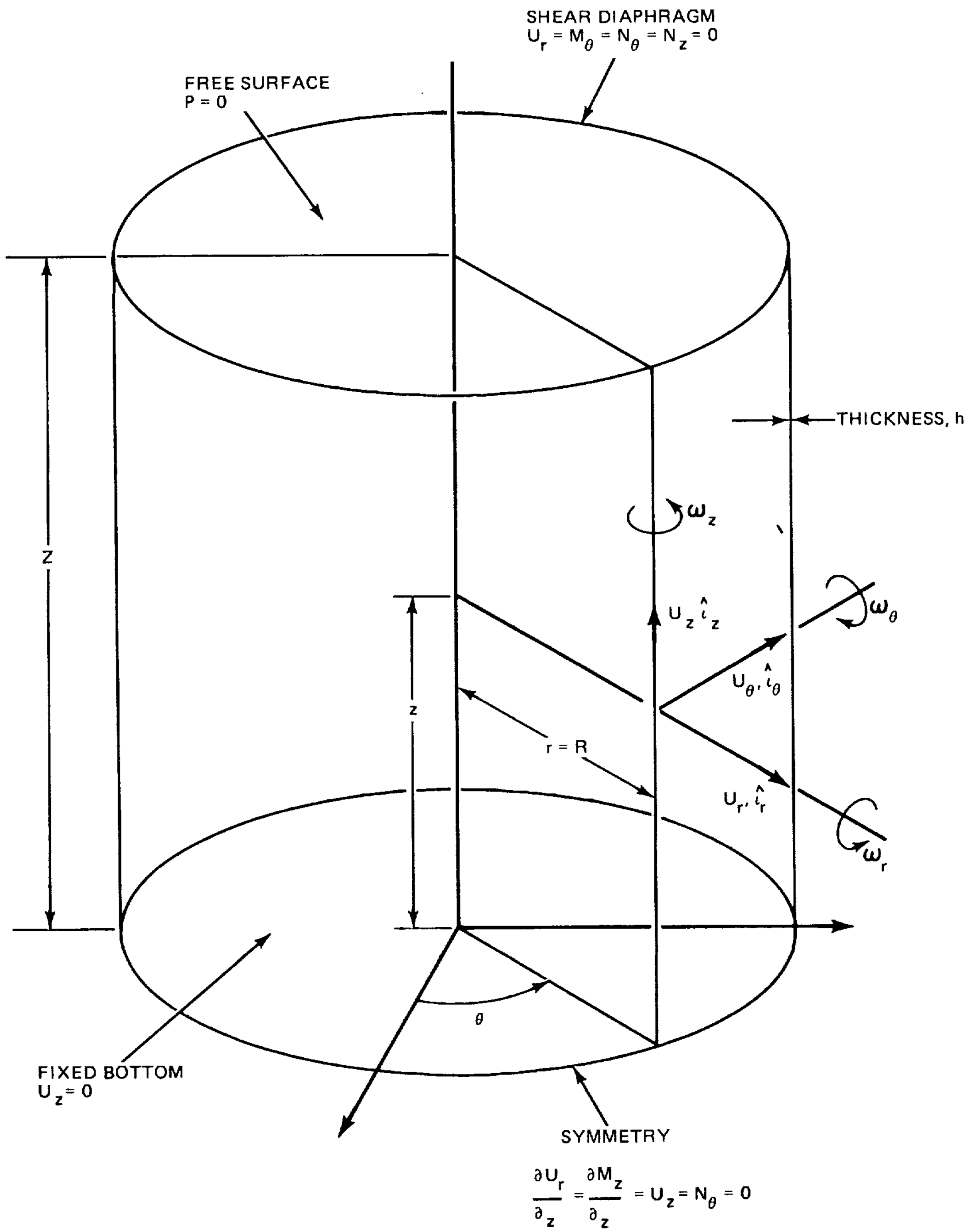

Fig. 4-4 Fluid Filled Circular Cylindrical Shell

Noting that the structural deformation shape Eq. 4.1-7a is the same as for an empty cylinder the hydroelastic natural frequencies are related to the empty structural frequencies $\omega_{E_{mn}}$ as

$$\omega_{mn} = \frac{\omega_{E_{mn}}}{\sqrt{1 + \frac{m_f}{m_s}}} \tag{4.1-9a}$$

where m_f and m_s represent the effective fluid and structural masses

$$m_f = \frac{\rho_f I_n\left(\frac{m\pi R}{2Z}\right)}{\left(\frac{m\ \pi}{2Z}\right)\frac{d}{dr}\left(I_n\left(\frac{m\pi r}{2Z}\right)\right)_{r=R}} \tag{4.1-9b}$$

$$m_s = \rho sh \tag{4.1-9c}$$

The empty shell frequencies $\omega_{E_{mn}}$ are known exactly on the basis of Flugge's shell theory (Ref. 11).

The finite element models of the shell and fluid are illustrated in Fig. 4-5. The structural grid for the quarter shell consists of 924 degrees of freedom and the fluid grid consists of 165 degrees of freedom (55 nodes of rotation, circumferential harmonics n = 0, 2, 4). The harmonic transformation retaining harmonics n = 0, 2, 4, application of single point constraints to enforce boundary conditions, and a small Guyan reduction retaining only radial displacements ultimately resulted in a 30-degree of freedom analysis set. Listings of the NASTRAN Rigid Format 7 and Rigid Format 3 data for this problem are presented in Appendix B of Volume II.

All natural frequencies and 25 mode shapes with and without the fluid included were calculated in Rigid Format 3 by the Givens method. The mode shapes in both cases were nearly identical to one another as concluded in the exact analysis. Selected mode shapes for the liquid filled case are illustrated in Fig. 4-6. Frequency spectra for the empty and fluid filled shells are presented in Fig. 4-7 illustrating excellent comparison between finite element NASTRAN and exact results in both cases.

$\left(\frac{L}{R}\right) = 2, \left(\frac{h}{R}\right) = 0.01, \rho_f/\rho_s = 0.333, \nu = 0.3$

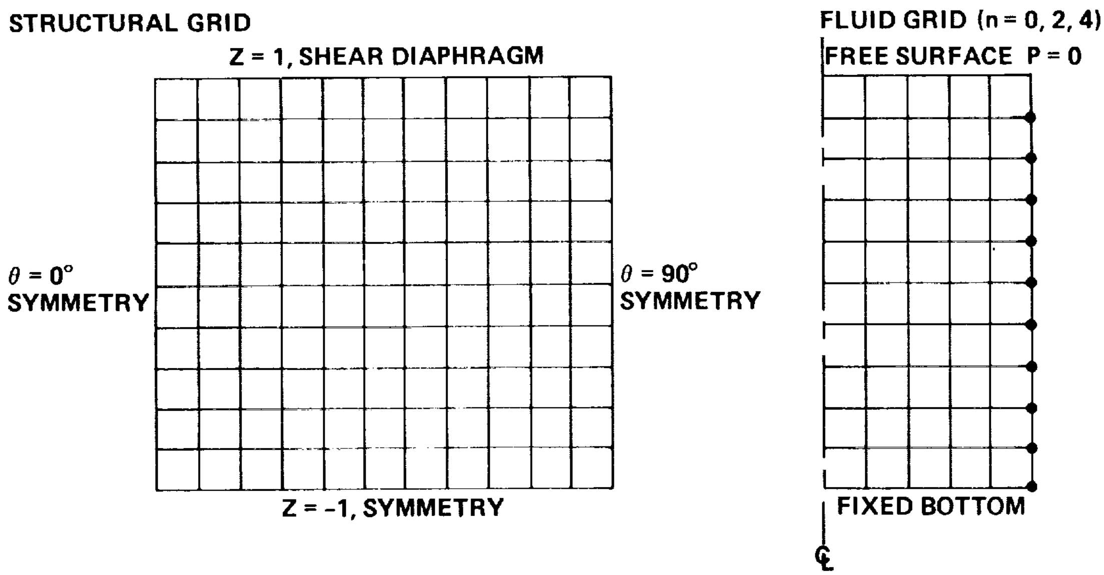

GRID SET = 726 + 198 = 924 DOF
HARMONIC SET = 66 X 3 HARM
= 198 DOF
ANALYSIS SET = 30 DOF

• DENOTES INDEPENDENT FLUID PRESSURE NODE

PRESSURE GRID = 55 X 3 HARM = 165 DOF
INDEPENDENT PRESSURES = 10 X 3 HARM
= 30 DOF

Fig. 4-5 Circular Cylindrical Shell with Fluid – Finite Element Model

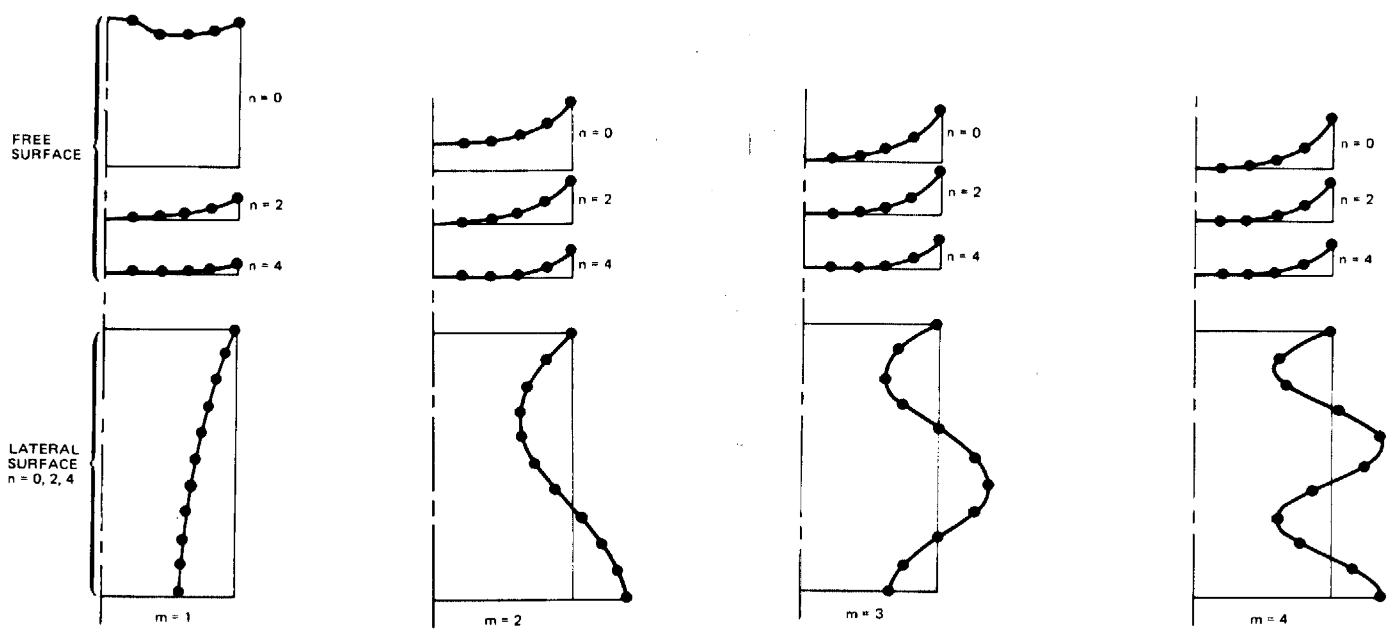

Fig. 4-6 Circular Cylinder Hydroelastic Mode Shapes

$\left(\frac{L}{R}\right) = 2, \left(\frac{h}{R}\right) = 0.01, \rho_f/\rho_s = 0.333, \nu = 0.3$

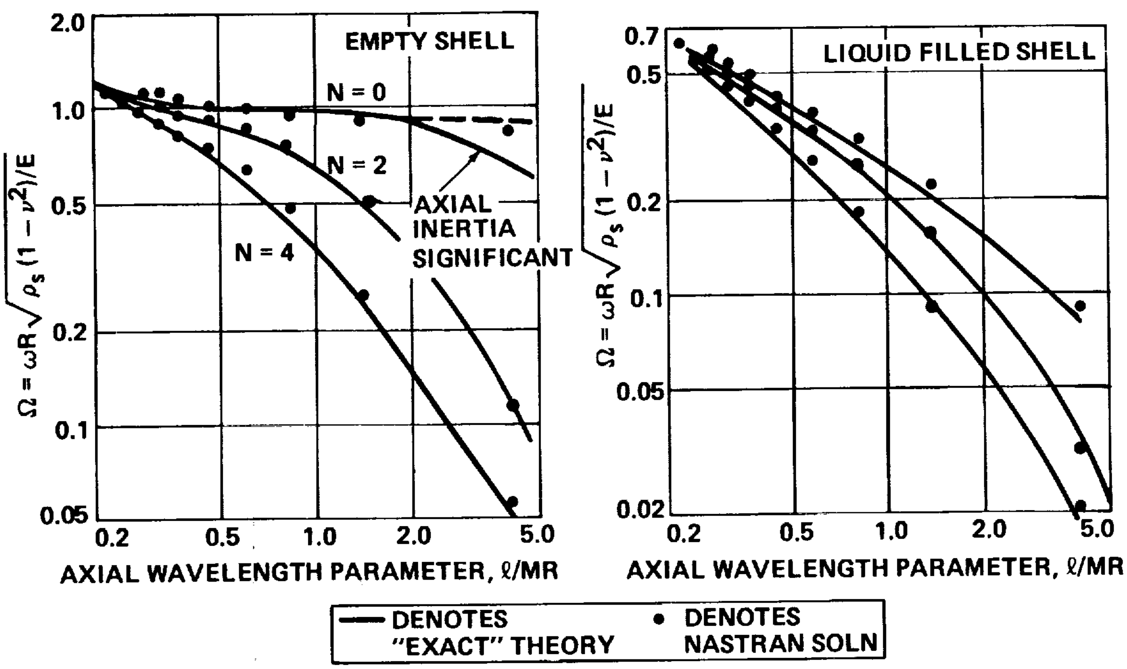

Fig. 4-7 Circular Cylindrical Shell Frequency Spectra

A characteristic of the modified NASTRAN hydroelastic analysis which is as significant as numerical accuracy is computational economy. On the Grumman IBM 370/165 computer the Rigid Format 3 solution time for the empty cylinder was 2 min. 2 sec; for the fluid filled cylinder the Rigid Format 7 and 3 solution times were 1 min 15 sec and 2 min 6 sec, respectively. These computation times represent considerable cost savings for NASTRAN hydroelastic analysis and empty-structure modal analysis.

Ex. 3. Pressurized Fluid Filled Circular Cylindrical Shell

The above described fluid filled cylindrical shell is now considered in a uniformly pressurized state. A closed form free vibration solution in this case follows Eq. 4.1-6 through 4.1-9 with $\omega^P_{E_{mn}}$ representing the empty pressurized shell frequencies. An approximate expression for the adjusted empty shell frequency with pressurization, P_o, (Ref. 10) is

$$\frac{\omega^P_{E_{mn}}}{\omega_{E_{mn}}} = 1 + \frac{(1-\nu^2)P_oR}{Eh}\left[n^2 + \frac{1}{2}\left(\frac{m\pi R}{2Z}\right)^2\right] \qquad (4.1\text{-}10)$$

The mode shapes in the pressurized case are the same as in the unpressurized case.

A modified version of Rigid Format 13 (normal modes with differential stiffness) was used to calculate modal data for the empty and fluid filled cylinder representation, with a pressurization level $(1-\nu^2)P_oR/Eh = 0.001$. The models used for this analysis and all reductions are the same as for the unpressurized case. The frequency spectra for the pressurized empty and fluid filled shells are presented in Fig. 4-8 for the n=4 modes only; pressurization caused negligible changes in the n=0, 2 modes. The natural frequencies resulting from the NASTRAN analysis are in excellent agreement with the results based on Eq. 4.1-10. In addition, as in the unpressurized analysis, computation times were quite satisfactory. Rigid Format 13 modal analysis CPU times were 3 min 2 sec and 3 min 20 sec for the empty and fluid filled cylinders, respectively; approximately 1 min CPU time was required to generate the differential stiffness terms in Rigid Format 13. Rigid Format 13 data for this problem are presented in Appendix B of Volume II.

4.2 COMPARISONS WITH EXPERIMENTAL DATA

Ex. 1 Liquid Filled Cylinders Under Static Pressurization

A detailed experimental study of the dynamics of structurally axisymmetric and asymmetric circular cylinders under various liquid (water) fill and static pressurization conditions has been conducted at NASA Langley Research Center by Mr. Robert Herr. Data resulting from these tests (unpublished) are very complete and serve as excellent information for analysis/test correlation studies. The test articles are aluminum cylinders with mean radius 25.4 cm and height 50.8 cm. The cylinder walls are welded at the top and bottom to heavy aluminum plates as illustrated in Fig. 4-9. The axisymmetric test article has a cylinder wall thickness of .08128 cm and the asymmetric test article has a wall thickness variation around the circumference 0.0508 – 0.1016 according to the equation

$$\frac{h}{h_{max}} = 0.75 - 0.25 \cos\theta \qquad (4.2\text{-}1)$$

The NASTRAN finite element fluid and structural grid representations for the 1/2 fill condition are illustrated in Fig. 4-10. The structural model for a 1/2 cylinder ($0^\circ \leq \theta \leq 180^\circ$) is described by a sufficiently fine grid to simulate the higher circumferential harmonic shapes (e.g. n=0-15) which are known a priori from the experimental results to dominate in the lowest frequency modes. The fluid representation consists of a fine radial grid near the structural wall to insure simulation of the sharp pressure gradients in the higher circumferential harmonics; the generalized fluid pressures are expressed in terms of the symmetric harmonics ($\cos n\theta$) for n = 0 to 15. The grid set for the half filled cylinder consists of 480 pressure degrees of freedom and 2,046 structural degrees of freedom. The structural description in this case is not reduced by harmonic reduction since all harmonics up to n=15 are of interest and insignificant computational economization would be gained by the harmonic transformation.

$(\frac{Z}{R}) = 2,\ (\frac{h}{R}) = 0.01,\ \rho f/\rho s = 0.333,\ \nu = 0.3$

PRESSURIZATION: $\frac{(1-\nu^2)PoR}{Eh} = 0.001$

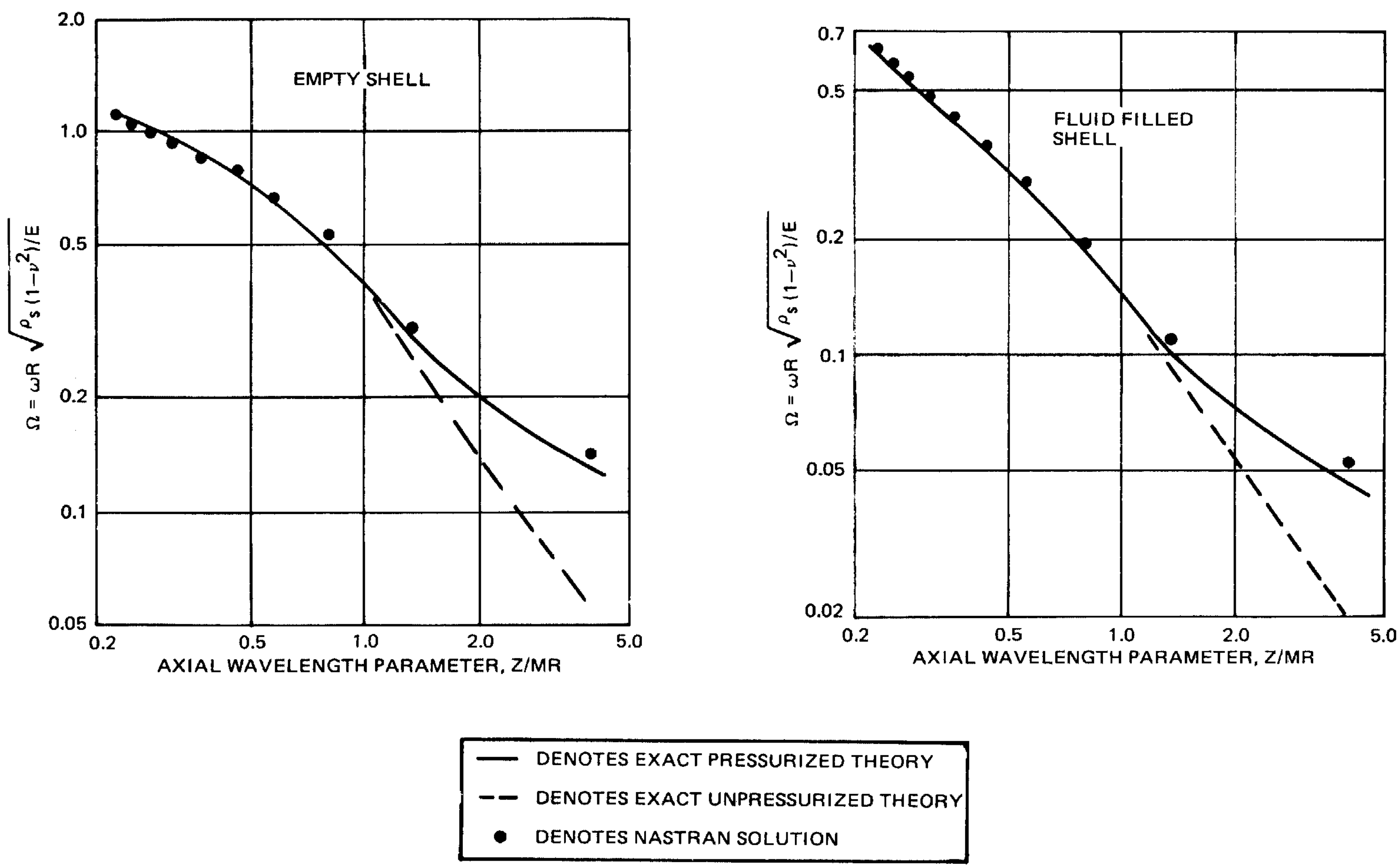

Fig. 4-8 Pressurized Circular Cylindrical Shell n = 4 Frequency Spectra

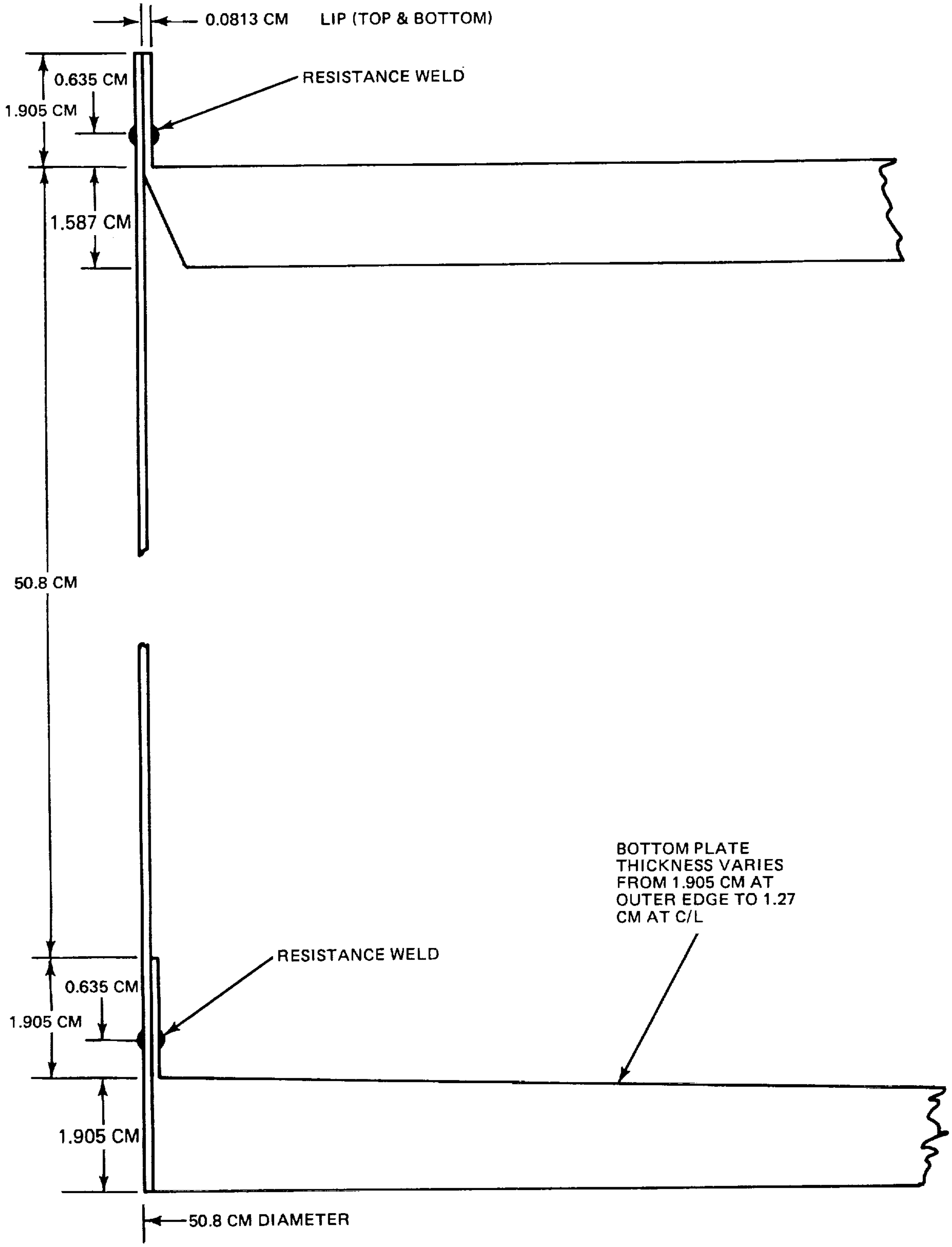

Fig. 4-9 Circular Cylindrical Shell Test Article

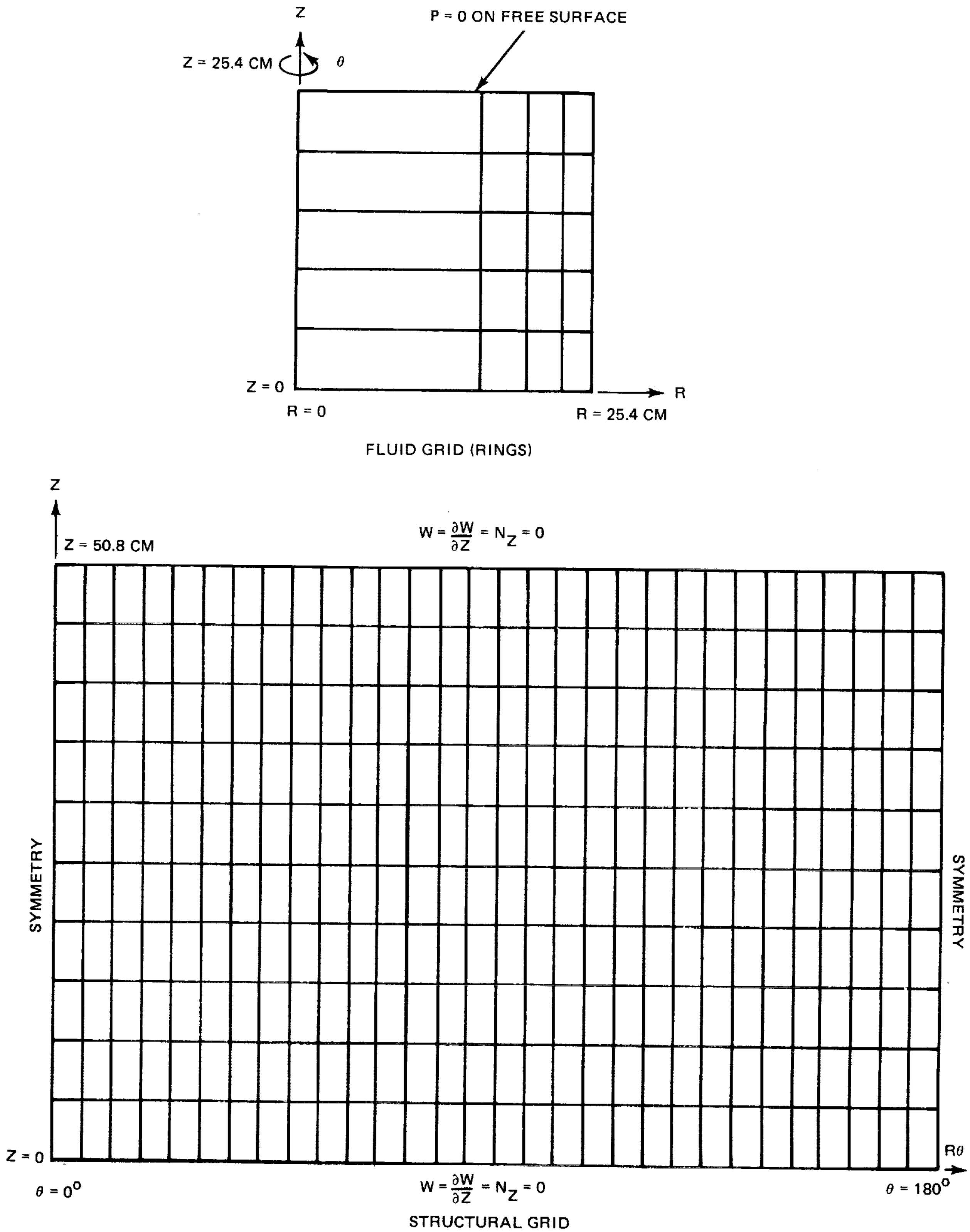

Fig. 4-10 Finite Element Idealization for 1/2-Filled Circular Cylindrical Shell

The first series of problems studied pertained to the cylinder of uniform thickness. The empty cylinder was first considered with an assumed axial plane of symmetry at z=25.4 cm such that only m=1, 3, 5 modes would be calculated. The grid set of 1116 degrees of freedom consisting of nodes below z=25.4 cm was reduced by Guyan reduction to an analysis set of 276 radial degrees of freedom with the base assumed completely fixed (clamped). The analysis on Rigid Format 13 was performed for the test conditions of zero pressurization and static pressurization at $5.516 \times 10^4 N/m^2$. The frequency spectrum of $m=1$, $n \geq 4$ modes is illustrated in Fig. 4-11 along with the test results. The calculated frequency spectrum was higher in both cases than the experimental frequency spectrum. A series of structural model modifications to reconcile the differences in results were considered and it was finally concluded that axial flexibility in the cylinder/plate weld provided the proper correction. Incorporation of the boundary conditions

$$U_r = \frac{\partial U_r}{\partial z} = N_z = 0 \ @ \ z = 0, \ 50.8 \text{ cm} \qquad (4.2\text{-}2)$$

resulted in extremely accurate frequency spectra for the empty 0 and $5.516 \times 10^4 N/M^2$ pressurization conditions, respectively, as illustrated in Fig. 4-11.

The half filled, unpressurized condition was then considered. The liquid free surface was described in terms of single point constraints applied to the surface pressures; free surface displacements were not desired as output information. Retaining only the radial displacements below the free surface in the analysis set a 248 degree of freedom fluid mass matrix and pressure recovery matrix were calculated with the modified version of Rigid Format 7. The cylinder structure in this case does not have a dynamic plane of symmetry at $z = 25.4$ cm; the lower portion ($z \leq 25.4$ cm) is loaded by the fluid inertia and small structural inertia while the upper portion ($z \geq 25.4$ cm) is loaded only by the structural inertia. This provides motivation for Guyan reduction with all degrees of freedom at and above $z = 25.4$ cm (not including the supported degrees of freedom) "omitted". A Guyan reduction on the structure was then performed resulting in an analysis set consisting of 248 radial degrees of freedom. Hydroelastic modes based on the clamped and modified clamped Eq. 4.2-2 end conditions were then

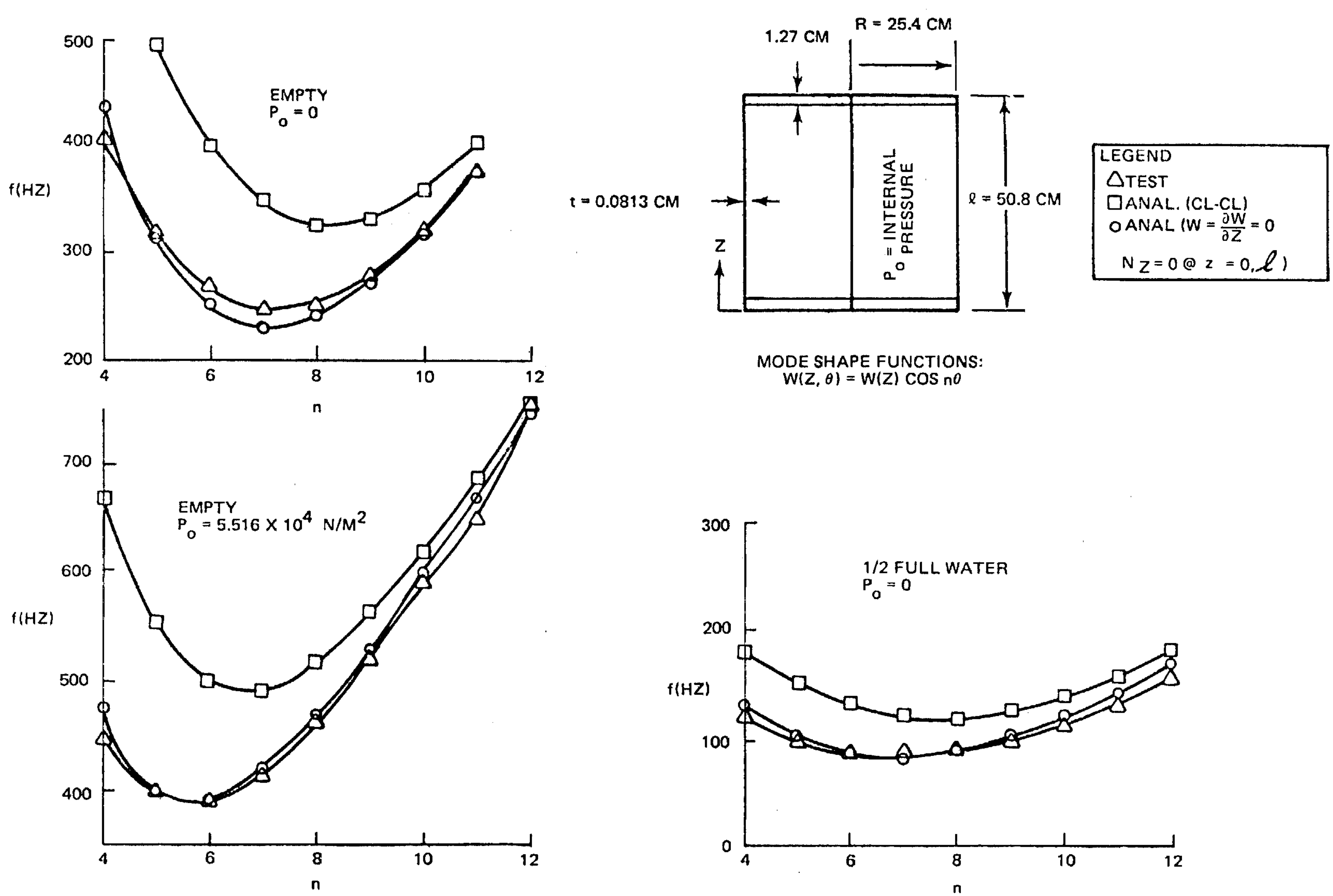

Fig. 4-11 Axisymmetric Cylinder Frequency Spectra (m = 1 Modes)

calculated. The $m = 1$, $n \geq 4$ modal frequency spectra illustrated in Fig. 4-11 show that the representation with the modified end conditions is quite accurate as concluded in the empty cases. At this point it was felt that a hydroelastic analysis with pressurization was not required since enough confidence in the model was gained from the three cases considered above. A study of the unsymmetric cylinder dynamics was then initiated.

The unsymmetric cylinder structural model consists of the same grid set as in the case of the axisymmetric cylinder with circumferential thickness variation. The hydroelastic study of this cylinder was limited to the half filled condition with 0 and $5.516 \times 10^4 \ N/m^2$ pressurization and the realistic edge condition Eq. 4.2-2 was applied. The $m = 1$ mode shapes calculated in Rigid Format 13 for the unpressurized and pressurized conditions illustrated in Figs. 4-12 and 4-13, respectively, are in excellent agreement with the test results as are the modal frequencies (presented in the illustrations).

Computation times for the cylinder study were moderate since harmonic reduction was not appropriate and thus not utilized. In all cases considered, all eigenvalues and 25 eigenvectors were calculated by the Givens method. Computation times for the empty axisymmetric cylinder (1116 DOF g-set, 276 DOF a-set) were 509 CPU sec and 524 CPU sec for the unpressurized and pressurized cases, respectively. Preparation of fluid matrix data in Rigid Format 7 required 97 CPU sec and computation of hydroelastic modes (2,046 DOF g-set, 248 DOF a-set) required 1,193 CPU sec and 1254 CPU sec for the unpressurized and pressurized cases, respectively. The increased CPU time required is predominantly due to the increased structural grid set size of the fluid filled cases; the increase in Guyan reduction time for systems of equivalent matrix bandwidth is proportional to the increase in g-set degrees of freedom. Computation times for the unsymmetric cylinder were similar to those required for the axisymmetric cylinder.

Ex. 2 1/8-Scale Space Shuttle External Tank

An investigation of 1/8 scale space shuttle external tank dynamics in a free-free supported condition has been undertaken. The 1/8 scale external tank consists of two separate propellant tanks connected by a cylindrical section. The finite element hydroelastic model described in detail in Volume II and Ref. 12 consists of a grid set of 348 pressure degrees of freedom, 2,058 structural degrees of freedom and 768 harmonic structural degrees of freedom. Harmonics n=0, 1, 2, 3 were chosen to describe asymmetric dynamics with the pitch plane taken as an axis of symmetry. The analysis set of displacements resulting from a combination of harmonic and Guyan reductions consists of 128 harmonic degrees of freedom associated with outward normal motion of the tank wall.

Three liquid fill conditions have been studied consisting of liftoff, post max Q and empty. In terms of liquid height above the respective bulkheads, the conditions are identified as:

- liftoff $h_{LOX} = 190.5$ cm, $h_{LH_2} = 358.14$ cm
- post max Q: $h_{LOX} = 127$ cm, $h_{LH_2} = 330.2$ cm
- empty: $h_{LOX} = h_{LH2} = 0$ cm

The liquid free surfaces are taken normal to the tank axis thus ignoring some free surface tilt to be experienced in flight since the NASTRAN hydroelastic analysis is currently limited to axisymmetric fluid configurations. This limitation, however, can be overcome by utilization of heat conduction polyhedral finite elements as fluid elements according to the analogy presented in Appendix B.

For each of the fill conditions, 128 natural frequencies and 25 mode shapes and modal pressure distributions were calculated with very good computational efficiency. About 20 CPU minutes per liquid level on the Grumman IBM 370/165 computer was required to perform the entire analysis including matrix assembly, reduction and modal analysis. In previous attempts to study the dynamics of the same finite element representation with the old NASTRAN hydroelastic analysis, computation times were in excess of 70 CPU minutes with only one natural frequency and mode shape computed.

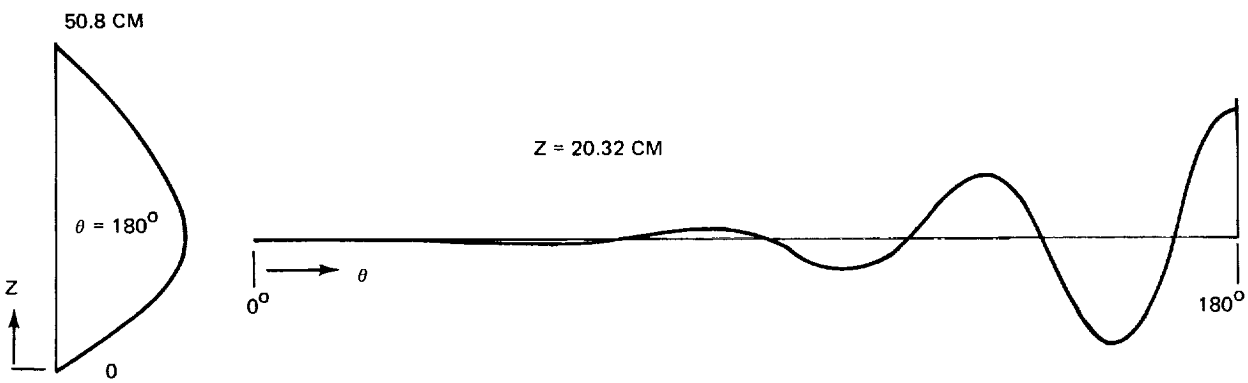

MODE 1 $f_{ANAL.}$ = 67.4 HZ, f_{TEST} = 66 HZ

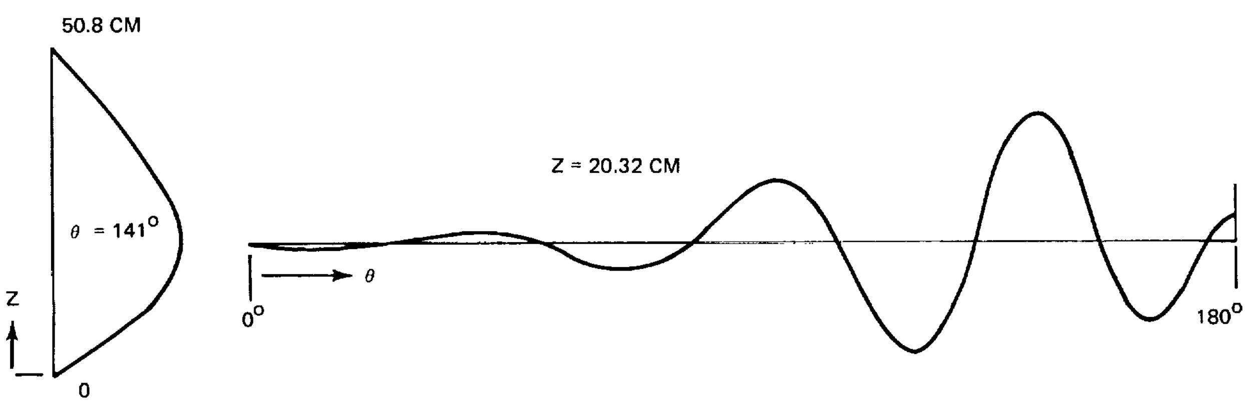

MODE 2 $f_{ANAL.}$ = 78.5 HZ, f_{TEST} = 74 HZ

Fig. 4-12 Unsymmetric Cylinder Hydroelastic Modes – 1/2-Filled with Water (P_o = 0)

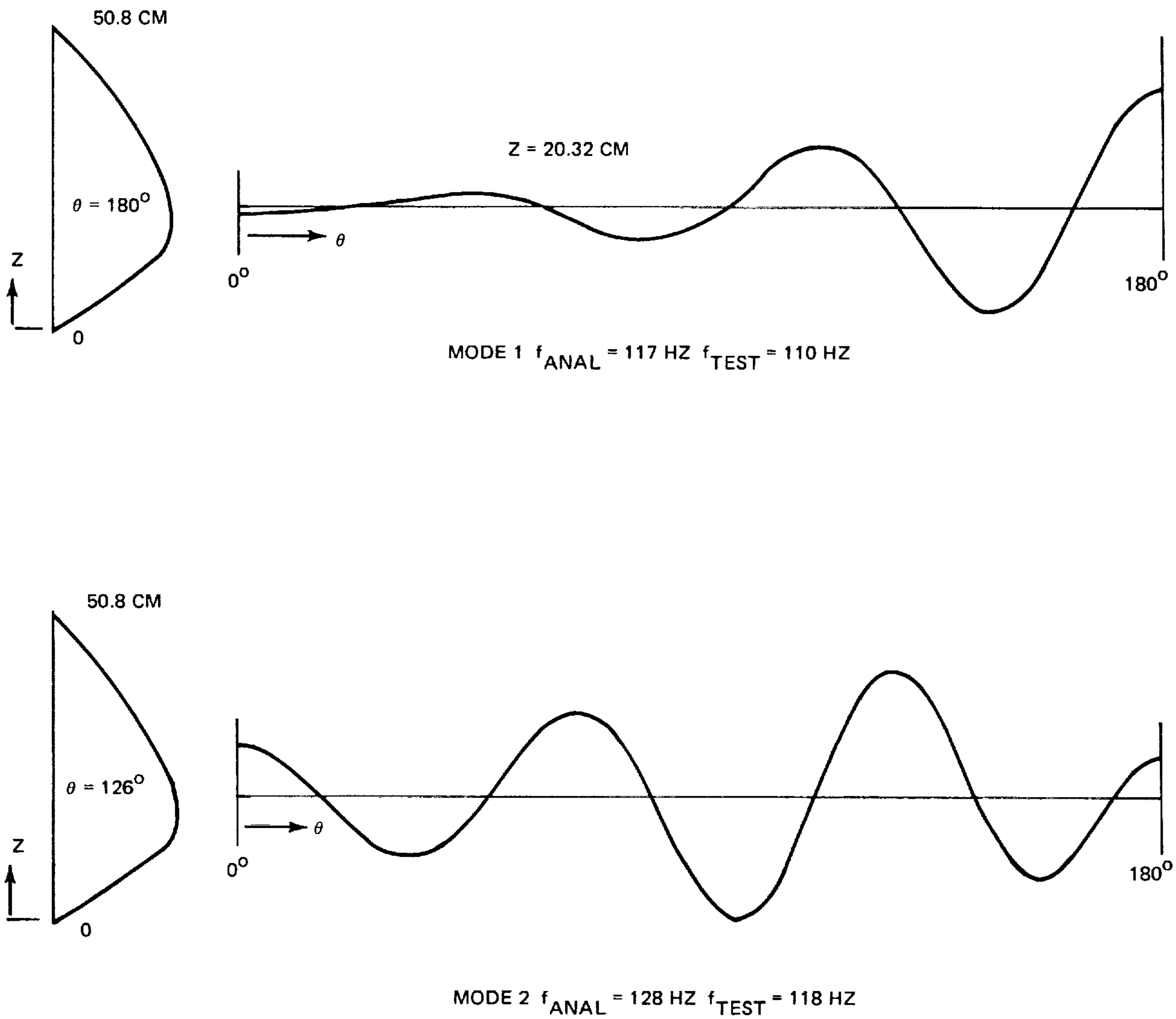

Fig. 4-13 Unsymmetric Cylinder Hydroelastic Modes – 1/2-Filled with Water (P_o = 5.516 X 10^4 N/M^2)

Modal data for each of the three fill conditions studied are summarized in Tables 4-2 through 4-4 with dome pressure gain presented as a measure of relative significance in Pogo susceptibility. The pressure gain is defined as the dome pressure (LO_2 and LH_2) in the vicinity of the feedline interface near the respective tank bottoms resulting from a unit modal acceleration. Plots of the mode shapes corresponding to the intermediate post max Q fill condition are presented in Figs. 4-14 through 4-35.

Excellent agreement between analysis and experimental frequencies occurred in the first axial mode but poor agreement occurred in the bending modes. The source of the discrepency is believed to be in the finite element representation of the structure and efforts to resolve the discrepency are discussed in Volume II.

Table 4-2 1/8-Scale External Tank Hydroelastic Mode Summary (at Liftoff)

Mode No.	Freq. (Hz)	Modal Mass	Description of Mode	LO_2 Dome Pressure Gain X 10^3	LH_2 Dome Pressure Gain X 10^3
4*	29.7	4.751	ET 1st Axial n=0	0.130	0.034
5	34.5	0.857	LO_2 n=2 (No Dome)	0.003	0.001
6*	35.7	0.760	ET 1st Bending n=1	0.040	0.017
7	36.6	0.428	LO_2 n=3 (No Dome)	0.008	0.005
8*	54.9	2.667	ET 2nd Axial n=0	0.067	0.091
9*	57.8	0.131	LH_2 Cylinder n=2,3	0.016	0.019
10*	61.4	0.067	LH_2 Cylinder n=3,2	0.017	0.034
11	62.1	0.395	LO_2 n=3 (No Dome)	0.011	0.005
12*	63.8	0.520	ET 2nd Bending n=1	0.070	0.006
13	68.4	0.581	LO_2 n=2 (No Dome)	0.002	0.003
14*	96.0	0.618	LO_2 n=1	0.102	0.001
15*	96.1	0.433	LO_2 n=0	0.302	0.006
16*	109.4	0.455	LO_2, LH_2 n=0	0.155	0.028
17	114.5	0.741	LO_2, LH_2 n=2,3	0.009	0.001
18	117.8	0.277	LO_2 n=3 (No Dome)	0.006	0
19*	119.7	0.142	LH_2 Cylinder, LOX n=2,0	0.085	0.002
20*	119.8	0.254	LO_2 n=0	0.276	0.017
21*	124.2	0.221	LO_2 n=1	0.253	0.003
22	128.6	0.062	LH_2 Cylinder n=3	0.002	0.001
23*	135.0	0.475	LO_2 n=0	0.150	0.025
24*	135.9	0.431	ET, LOX Dome n=1,0	0.194	0.005
25	138.2	0.589	LO_2 n=2	0.006	0.002

*Denotes POGO Sensitive Mode
NOTE: Modes 1, 2, 3 are Rigid Body Pitch Plane Modes

Table 4-3 1/8-Scale External Tank Hydroelastic Mode Summary (Post Max Q)

Mode No.	Freq. (Hz)	Modal Mass	Description of Mode	LO_2 Dome Pressure Gain X 10^3	LH_2 Dome Pressure Gain X 10^3
4	42.0	0.549	LO_2 n=2 (No Dome)	0.013	0.009
5	45.5	0.294	LO_2 n=3 (No Dome)	0.007	0.006
6*	49.2	0.427	ET 1st Bending n=1	0.078	0.074
7*	51.8	1.809	ET 1st Axial n=0	0.124	0.106
8	58.6	0.140	LH_2 Cylinder n=2, 3	0.006	0.005
9*	61.7	0.074	LH_2 Cylinder n=3,2	0.019	0.015
10*	79.2	1.158	ET 2nd Axial n=0	0.082	0.040
11*	79.7	1.135	ET 2nd Bending n=1	0.111	0.016
12	105.7	0.359	LO_2 n=2 (No Dome)	0.003	0.001
13	107.8	0.177	LO_2 n=3 (No Dome)	0.005	0.001
14*	113.7	0.244	LO_2 n=0	0.422	0.005
15*	120.7	0.160	LO_2 n=1, ET n=1	0.412	0.003
16*	120.9	0.346	LO_2 n=0	0.198	0.033
17	125.5	0.126	LH_2 Cylinder n=3,2	0.006	0.
18	130.6	0.106	LH_2 Cylinder n=3,2	0.013	0.002
19	144.6	0.396	LO_2 n=2	0.015	0.002
20*	146.2	0.125	LO_2 n=1	0.401	0.009
21*	148.6	0.338	LO_2 n=0	0.194	0.015
22	149.1	0.211	LO_2 n=3 (No Dome)	0.005	0.001
23*	150.6	0.283	ET Bending, LOX Dome n=1	0.128	0.018
24*	162.9	0.089	LO_2 n=2	0.141	0.001
25*	167.8	0.079	LO_2 Dome, ET n=0	0.662	0.273

*Denotes POGO Sensitive Mode

Table 4-4 Empty 1/8-Scale External Tank Mode Summary

Mode No.	Freq. (Hz)	Modal Mass	Description of Mode
4	105.6	0.0425	ET 1st Bending n=1
5	153.0	0.0094	LH_2 Cylinder n=3
6	161.7	0.0172	LH_2 Cylinder n = 2, 3
7	226.0	0.0497	ET 2nd Bending n=1
8	257.8	0.0770	ET 1st Axial n=0
9	274.7	0.0271	LH_2 Cylinder n=2,3
10	328.3	0.0122	LH_2 Cylinder, LOX n=3,2
11	332.0	0.0149	LO_2, LH_2 n=3,2
12	332.8	0.0234	LO_2, LH_2 n=3,2
13	343.7	0.0118	ET n=3
14	357.8	0.0696	ET Bending n=1,3
15	431.0	0.0210	LH_2 Cylinder n=2
16	459.1	0.0615	LH_2 Cylinder n=3, ET n=1
17	472.9	0.0114	LH_2 Cylinder n=3
18	482.2	0.0185	ET n=2
19	498.6	0.0076	LO_2 n=3
20	513.2	0.0697	ET n=1, 2, 3
21	533.1	0.0243	ET n=2, 1
22	567.2	0.0487	ET n=1, 2, 3
23	604.6	0.0391	ET n=2, 1, 3
24	625.4	0.0116	LO_2 n=3
25	628.0	0.0144	ET n=3,2

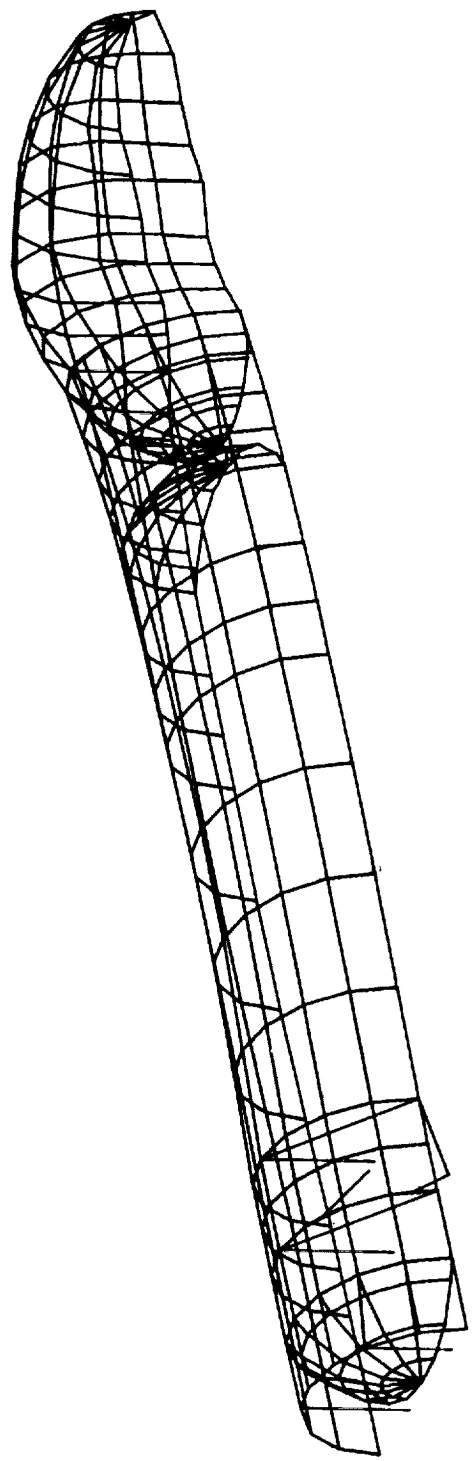

Fig. 4-14 1/8-Scale Space Shuttle External Tank — Post Max Q, Mode 4

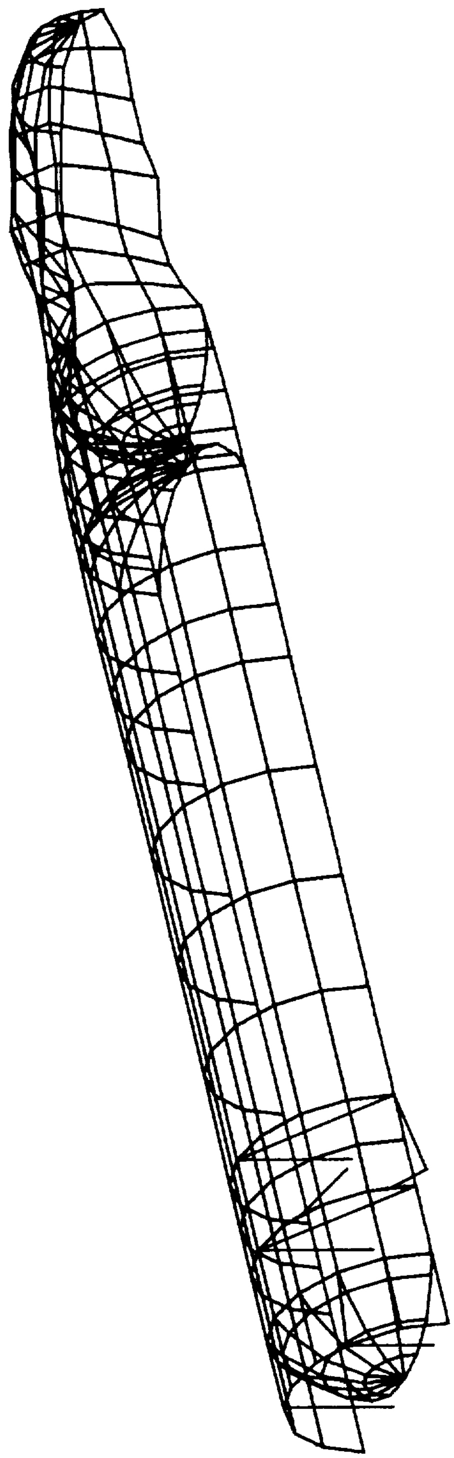

Fig. 4-15 1/8-Scale Space Shuttle External Tank – Post Max Q, Mode 5

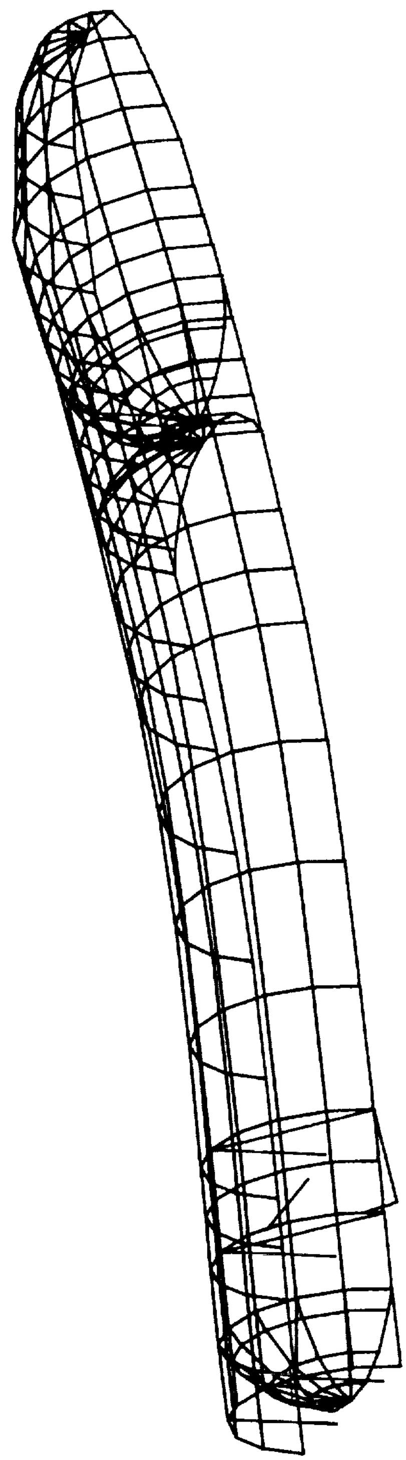

Fig. 4-16 1/8-Scale Space Shuttle External Tank — Post Max Q, Mode 6

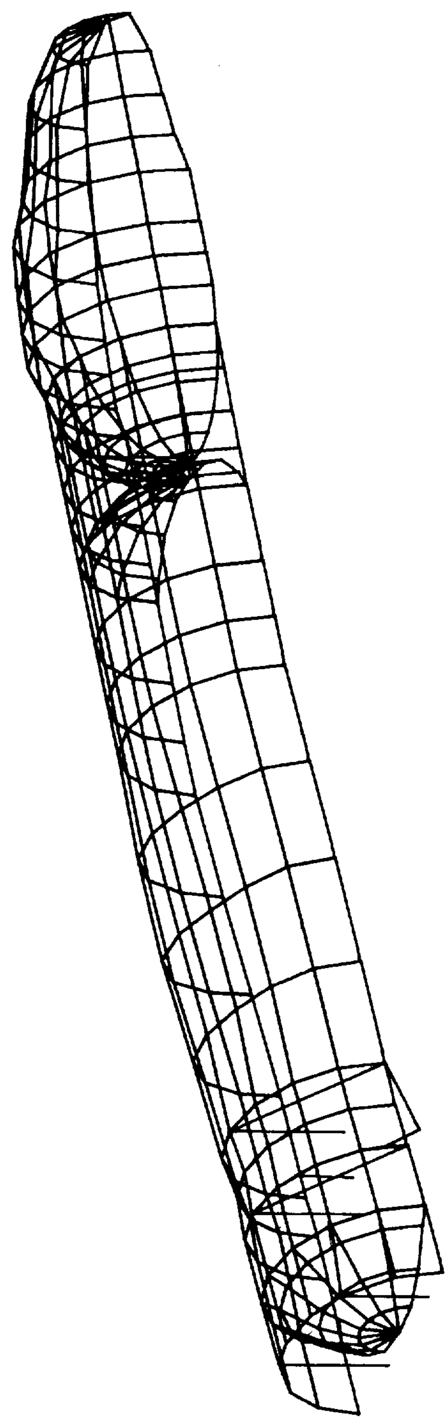

Fig. 4-17 1/8-Scale Space Shuttle External Tank — Post Max Q, Mode 7

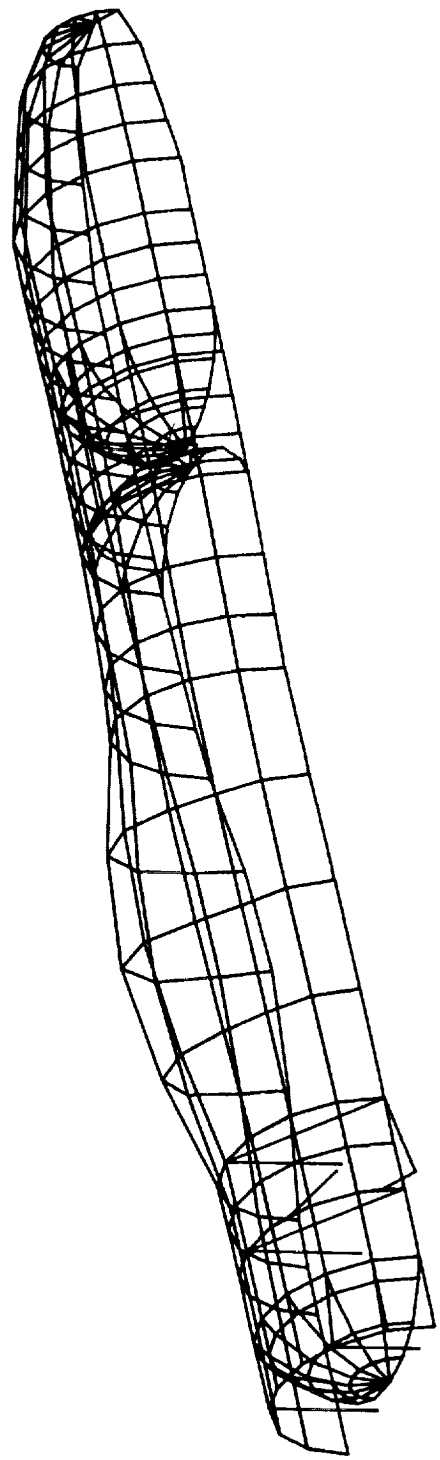

Fig. 4-18 1/8-Scale Space Shuttle External Tank — Post Max Q, Mode 8

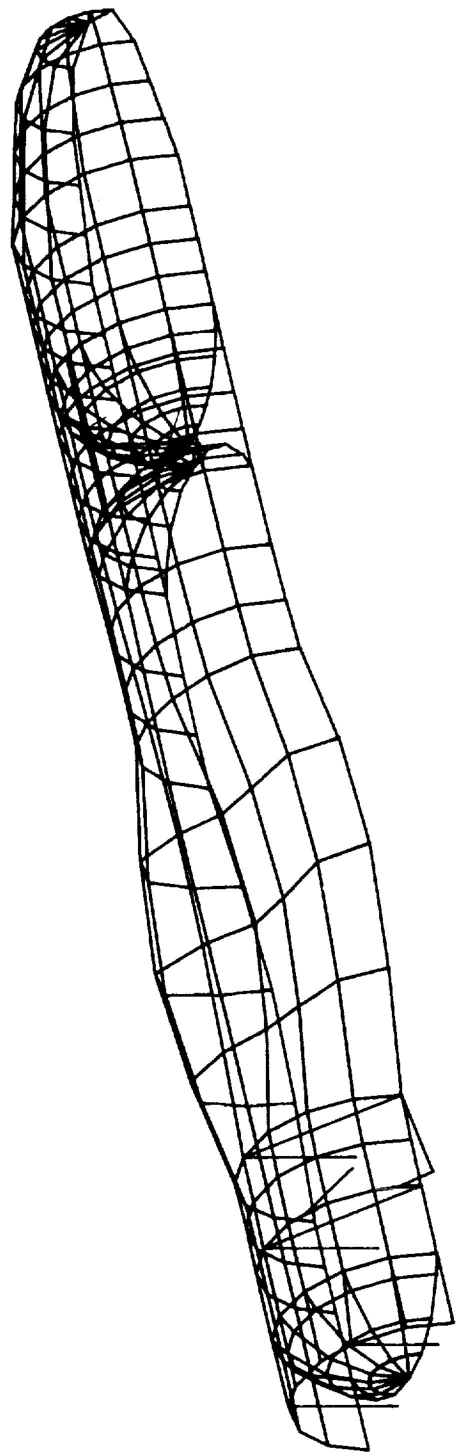

Fig. 4-19 1/8-Scale Space Shuttle External Tank — Post Max Q, Mode 9

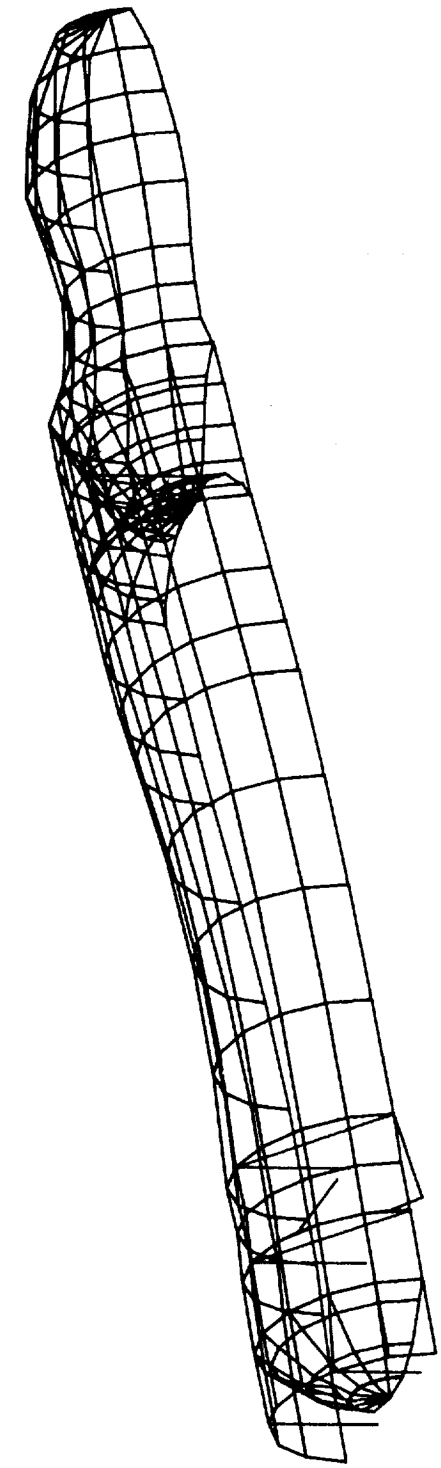

Fig. 4-20 1/8-Scale Space Shuttle External Tank - Post Max Q, Mode 10

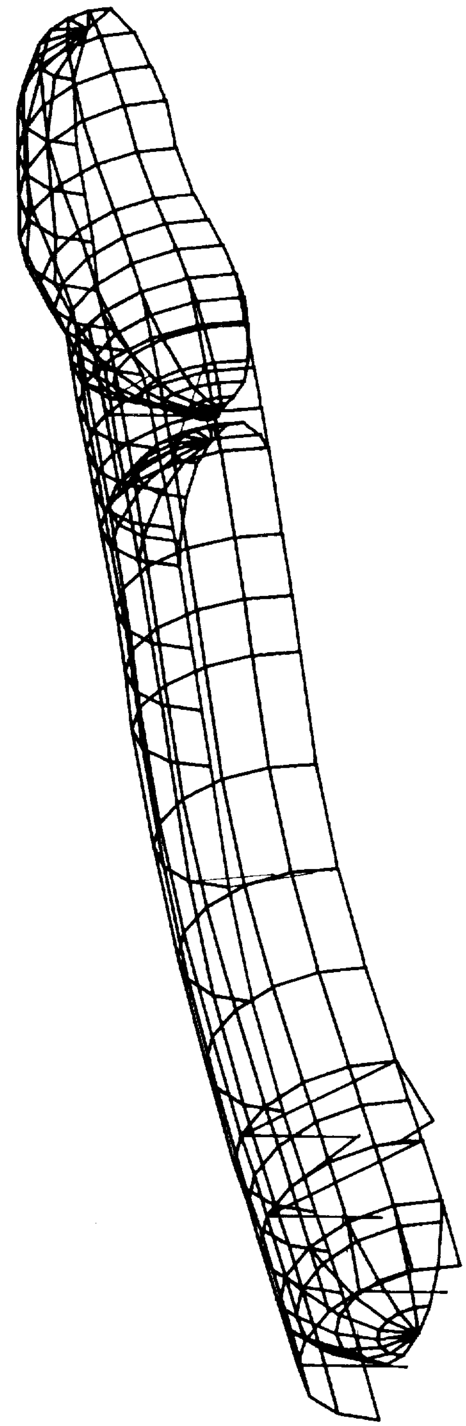

Fig. 4-21 1/8-Scale Space Shuttle External Tank – Post Max Q, Mode 11

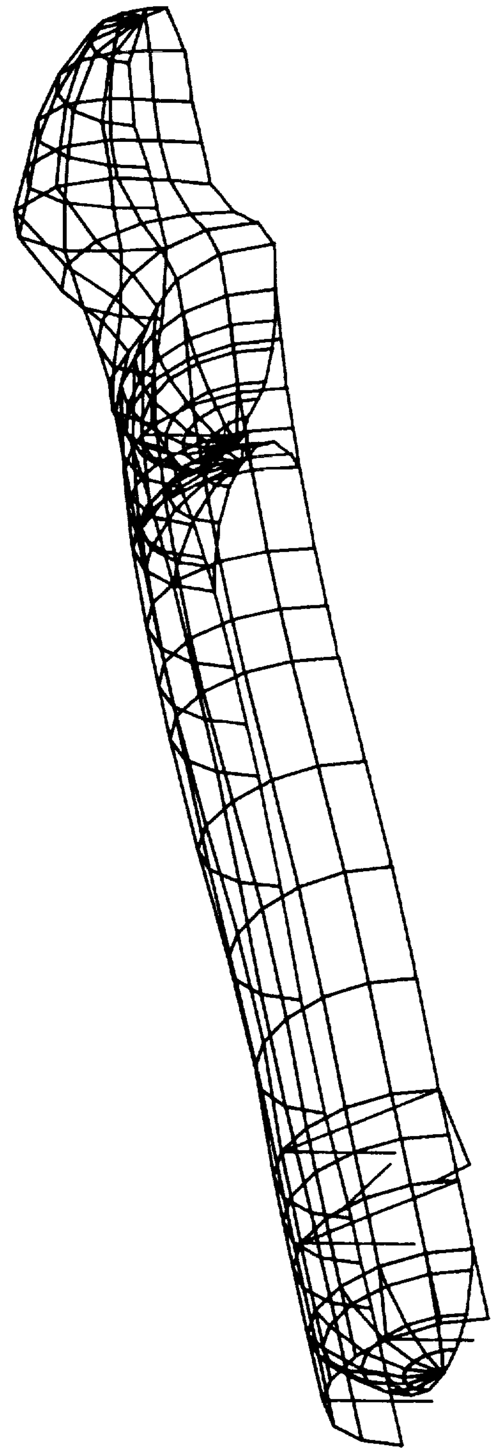

Fig. 4-22 1/8-Scale Space Shuttle External Tank – Post Max Q, Mode 12

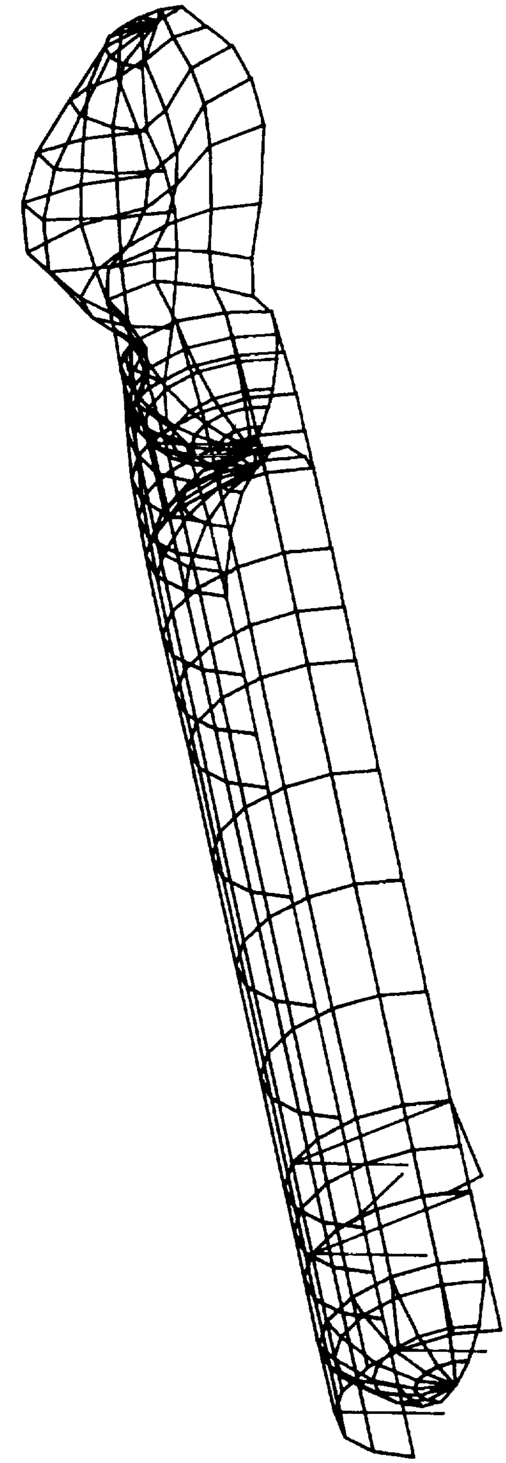

Fig. 4-23 1/8-Scale Space Shuttle External Tank — Post Max Q, Mode 13

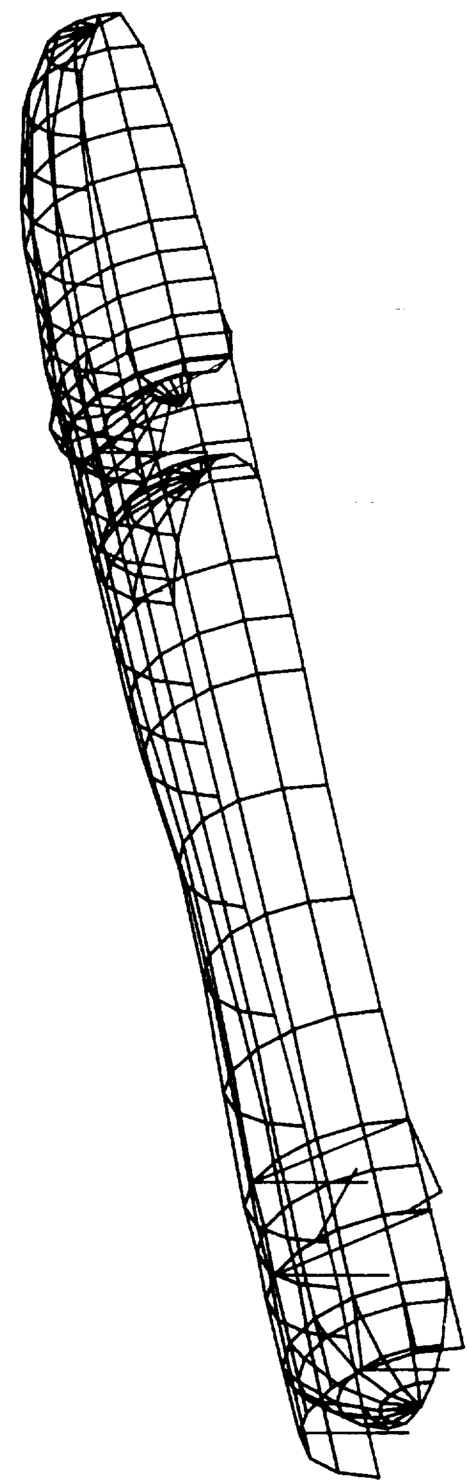

Fig. 4-24 1/8-Scale Space Shuttle External Tank – Post Max Q, Mode 14

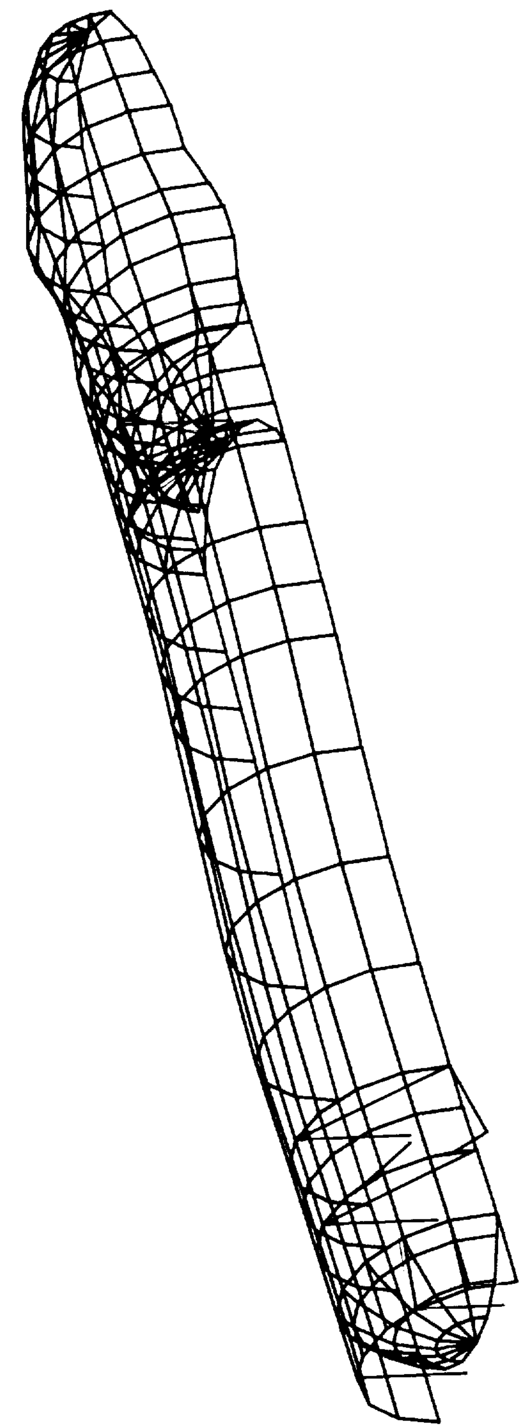

Fig. 4-25 1/8-Scale Space Shuttle External Tank — Post Max Q, Mode 15

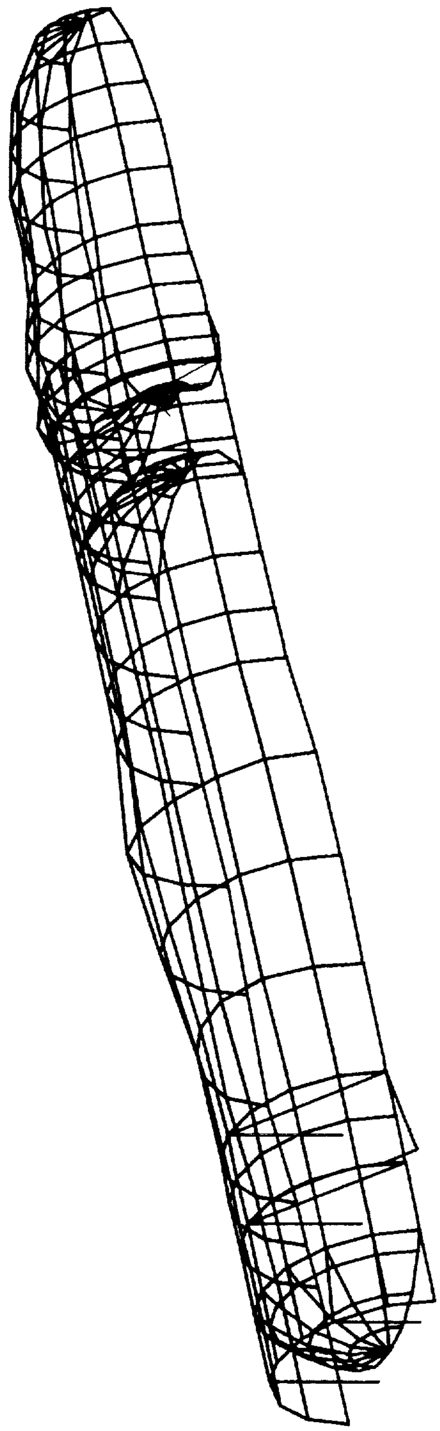

Fig. 4-26 1/8-Scale Space Shuttle External Tank — Post Max Q, Mode 16

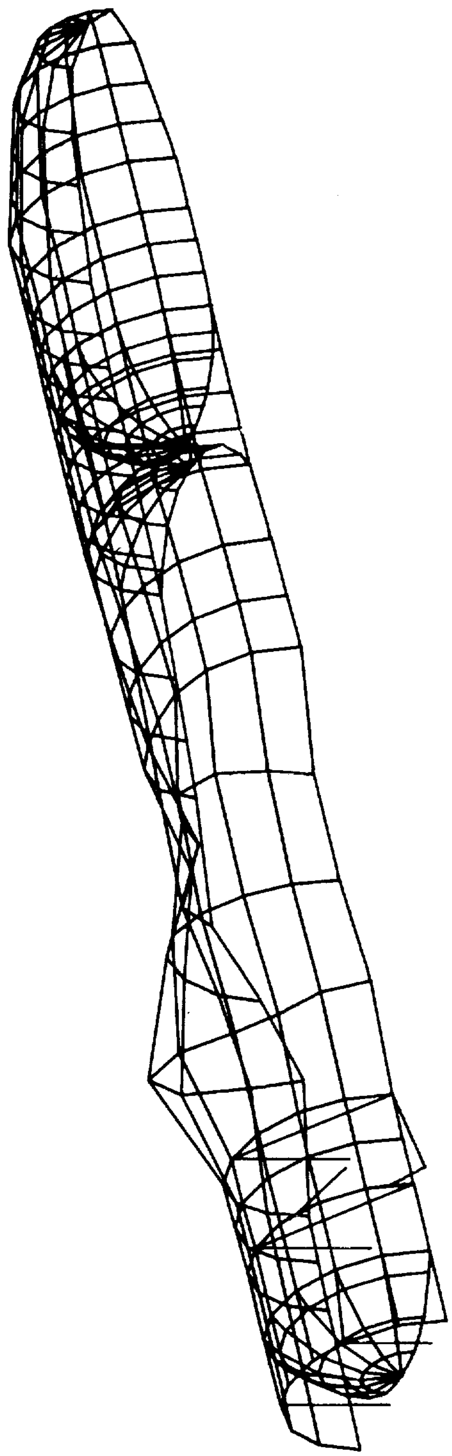

Fig. 4-27 1/8-Scale Space Shuttle External Tank – Post Max Q, Mode 17

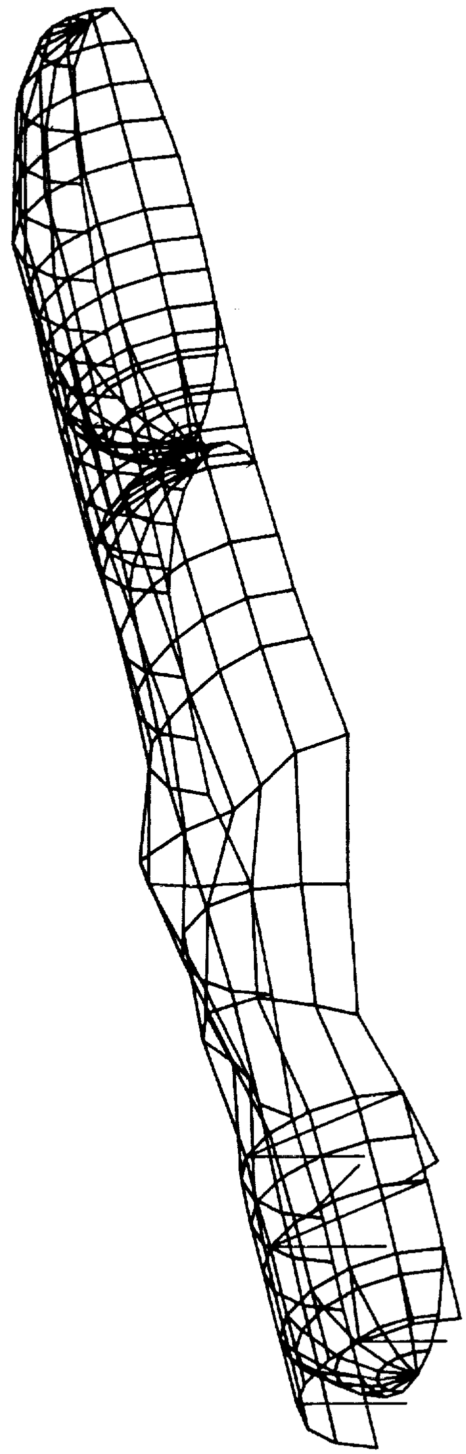

Fig. 4-28 1/8-Scale Space Shuttle External Tank – Post Max Q, Mode 18

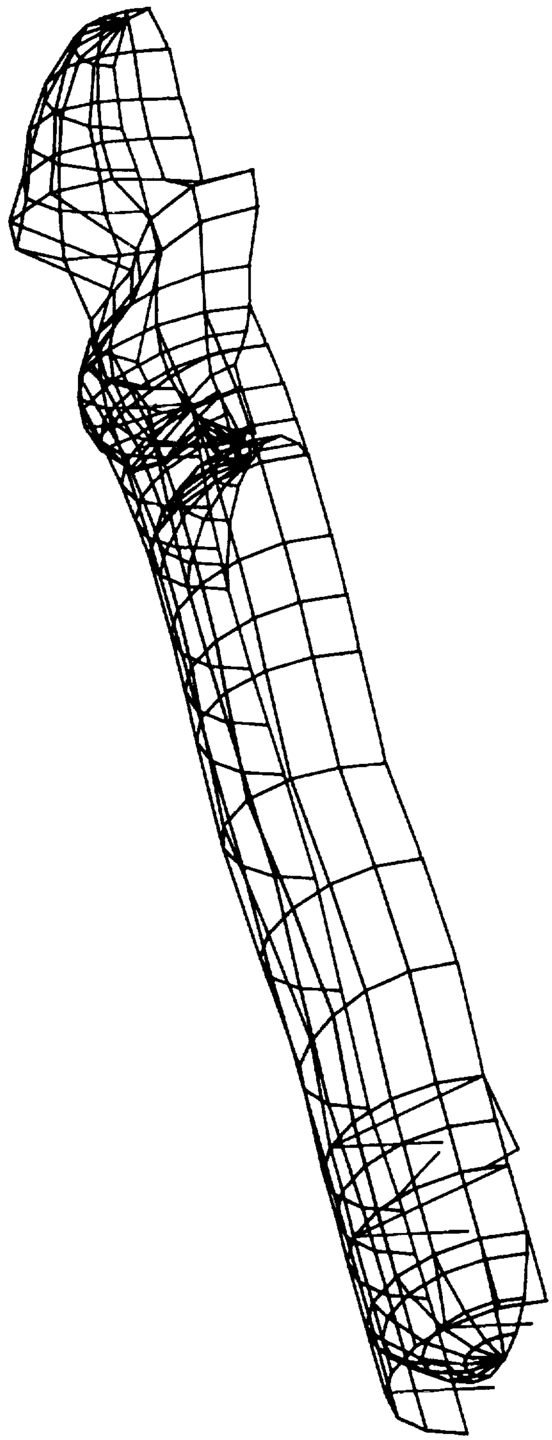

Fig. 4-29 1/8-Scale Space Shuttle External Tank – Post Max Q, Mode 19

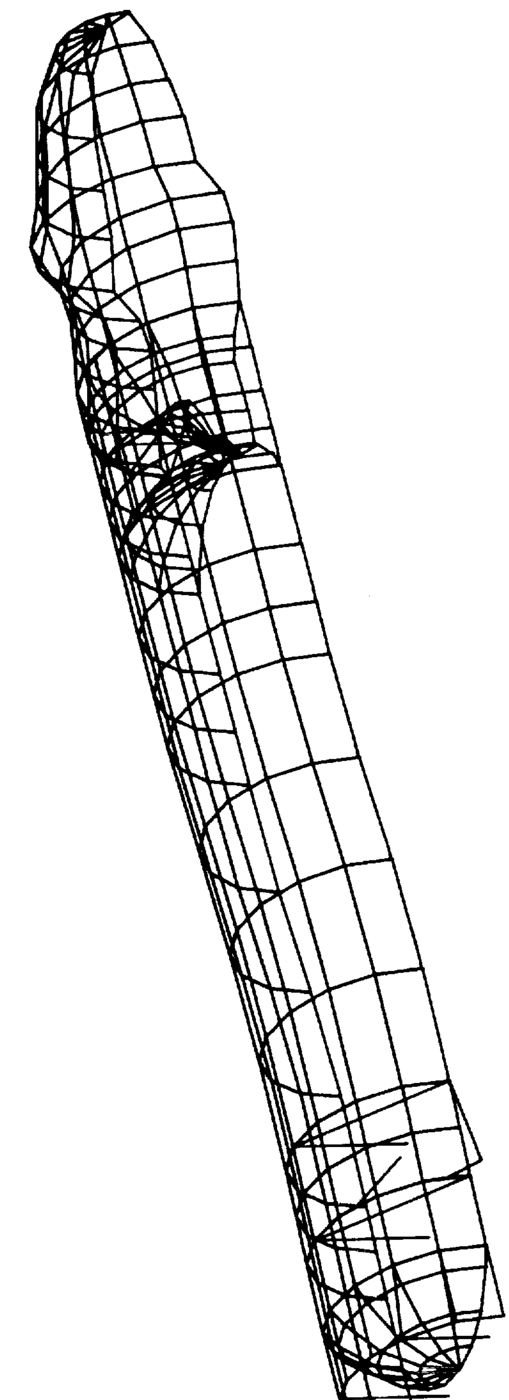

Fig. 4-30 1/8-Scale Space Shuttle External Tank — Post Max Q, Mode 20

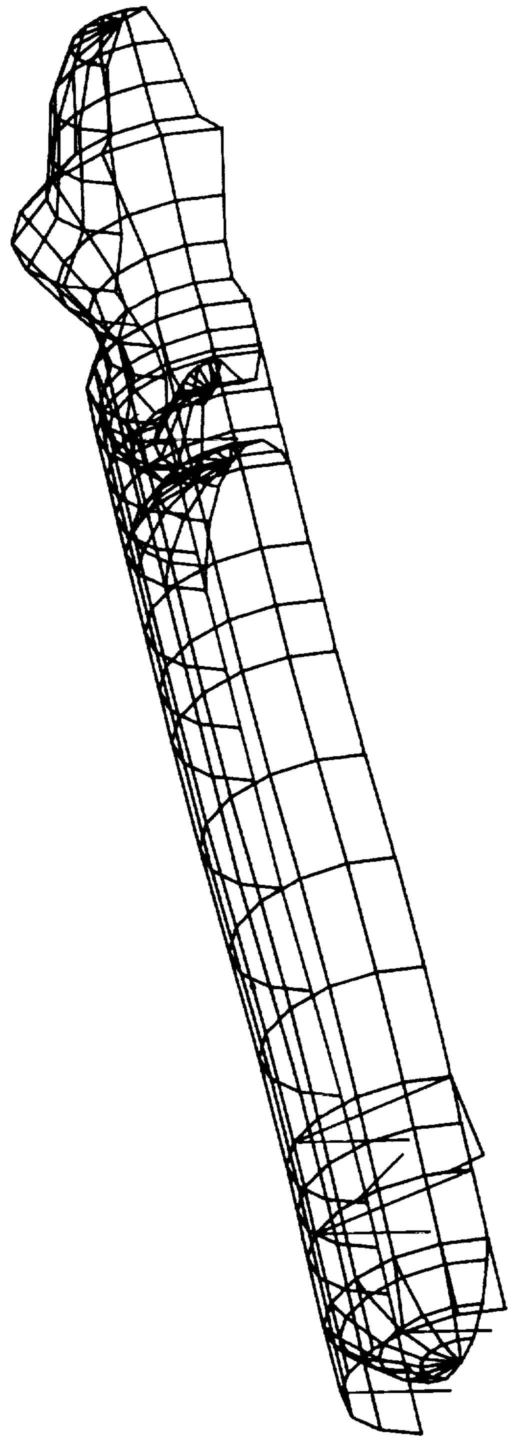

Fig. 4-31 1/8-Scale Space Shuttle External Tank — Post Max Q, Mode 21

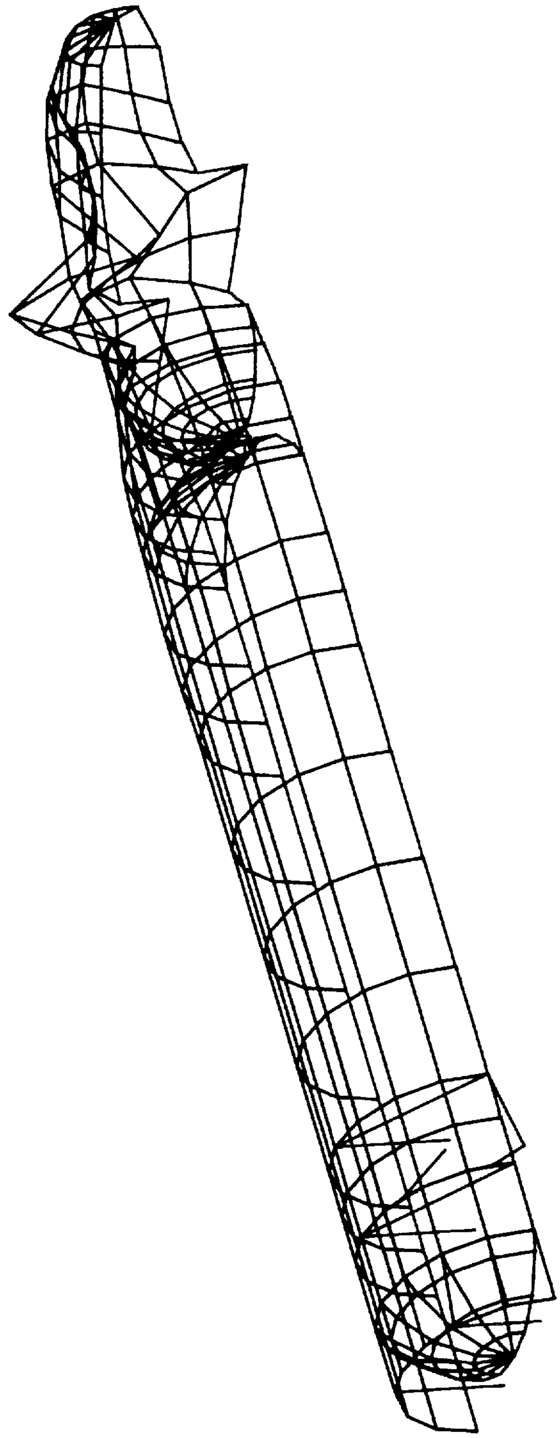

Fig. 4-32 1/8-Scale Space Shuttle External Tank – Post Max Q, Mode 22

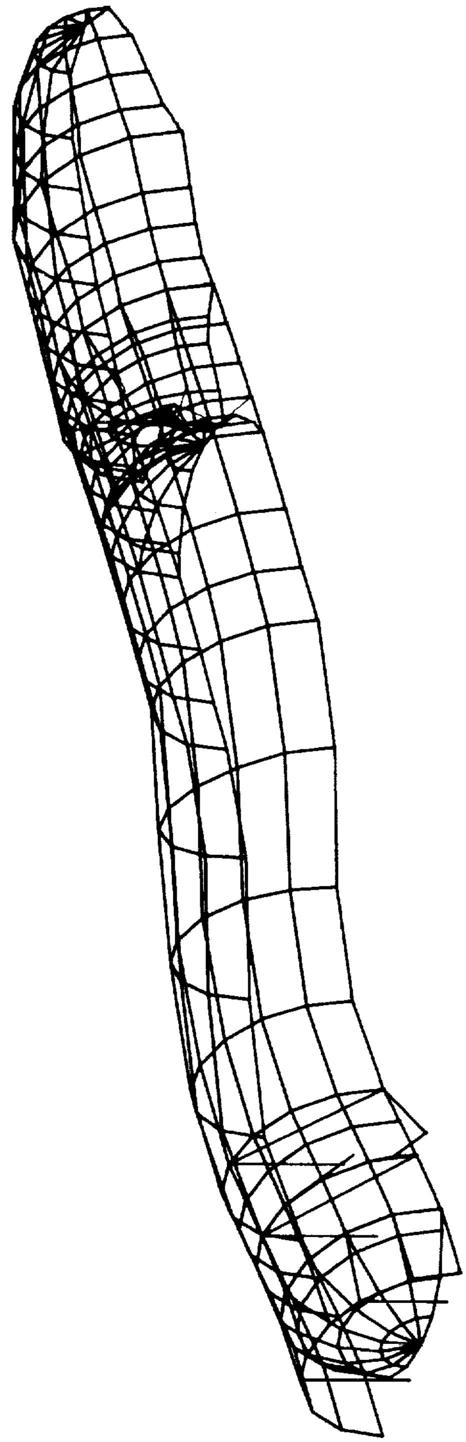

Fig. 4-33 1/8-Scale Space Shuttle External Tank — Post Max Q, Mode 23

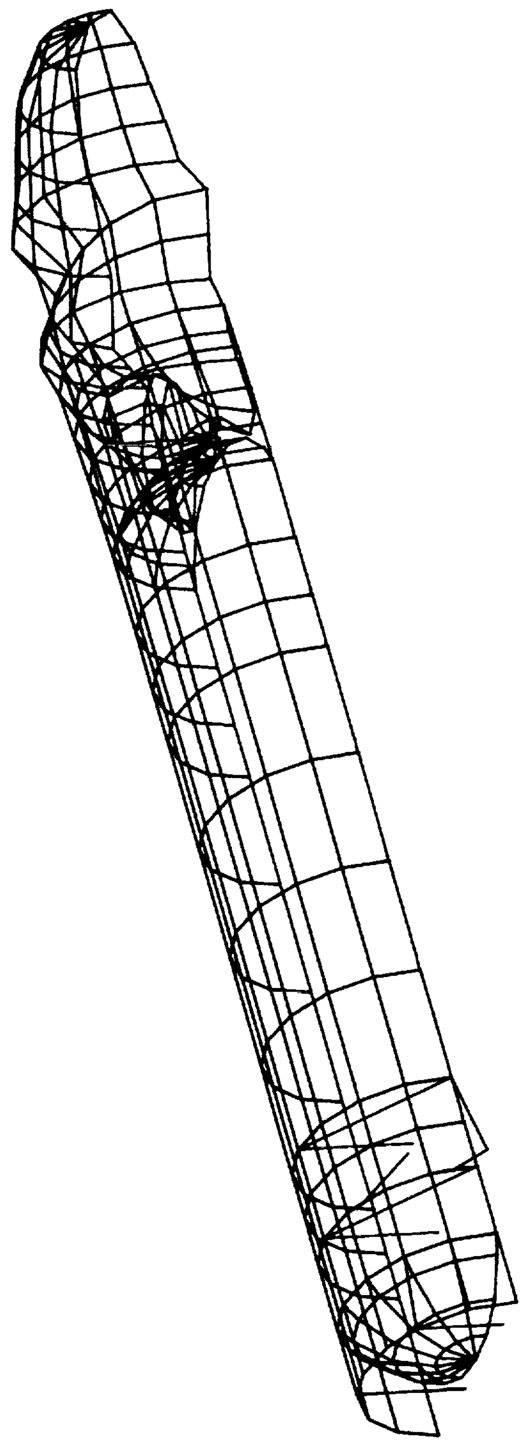

Fig. 4-34 1/8-Scale Space Shuttle External Tank — Post Max Q, Mode 24

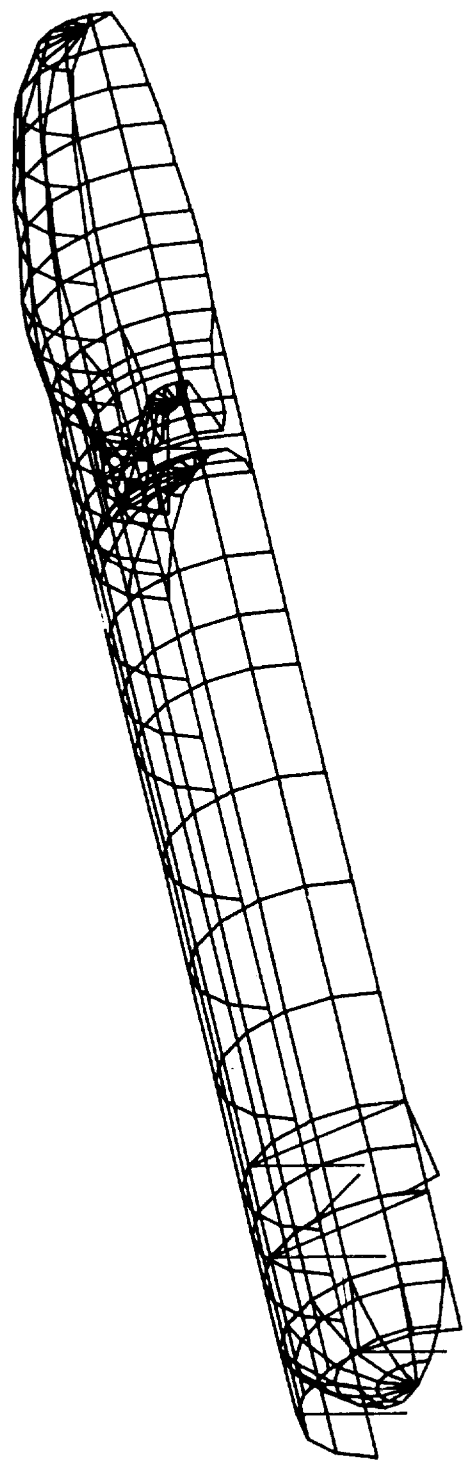

Fig. 4-35 1/8-Scale Space Shuttle External Tank – Post Max Q, Mode 25

5 - CONCLUSIONS

Symmetric finite element matrix formulations for compressible and incompressible hydroelasticity have been developed on the basis of Toupin's complementary formulation of classical mechanics. The incompressible formulation applicable in propellant tank hydroelastic analysis has been implemented in NASTRAN to replace the unsymmetric matrix formulation. The new technique which utilizes existing fluid and structural finite elements has been verified and demonstrated to be accurate and efficient.

The fluid representation according to the new technique consists of a symmetric fluid mass matrix described in terms of surface deformation only and an additional surface stiffness matrix when gravitational potential and ullage pressure stiffness are included in the fluid idealization. The fluid mass and stiffness matrices are then added directly to the structural mass and stiffness matrices, respectively, forming a symmetric set of hydroelastic equations in terms of structural displacements. As a result of the extensive NASTRAN structural modeling capability, differential stiffness effects due to static pressurization and fluid weight may be accounted for in the structural idealization. Modal hydroelastic analysis is performed with the same efficiency as in the case of a non-fluid filled structure as a result of very few additional degrees of freedom being required for the fluid.

The efficiency of the new hydroelastic analysis technique has been enhanced for both fluid and structure by introduction of harmonic reduction, applicable to geometrically axisymmetric structures, as an alternative to Guyan reduction. When the number of harmonics utilized is much less than the number of discrete nodes about a circumference, overall matrix size and bandwidth are significantly reduced. Harmonic reduction which was developed early in the present study was first demonstrated on a 60° spherical cap exhibiting superior accuracy and efficiency relative to Guyan reduction for an axisymmetric structure.

The formulation has been verified by comparison with exact analytical results for a fluid filled hemispherical container, a fluid filled circular cylindrical shell and a pressurized fluid circular cylindrical shell. In all three cases, excellent correlation was exhibited as well as very good computational efficiency.

Analysis/test discrepancies on the 1/8-scale external tank model have not yet been resolved. The efficiency of the current 1/8-scale external tank analysis, however, is very encouraging upon comparison of computation times between the present analysis and the standard unsymmetric NASTRAN hydroelastic formulation. Approximately 20 CPU minutes of computer time is required to extract 128 natural frequencies and 25 mode shapes with the present analytical technique while more than 70 CPU minutes was required with the standard NASTRAN hydroelastic analysis to extract a single natural frequency and mode shape.

The analysis/test correlation study on symmetric and unsymmetric circular cylindrical shells under various fluid fill conditions and static pressurization is considered very good.

It is strongly recommended that the present NASTRAN hydroelastic analysis be extended to include the capability for modeling non-axisymmetric fluid geometries by use of polyhedral heat condition finite elements. Long term goals anticipating future analytical requirements should also be pursued including implementation of the symmetric compressible hydroelastic formulation and development of general polyhedral compressible fluid elements.

6 - REFERENCES

1. "A Finite Element Method for Nonaxisymmetric Vibrations of Pressurized Shells of Revolution Partially Filled with Liquid", L.D. Pinson and C.G. Brown, AIAA Paper No. 73-399, March 1973.

2. "Dynamics of a Flexible Bulkhead and Contained Fluid", G.C. Feng and C.E. Jones, Lockheed Missiles and Space Co., Huntsville Res. and Eng. Center. Final Report LMSC - HREC TR D306476, May 1973.

3. "Calculation of Axisymmetric Longitudinal Modes for Fluid-Elastic Tank-Ullage Gas Systems and Comparison With Model Test Results", J. H. Palmer and G. W. Asher. AIAA Symposium on Structural Dynamics and Aeroelasticity, 1965, pp 189-193.

4. "Study on Dynamics of an Ellipsoidal Bulkhead Containing Fluid" R. J. Guyan, Rockwell International, Space Div. Technical Summary Report SD71-183, Sept. 1971.

5. "Longitudinal Vibration Analysis of Partially Filled Ellipsoidal Tanks by Finite Differences, R.L. Goldman, RIAS Technical Report No. TR70-6C, Aug. 1970.

6. "A Variational Principle for the Mesh-Type Analysis of a Mechanical System" R.A. Toupin, Journal of Applied Mechanics, June 1952, pp 151-152.

7. "A Numerically Efficient Finite Element Hydroelastic Analysis - Volume II Implementation in NASTRAN" R.N. Coppolino, NASA CR 132684, November 1974.

8. "Numerical Analysis of Stiffened Shells of Revolution", V. Svalbonas and P. Ogilvie, NASA CR-2273, Sept. 1973.

9. "Exact Hydroelastic Solution for an Ideal Fluid in a Hemispherical Container" R.N. Coppolino, Journal of Spacecraft and Rockets, Vol. 10 No. 9 Sept. 1973, pp 612-613.

10. "The Dynamic Behavior of Liquids in Moving Containers", H.N. Abramson, ed., NASA SP-106, 1966, pp 321-338.

11. "Vibration of Shells", A.W. Leissa, NASA SP-288, 1973, pp 62-64, 248-265.

12. "Development of Technology for Fluid-Structure Interaction Modeling of a 1/8-Scale Dynamic Model of the Shuttle External Tank (ET)" M. Bernstein, R. Coppolino, J. Zalesak, P.W. Mason, NASA CR-132549, Aug. 1974.

APPENDIX A - TOUPIN'S VARIATIONAL PRINCIPLE

A complementary variational formulation of classical mechanics utilizing impulse quantities as generalized coordinates was introduced by Toupin in 1952 (Ref. 6). This formulation, which may be interpreted as a dynamic generalization of the complementary energy principle of statics, has not received much attention in the development of analytical methodology; it is advantageous in most analyses to utilize displacement quantities as generalized coordinates. As in the displacement formulation of mechanics, complementary counterparts of D'Alembert's Principle, Hamilton's Principle and the Euler-Lagrange equations are derivable as consequences of Newton's laws. The development presented here closely parallels the derivation of the variational displacement formulation in mechanics.

Newton's second law states that for a particle

$$\frac{d}{dt}(m_o\dot{\vec{r}}) = \ell_o\vec{F} \tag{A-1}$$

with $\dot{\vec{r}}$ and $\vec{F}$ representing the velocity and force vectors, respectively, and with m_o and ℓ_o taken as constants. Newton arbitrarily defined m_o as the particle mass and ℓ_o as unity thus setting the course for development of displacement oriented formulations in mechanics. By arbitrarily defining m_o as unity and ℓ_o as the particle inertance the course is now set for development of alternative formulations; the inertance is simply the inverse of mass. Integration of (A-1) with respect to time results in

$$\dot{\vec{r}}(t) = \ell_o\int_o^t \vec{F}\,dt + \dot{\vec{r}}(o) \tag{A-2a}$$

or by taking the initial velocity as a consequence of all previously applied force

$$\dot{\vec{r}}(o) = \ell_o\int_{-\infty}^{o} \vec{F}\,dt \tag{A-2b}$$

the concise integrated statement of Newton's law is

$$\dot{\vec{r}}(t) = \ell_o\,\hat{F}(t) \tag{A-2c}$$

with

$$\hat{F}(t) = \int_{-\infty}^{t} \vec{F}(t)\, dt \qquad \text{(A-2d)}$$

The quantity $\hat{F}(t)$ is the total impulse which has brought the particle from rest to the current velocity. The above statements also hold for aggregates of particles.

It is now postulated that a system of n particles moves such that under the arbitrary virtual impulses, $\delta \hat{F}_i$,

$$\sum_{i=1}^{n} (\dot{\vec{r}}_i - \ell_{oi} \hat{F}_i) \cdot \delta \hat{F}_i = 0 \qquad \text{(A-3)}$$

where $\vec{r}_i$ denotes the position vector with respect to a Newtonian reference frame. The above is the complementary counterpart of D'Alembert's principle. Integration of the above expression over the time interval (t_o, t_1) results in

$$\int_{t_o}^{t_1} \sum_{i=1}^{n} (\dot{\vec{r}}_i \cdot \delta \hat{F}_i)\, dt - \int_{t_o}^{t_1} \sum_{i=1}^{n} \ell_{oi} \hat{F}_i \cdot \delta \hat{F}_i\, dt = 0 \qquad \text{(A-4)}$$

At this point it is convenient to define the complementary kinetic energy and virtual work functions which are

$$T_c = 1/2 \sum_{i=1}^{n} \ell_{oi} \hat{F}_i \cdot \hat{F}_i \qquad \text{(A-5a)}$$

and

$$\delta W_c = \sum_{i=1}^{n} \vec{r}_i \cdot \delta \dot{\hat{F}}_i \qquad \text{(A-5b)}$$

respectively. The time integral of the virtual work function integrated by parts is

$$\int_{t_o}^{t_1} \delta W_c\, dt = \int_{t_o}^{t_1} \sum_{i=1}^{n} (\vec{r}_i \cdot \delta \dot{\hat{F}}_i)\, dt$$

$$= \sum_{i=1}^{n} \vec{r}_i \cdot \delta \hat{F}_i \Bigg|_{t_o}^{t_1} - \int_{t_o}^{t_1} \sum_{i=1}^{n} (\dot{\vec{r}}_i \cdot \delta \hat{F}_i)\, dt \qquad \text{(A-6a)}$$

By imposing the constraints

$$\delta \hat{F}_i\,(t_o) = \delta \hat{F}_i\,(t_1) = 0 \qquad \text{(A-6b)}$$

the complementary virtual work function is expressible in the alternate form

$$\delta W_c = - \sum_{i=1}^{n} (\dot{\vec{r}}_i \cdot \delta \hat{F}_i) \qquad \text{(A-6c)}$$

Incorporation of Eq. A-5a and Eq. A-6c into Eq. A-4 yields the statement of the complementary Hamilton's principle

$$\int_{t_o}^{t_1} (\delta T_c + \delta W_c)\, dt = 0 \qquad \text{(A-7)}$$

If the complementary work function, W_c, is expressible as

$$W_c = - U_c + W_c' \qquad \text{(A-8)}$$

where U_c defined as the complementary potential energy function has the general functional dependence

$$U_c = U_c\,(\hat{F}_1, \ldots, \hat{F}_n, \dot{\hat{F}}_1, \ldots, \dot{\hat{F}}_n\,; t) \qquad \text{(A-9)}$$

and W_c' is the remaining part of the work function best thought of as dependent on externally applied displacements (or velocities) such that

$$\delta W_c' = - \sum_{i=1}^{n} (\dot{\vec{r}}_{i_e} \cdot \delta \hat{F}_i) \qquad \text{(A-10)}$$

The complementary Lagrangian function is now designated as

$$L_c = T_c - U_c \qquad \text{(A-12)}$$

and the complementary form of Hamilton's principle is

$$\delta \int_{t_o}^{t_1} L_c (\hat{F}_1, \ldots, \hat{F}_n, \dot{\hat{F}}_1, \ldots, \dot{\hat{F}}_n, t)\, dt + \int_{t_o}^{t_1} \delta W_c' \, dt = 0 \qquad \text{(A-12)}$$

In order to derive a general set of complementary Euler-Lagrange equations (Toupin's equations) the notation of generalized impulse coordinates is introduced. The generalized impulses are defined as those which

- Determine the dynamic configuration of the system
- May be varied arbitrarily and independently without violating the constraints of the system.

Consider now a system of n particles for which the individual impulses are functions of m ($m \leq n$) generalized impulses, i.e.,

$$\hat{F}_i = \hat{F}_i (\hat{Q}_1, \ldots, \hat{Q}_m, t), \; i = 1, \ldots, n \qquad \text{(A-13)}$$

The functions $\hat{F}_i$ are assumed continuous with continuous partial derivatives and the time derivative of the total impulse $\hat{F}_i$ is

$$\dot{\hat{F}}_i = \frac{\partial \hat{F}_i}{\partial \hat{Q}_1} \dot{\hat{Q}}_1 + \ldots + \frac{\partial \hat{F}_i}{\partial \hat{Q}_m} \dot{\hat{Q}}_m + \frac{\partial \hat{F}_i}{\partial t} \qquad \text{(A-14)}$$

Thus the complementary Lagrangian has the functional dependence

$$L_c = L_c (\hat{Q}_1, \ldots, \hat{Q}_m, \dot{\hat{Q}}_1, \ldots, \dot{\hat{Q}}_m, t) \qquad \text{(A-15)}$$

The variation of impulse, $\hat{F}_i$, is

$$\delta \hat{F}_i = \frac{\partial \hat{F}_i}{\partial \hat{Q}} \delta \hat{Q}_1 + \ldots + \frac{\partial \hat{F}_i}{\partial \hat{Q}_m} \delta \hat{Q}_m \qquad \text{(A-16)}$$

and the external complementary virtual work Eq. A-10 is expressed as

$$\delta W_c' = - \left[\dot{q}_{1_e} \quad \hat{Q}_1 + \ldots + \dot{q}_{m_e} \delta \hat{Q}_m \right] \qquad \text{(A-17a)}$$

where

$$\dot{q}_{je} = \sum_{i=1}^{n} \left(\frac{\partial \hat{F}_i}{\partial \hat{Q}_j} \cdot \dot{\vec{r}}_{i_e} \right); \; j = 1, \ldots, m \tag{A-17b}$$

Substitution of Eq. A-15 and Eq. A-17 into Eq. A-12 results in

$$\sum_{j=1}^{m} \int_{t_o}^{t_1} \left[\left(\frac{\partial L_c}{\partial \hat{Q}_j} - \dot{q}_{je} \right) \delta \hat{Q}_j + \frac{\partial L_c}{\partial \dot{\hat{Q}}_j} \delta \dot{\hat{Q}}_j \right] dt = 0 \tag{A-18}$$

Integration by parts noting the constraints at the limits

$$\delta Q_j (t_o) = \delta \hat{Q}_j (t_1) = 0 \tag{A-19}$$

yields

$$\sum_{j=1}^{m} \int_{t_o}^{t_i} \left[\frac{\partial L_c}{\partial \hat{Q}_j} - \frac{d}{dt} \left(\frac{\partial L_c}{\partial \dot{\hat{Q}}_j} \right) - \dot{q}_{je} \right] dt = 0 \tag{A-20a}$$

where the Euler-Langrange equations are the integrands

$$\frac{d}{dt} \frac{\partial L_c}{\partial \dot{\hat{Q}}_j} - \frac{\partial L_c}{\partial \hat{Q}_j} + \dot{q}_{je} = 0 \tag{A-20b}$$

Application of the complementary principle to large deformation and other non-linear problems requires a re-education of the analyst; one's physical intuition must be reoriented towards kinetic rather than kinematic considerations. Restricting further discussion to small deformation problems (in particular conservative small vibration problems), the kinetic and potential energy expressions reduce to the quadratic forms

$$\begin{aligned} T_c &= T_c (\hat{Q}_1, \ldots, \hat{Q}_m) \\ &= \frac{1}{2} \sum_{i=1}^{m} \sum_{j=1}^{m} L_{ij} \hat{Q}_i \hat{Q}_j \end{aligned} \tag{A-21a}$$

and

$$U_c = U_c\,(\dot{\hat{Q}}_1, \ldots, \dot{\hat{Q}}_m)$$
$$= \frac{1}{2} \sum_{i=1}^{m} \sum_{j=1}^{m} C_{ij}\, \dot{\hat{Q}}_i\, \dot{\hat{Q}}_j \qquad \text{(A-21b)}$$

respectively. The matrix set of Euler-Langrange equations resulting from Eq. A-22 is

$$(L) \left\{\ddot{\hat{Q}}\right\} + (C) \left\{\hat{Q}\right\} = \left\{\dot{q}_e\right\} \qquad \text{(A-22a)}$$

Taking the time derivative (noting that $\dot{\hat{Q}} = Q$) the result is

$$(L) \left\{\ddot{Q}\right\} + (C) \left\{Q\right\} = \left\{\ddot{q}_e\right\} \qquad \text{(A-22b)}$$

where $\{Q\}$ is the generalized force vector, (L) is the generalized inertance matrix and (C) is the generalized flexibility matrix. The significance of the matrices becomes apparent when the equations are rearranged as

$$(L) \left\{\ddot{Q}\right\} = \left\{\ddot{q}_e\right\} + \left\{\ddot{q}_d\right\} = \left\{\ddot{q}_{TOT}\right\} \qquad \text{(A-23)}$$

where

$$\left\{\ddot{q}_d\right\} = -\ (C) \left\{Q\right\} \qquad \text{(A-24)}$$

are interpreted as "complementary D'Alembert accelerations". Thus (L) is the inverse of the generalized mass matrix (M). In the case of statics the kinetic energy is null and the special equation (integrated twice)

$$(C) \left\{Q\right\} = \left\{q_e\right\} \qquad \text{(A-25)}$$

represents a statement of static equilibrium; and the flexibility matrix (C) is identified as the inverse of the generalized stiffness matrix.

The qualities of a complementary formulation are best illustrated by a set of simple examples.

Example 1:

Consider first the simple oscillator with base excitation, $\dot{U}_e$, illustrated in Fig. A-1. The kinetic and strain energies are

$$T_c = \frac{1}{2} L\hat{F}^2, \; U_c = \frac{1}{2} C\dot{\hat{F}}^2 \tag{A-26}$$

respectively and the complementary virtual work is

$$\delta W_c' = - \dot{U}_e \; \delta\hat{F} \tag{A-27}$$

The resulting Euler-Lagrange equation is

$$L\hat{F} + C\ddot{\hat{F}} = \dot{U}_e \tag{A-28}$$

Noting that the inertance and compliance are inverses of mass and stiffness, respectively, the natural frequency is

$$\omega = \sqrt{\frac{L}{C}} = \sqrt{\frac{K}{M}} \tag{A-29}$$

Example 2:

Consider now the free-free system illustrated in Fig. A-2. The kinetic and strain energies are

$$T_c = \frac{1}{2} L_1 \hat{F}^2 + \frac{1}{2} L_2 (\hat{F} + \hat{F}_e)^2 \tag{A-30a}$$

$$U_c = \frac{1}{2} C\dot{\hat{F}}^2 \tag{A-30b}$$

Noting that the external impulse $\hat{F}_e$ is prescribed and has no variation ($\delta Fe = 0$) the Euler-Lagrange equation is

$$(L_1 + L_2) \hat{F} + C\ddot{\hat{F}} = -L_2 \hat{F}_e \tag{A-31}$$

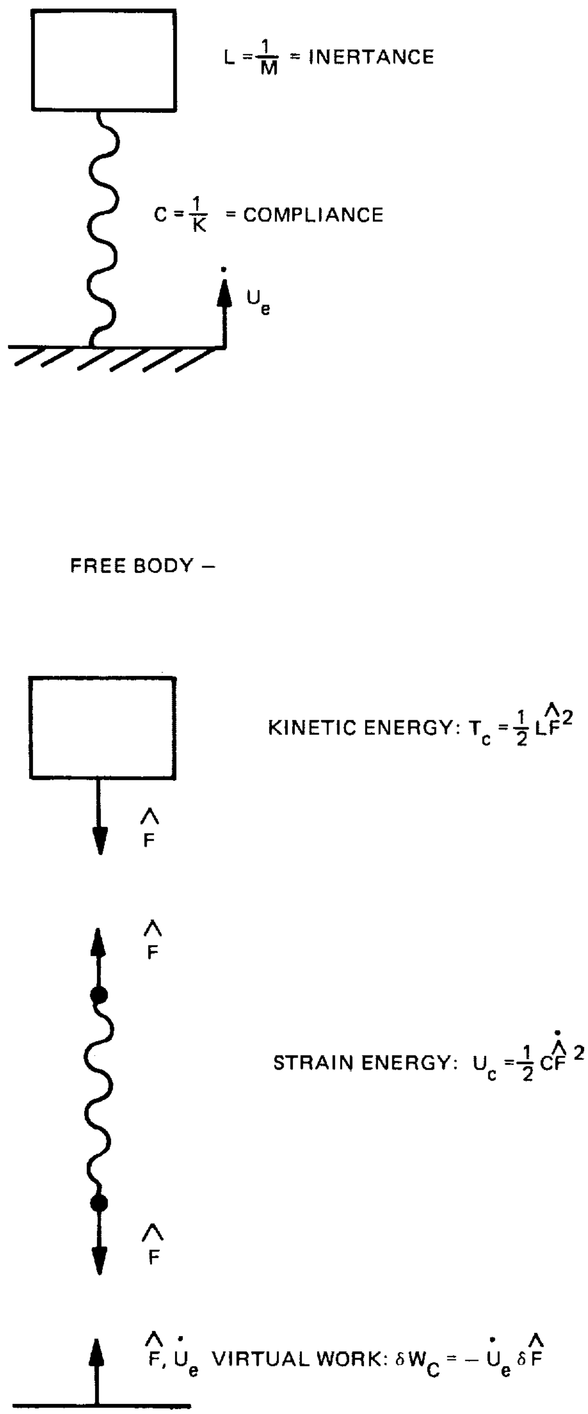

Fig. A-1 Simple Oscillator with Base Excitation

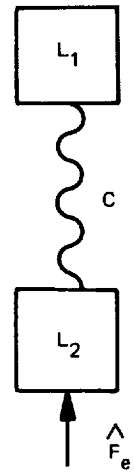

FREE BODY –

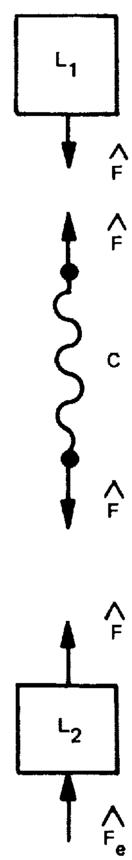

Fig. A-2 Free-Free System

In terms of the particle masses, (M_1, M_2), the inertance of the system is

$$(L_1 + L_2) = \left(\frac{1}{M_1} + \frac{1}{M_2}\right) = \left(\frac{M_1 M_2}{M_1 + M_2}\right) \tag{A-32}$$

which is immediately recognized as the inverse of the relative mass. Rigid body motion singularities are automatically removed in the complementary formulation. The complementary forcing function

$$L_2 \hat{F}_e = \frac{1}{M_2} \hat{F}_e = \dot{U}_e \tag{A-33}$$

is equivalent to an effective base motion input.

Example 3:

Consider the two-degree of freedom system illustrated in Fig. A-3. The kinetic and strain energies are

$$T_c = \frac{1}{2} L_1 \hat{F}_1^{\,2} + \frac{1}{2} L_2 (\hat{F}_2 - \hat{F}_1)^2 \tag{A-34a}$$

$$U_c = \frac{1}{2} C_1 \dot{\hat{F}}_1^{\,2} + \frac{1}{2} C_2 \dot{\hat{F}}_2^{\,2} \tag{A-34b}$$

and the Euler-Lagrange equations are

$$\begin{pmatrix} C_1 & 0 \\ 0 & C_2 \end{pmatrix} \begin{Bmatrix} \ddot{\hat{F}}_1 \\ \ddot{\hat{F}}_2 \end{Bmatrix} + \begin{pmatrix} L_1 + L_2 & L_2 \\ L_2 & L_2 \end{pmatrix} \begin{Bmatrix} \hat{F}_1 \\ \hat{F}_2 \end{Bmatrix} = \begin{Bmatrix} 0 \\ 0 \end{Bmatrix} \tag{A-35}$$

The flexibility and inertance matrices are inverses of the stiffness and mass matrices respectively of the system when the relative displacements X_1 and $(X_2 - X_1)$ are taken as the generalized displacements. If in the complementary formulation the net impulses are taken as generalized coordinates, i.e.,

$$\hat{F}_1' = \hat{F}_1 \tag{A-36a}$$

$$\hat{F}_2' = \hat{F}_2 - \hat{F}_1 \tag{A-36b}$$

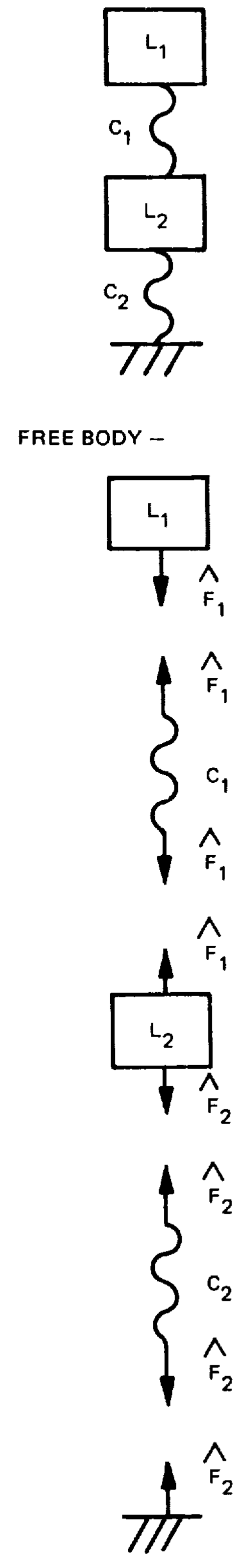

Fig. A-3 Supported Two-Degree of Freedom System

the kinetic and strain energies are expressed as

$$T_c = \frac{1}{2} L_1 \hat{F}_1'^2 + \frac{1}{2} L_2 \hat{F}_2'^2 \tag{A-37a}$$

$$U_c = \frac{1}{2} C_1 \dot{\hat{F}}_1'^2 + \frac{1}{2} C_2 (\dot{\hat{F}}_2' + \dot{\hat{F}}_1')^2 \tag{A-37b}$$

and the Euler-Lagrange equations are

$$\begin{pmatrix} C_1+C_2 & C_2 \\ C_2 & C_2 \end{pmatrix} \begin{Bmatrix} \ddot{\hat{F}}_1' \\ \ddot{\hat{F}}_2' \end{Bmatrix} + \begin{pmatrix} L_1 & 0 \\ 0 & L_2 \end{pmatrix} \begin{Bmatrix} \hat{F}_1' \\ \hat{F}_2' \end{Bmatrix} = \begin{Bmatrix} 0 \\ 0 \end{Bmatrix} \tag{A-38}$$

The above flexibility and inertance matrices are the inverses of the stiffness and mass matrices, respectively, of the system when the absolute displacements are taken as generalized coordinates.

It is interesting to note that the use of absolute impulse as a generalized coordinate results in a relative displacement equivalent formulation while use of relative (net) impulse generalized coordinates results in an absolute displacement equivalent formulation.

APPENDIX B - HEAT CONDUCTION - FLUID FLOW ANALOGY

The current NASTRAN hydroelastic modeling capability is limited to axisymmetrically shaped fluid configurations modeled with the cylindrical core and toroidal elements defined on CFLUID2, CFLUID3 and CFLUID4 connect cards. The possible need for a tilted liquid free surface fluid model for space shuttle external tank analysis necessitates the use of generally configured fluid finite elements. Tetrahedral and hexahedral finite elements would satisfy this requirement as well as any future requirement to model general non-axisymmetric fluid geometries. The desired general fluid elements are available in NASTRAN in the form of heat conduction elements; these may be utilized as incompressible fluid dynamic finite elements by implementation of the analogy presented below.

The field equation and flow boundary condition for an incompressible, inviscid fluid undergoing small motion are:

$$\nabla^2 P = 0 \qquad \text{in V} \tag{B-1}$$

and

$$\nabla P \cdot \hat{n} = \frac{\partial P}{\partial x_n} = -\rho \ddot{u}_n \qquad \text{on S} \tag{B-2}$$

On the boundary surface (outward normal x_n, $\hat{n}$). The field equation and heat flux boundary condition for an isotropic solid under steady state thermal loading are:

$$\nabla^2 \tau = 0 \qquad \text{in V} \tag{B-3}$$

and

$$\nabla \tau \cdot \hat{n} = \frac{\partial \tau}{\partial x_n} = -\frac{1}{K_T} f_n \qquad \text{on S} \tag{B-4}$$

The analogy is now immediately apparent with the following variables taking equivalent roles:

pressure, P: temperature, T

outward normal acceleration, $\ddot{u}_n$: outward normal flux/area, f_n inverse

mass density, ρ: inverse thermal conductivity, $1/K_T$

Consider the "generalized energy" principles utilized to derive the finite element fluid flow and heat conduction equations. The fluid "generalized potential energy" is (Ref. 12):

$$U_{f_V} = \frac{1}{2} \int_V \frac{1}{\rho} (\nabla P . \nabla P) \, dV \tag{B-5}$$

the corresponding thermal potential function is (Ref. 12):

$$U_{T_V} = \frac{1}{2} \int_V K_T (\nabla \tau . \nabla \tau) \, dV \tag{B-6}$$

in the special case of an isotropic material.

The variation of outward flow potential for the fluid and the corresponding quantity for the thermal surface potential are:

$$\delta U_{f_B} = - \int_S \delta P (\frac{1}{\rho} \nabla P) \cdot \hat{n} dS = \int_S \delta P \ddot{U}_n dS \tag{B-7}$$

and

$$\delta U_{T_B} = - \int_S \delta \tau (K \nabla \tau) \cdot \hat{n} dS = \int_S \delta \tau f_n dS \tag{B-8}$$

respectively.

The generalized energy expressions Eqs. B-5, B-6, B-7 and B-8 form the basis for derivation of mathematically equivalent incompressible fluid flow and thermal finite elements. The sets of algebraic equations describing fluid dynamic and thermal states, respectively, are

$$K_{f_{ij}} P_j = -S_i \ddot{U}_i \tag{B-9}$$

and

$$K_{T_{ij}} \tau_j = -S_i f_i \tag{B-10}$$

The utility of fluid flow and thermal elements has just been proven to be interchangeable; NASTRAN is capable of modeling general incompressible fluid flow configurations. The thermal elements required are defined by CTETRA, CHEXA1 and CHEXA2 connect cards. Thermal material properties following the analogy (mass density, ρ : inverse of thermal conductivity, K_T^{-1}) are specified on a MAT4 card.

NASA-Langley, 1976 CR-2662